Three-dimensional Nuclear Organization in Cancer: Examples from Mouse Plasmacytoma and Human Neuroblastoma

By

Alexandra Kuzyk

A Thesis submitted to the Faculty of Graduate Studies of

The University of Manitoba

In partial fulfillment of the requirements of the degree of

Doctor of Philosophy

Department of Biochemistry and Medical Genetics

University of Manitoba

Winnipeg, Manitoba, Canada

Abstract

Three-dimensional (3D) nuclear organization is the study of the spatial distribution of nuclear contents and components. Aspects of nuclear organization that are examined in this thesis were chromosome territories, chromosomal sub-regions and telomeres.

We began by examining nuclear disorganization in a transgenic mouse model. Mouse plasmacytoma (PCT) has different latency periods depending on the method of induction. Slow-onset PCTs are induced with pristane-only, take over 300 days to develop, and harbor activating *MYC/Ig* translocations. Fast-onset PCTs are induced with the v-*abl/myc* retrovirus, develop in an average of 45 days, do not harbor *MYC/Ig* translocations, but they display trisomy of cytoband 11E2. The nuclear location of the 11E2 cytoband was more central in the fast- compared to slow-onset PCTs and normal lymphocytes. The central location of this cytoband may increase the transcription of this region leading to the overexpression of genes located on 11E2. 3D telomere quantitative fluorescence *in situ* hybridization (Q-FISH) illustrated unique telomere profiles for fast- compared to slow-onset PCTs and normal lymphocytes. Fast-onset PCTs, compared to slow-onset PCTs and wild-type mice, had higher numbers of telomeres and telomeric aggregates per cell, more short telomeres, an altered distribution of telomeres throughout the nucleus, and a larger nuclear volume ($P < 0.0001$).

Our study of mouse PCT identified differences in the nuclear organization between aggressive and non-aggressive forms of the cancer. We further examined this distinction in a human context, looking for changes in nuclear organization in *MYCN* amplified compared to non-amplified neuroblastomas. Similar to PCT, neuroblastoma pathogenesis is driven by deregulation of the *MYC* family of oncogenes. Neuroblastoma also harbors chromosome aberrations in the syntenic region to mouse cytoband 11E2: human cytoband 17q25.

Neuroblastoma is the most common extracranial tumor in children. Multiple clinical features are considered poor prognostic factors such as higher tumor stage, unfavorable histology, older age at diagnosis, *MYCN* amplification and gain of chromosome arm 17q. Using dual-colored FISH and MYCN immunofluorescence on 16 neuroblastoma tissue samples, the unbalanced gain of 17q was found to be associated with high MYCN expression, no gain of 17q to be associated with medium MYCN expression, and numerical gain of chromosome 17 to be associated with low expression ($P < 0.0001$). The nuclear location of 17q also correlated with chromosome 17 copy number status: in tumors with unbalanced gain and no gain of chromosome 17, the 17q region occupies a location closer to the nuclear centre than in tumors with balanced gain ($P < 0.0001$). A more central nuclear location of 17q coincided with the increased expression of genes found within this chromosome arm. Telomere Q-FISH on 74 neuroblastoma tissue samples identified three tumor subgroups based on the measured telomere parameters, which represented unique levels of telomere dysfunction and genomic instability. Subgroups with higher levels of telomere dysfunction had more

telomeres and telomeric aggregates per cell, and greater percentages of short and long telomeres ($P < 0.0001$); these subgroups also were associated with poor prognostic clinical features ($P < 0.001$). Increased MYCN expression in two constitutively low-expressing neuroblastoma cell lines was correlated with unbalanced gain of 17q, more central nuclear location of 17q, and altered telomere organization.

In summary, this thesis illustrates the significance of multiple parameters of 3D nuclear organization in both PCT and neuroblastoma. The changes observed in the nuclear architecture of these cancers reflect increased telomere-mediated genomic instability that is driven by MYC and MYCN. Furthermore, the differences between aggressive and less-aggressive forms of the tumors suggest 3D nuclear organization could be used as a novel biomarker in cancer.

Acknowledgements

Firstly, I would like to thank Dr. Sabine Mai. From the time we first met, I knew I wanted to work in her laboratory. Sabine has been an amazing supervisor, mentor and friend. Her knowledge, ideas and views have strengthened my abilities and shaped my outlook on research in medicine. Her strength and compassion have inspired me.

I would like to thank all the present and former members of the Mai laboratory. Your knowledge and support was instrumental in my success. I will always treasure your friendships.

I would like to thank my committee members, Dr. Spencer Gibson, Dr. Sabine Hombach-Klonisch, Dr. James Johnston and Dr. Michael Mowat, for their guidance throughout my studies. I would also like to thank the laboratories of Dr. Sachin Katyal, Dr. Aaron Marshall, Dr. Kirk McManus, Dr. Michael Mowat and Dr. Leigh Murphy for their advice and help with specific techniques.

I would like to acknowledge the University of Manitoba's MD/PhD Program, and the past and present program directors, Dr. David Eisenstat and Dr. Kent Hayglass. I am grateful for the financial support of a CIHR MD/PhD studentship.

Lastly, I would like to thank my family and friends. This journey would not have been possible without the generous love and support of my parents.

In loving memory of my uncles

Peter Paul Kuzyk

and

Donald Ernest Boguski

Вічная Пам'ять

Table of Contents

List of Tables

List of Figures

List of Abbreviations

2D	Two-dimensional
3C	Chromosome Conformation Capture
3D	Three-dimensional
4C	Circularized Chromosomal Conformation Capture
5C	Carbon Copy Chromosome Conformation Capture
ALT	Alternative lengthening of telomeres
AML	Acute myeloid leukemia
ANOVA	Nested factorial analysis of variance
APB	ALT-associated promyelocytic leukemia nuclear bodies
ATM	Ataxia telangiectasia mutated
ATR	Ataxia telangiectasia and Rad3-related
BET	Bromodomain and extraterminal
BFB	Breakage-fusion-bridge
Can	Canonical variable
CGH	Comparative genomic hybridization
CML	Chronic myeloid leukemia
COG	Children's Oncology Group
CT	Chromosome territory
CTCF	CCCTC-binding factor
DAPI	4′6′-diamidino-2-pheylindole
DDR	DNA damage response

DHFR	Dihydrofolate reductase
DSB	Double-strand break
EE	Extrachromosomal element
FISH	Fluorescence *in situ* hybridization
H3Km3	Trimethylation of histone H3 at lysine K9
H4K20m3	Trimethylation of histone H4 at lysine K20
IC	Interchromatin Compartment
ICD	Interchromosomal Domain
Ig	Immunoglobulin
INSS	International Neuroblastoma Staging System
IP	Intraperitoneal
LOH	Loss of heterozygosity
mBANDing	Multicolor banding
MDS	Myelodysplastic syndrome
MEF	Mouse embryonic fibroblast
MGUS	Monoclonal gammopathy of undetermined significance
MKI	Mitosis-karyorrhexis index
MYCER	MYC-estrogen receptor fusion protein
NHEJ	Non-homologous end-joining
NM1β	Nuclear myosin 1 beta
OG	Oil granuloma
PBS	Phosphate-buffered saline
PCT	Plasmacytoma

PNA	Peptide nucleic acid
POT1	Protection of telomere-1
Q-FISH	Quantitative fluorescence *in situ* hybridization
Q-PCR	Quantitative polymerase chain reaction
RAP1	Repressor/Activator Protein 1
rcpT	Reciprocal translocation
RFU	Relative fluorescence units
ROS	Reactive oxygen species
STELA	Single telomere length analysis
TAD	Topologically associating domain
TERC	Telomerase RNA component
TERRA	Telomere repeat-containing RNA
TERT	Telomerase reverse transcriptase
TIN2	TRF1-interacting protein 2
TPP1	Tripeptidyl peptidase 1
TRF	Telomere restriction fragment
TRF1	Telomere repeat factor-1
TRF2	Telomere repeat factor-2
UV	Ultraviolet

List of Copyrighted Material for which Permission was Obtained

1. Kuzyk A and Mai S. (2012). Selected telomere length changes and aberrant three-dimensional nuclear telomere organization during fast-onset mouse plasmacytomas. *Neoplasia*. **14**(4): 344 – 51.

2. Kuzyk A, Booth S, Righolt C, Mathur S, Gartner J and Mai S. (2015). MYCN overexpression is associated with unbalanced copy number gain, altered nuclear location and overexpression of chromosome arm 17q genes in neuroblastoma tumors and cell lines. *Genes Chr Cancer.* **54**(10): 616 – 628.

Chapter 1:

Introduction

1.1. Chromosome Territories (CTs)

1.1.1. Structure, Models and Measurement Methods of CTs

CTs are distinct volume regions occupied by decondensed chromosomes in the interphase nucleus (1). CTs have been identified in animals (2), plants (3-5), and the single-cell eukaryotes, budding and fission yeast (6, 7). Although not completely defined, CTs are thought to be built from ~1 Mbp chromatin domains (8, 9), termed topologically associating domains (TADs) by Hi-C and Carbon Copy Chromosome Conformation Capture (5C) studies (10, 11). These ~ 1 Mbp chromatin domains join to form chromatin clumps that are in turn, folded and organized into CTs (12). TADs are conserved between cell types and during development, and are independent of epigenetic markings such as DNA methylation and histone modifications. It was found that TADs near the X-inactivation centre in mouse embryonic stem cells were aligned with repressive methylation markers; however, the removal of these markers did not alter TAD formation (11). CT folding may be influenced by function; for example, the inactive X chromosome is more compact than the active X chromosome (13, 14). The folding of chromatin into CTs is also physically advantageous, as long polymer molecules such as DNA can maximize entropy by limiting intermingling and forming intramolecular territories (15).

The most widely accepted model of CT architecture is the CT Interchromatin Compartment model (16). This model proposes that CTs are spatially associated with a contiguous three-dimensional (3D) network called the interchromatin compartment (IC). The IC channels from nuclear pores through higher-order chromatin. Although the IC is DNA free, it is separated from the CTs by a thin layer of decondensed chromatin, called perichromatin (17), which is the major site for transcription (18, 19), splicing (18-20), DNA replication (21) and DNA repair (22). The CT IC model stemmed from an earlier concept called the Interchromosomal Domain (ICD) model (23). This model stated that transcription occurred at the CT periphery, releasing RNA transcripts into the ICD; however, as genes were found to be transcribed both inside and outside of CTs (18, 24-26), this model fell out of favor. The Interchromatin Network model (27) suggests that chromatin fibers intermingle in a uniform way both inside CTs and between neighboring ones, which makes the distinction between the interior and periphery of CTs meaningless. The Giant-Loop model (28, 29) proposes giant loops of chromatin can reach across CTs to carry genes to remote sites for co-regulation or repression (30); this model incorrectly states there is no DNA-free space, which previous studies have proven by electron microscopy (16, 31).

Two main methods are used to study CTs: firstly, microscopic methods, such as fluorescence *in* situ hybridization (FISH) with probes that label entire or parts of chromosomes, are used to see chromatin structure and measure spatial distance between loci; secondly, non-microscopic methods, such as Chromosome Conformation Capture (3C) (32), use proximity-ligation assays of DNA to quantify the frequency of contact

between DNA segments, which is considered inversely proportional to their *in vivo* distance. Although microscopic resolution has previously limited the use of FISH, the implementation of super resolution microscopes (33, 34) has removed this barrier. While 3C examines pairwise interactions between loci on the same or different chromosomes, Circularized Chromosome Conformation Capture (4C) examines interactions of a locus of interest with the entire genome, and 5C and Hi-C examine pairwise interactions over the entire genome (35). Thresholding in both FISH and Hi-C methodologies must be used to avoid over-interpretation of interacting regions and sequences in CTs.

1.1.2. Factors Contributing to CT Arrangement

CTs are arranged in a non-random, cell-type specific manner in the nucleus (36-38). Their position is established early in G1 and is stable throughout interphase, until chromosomes must move to align in the metaphase plate during prophase (39-42). During interphase, CTs may undergo limited diffusion (43). CTs have been shown to undergo repositioning during cellular differentiation (44, 45) and tumorigenesis (36, 46-49).

One of the main factors thought to contribute to the arrangement of CTs is gene density. Early studies on human lymphocyte nuclei with chromosome probes for the gene-dense chromosome 19 and gene-poor chromosome 18, illustrated that CT 19 was consistently found in the nuclear interior and CT 18 at the nuclear periphery (50). This arrangement was confirmed in multiple normal cell types and tumor cell lines (48) and

was determined to be evolutionarily conserved in lymphoblastoid cells from primates, where orthologous segments of human chromosomes 18 and 19 were located at the nuclear periphery and centre, respectively (51). A gene density correlated radial arrangement was confirmed in all human chromosomes by Boyle *et al*. (52) and also found in rodents (53), cattle (54) and birds (55). A study of bovine embryos showed a radial arrangement of CTs depending on gene density was not present at the blastomere stage, but was established in the blastocyst (54). Although a size-based radial arrangement of CTs in human fibroblasts was initially proposed (56), a gene density correlated pattern was seen at the subchromosomal level with gene-dense Alu sequence-rich chromatin in the nuclear interior of the CTs. While bladder cells showed weak linear relationships with either gene density or size-based radial arrangements, the ratio of density:size showed a strong correlation (57).

The arrangement of CTs may also be due to DNA-binding factors or as a result of cellular preservation or function. Hi-C has identified CCCTC-binding factor (CTCF) as a highly conserved protein that plays a role in organizing DNA loops within chromosomes at specific loci (58). CTCF regulates gene expression by binding insulator sequences (59). At heterochromatin boundaries this creates barriers dividing chromatin into silent and active domains, which terminates the spread of histone marks and prevents interactions that activate transcription (60-64). Chromosomes have been found to be in closer proximity to a heterologue than a homologue (57, 65). This may be evolutionarily important to avoid homologous recombination, loss of heterozygosity (LOH) and damaging both copies of a chromosome from a single stress. A hallmark example of CT

arrangement that illustrates functionality was identified in rod cells of retinal tissue in nocturnal animals (66): whereas euchromatin is usually in the nuclear centre and heterochromatin at the periphery, nocturnal animals showed the opposite chromosome order with a MSR-positive chromocentre surrounded by a thick shell of gene-poor noncentromeric heterochromatin and thin outer shell of Alu sequence-rich euchromatin. This inverted arrangement was proposed to be an adaption of the animals to lower light conditions, as it allows for clearer night vision due to the higher refractive index when heterochromatin is in the nuclear interior. Although there are multiple theories about the arrangement of CTs, most groups agree that more than one factor contributes to the final arrangement.

1.1.3. CTs and Gene Regulation

Gene expression and gene location within a CT, and within the nucleus, are thought to influence each other (67). Studies have found transcriptionally active alleles to be located on the edges of CTs or looping outside the CT, whereas inactive alleles are embedded inside the CT (68). With increased transcription, gene-rich loops of chromosome 6, containing sections of the major histocompatibility complex, have been shown to loop outside of their CT (69). Furthermore, as genes in *cis* and *trans* can share the same transcription factory, they may relocate by looping out of their CT to reach transcription factories. For example, with induction, *MYC* rapidly relocated to the transcription factory occupied by *IgH* (70); this is functionally significant as *MYC* and *IgH* undergo frequent translocation in mouse plasmacytoma (PCT) and Burkitt

lymphoma. Additional studies have shown that chromatin looping is necessary for gene transcription: forced looping with a DNA binding protein between the IFN-β enhancer and a reporter gene stimulated the gene's transcription (71); tethering a looping factor to the murine *β-globin* locus triggered chromatin looping and *β-globin* transcription (72).

Traditionally, the nuclear periphery has been thought of as a repressive environment for transcription, and the nuclear interior as an area of transcriptional activity (73). Tethering a silencing-defective mating-type locus in yeast to the nuclear periphery restored its gene silencing (74). In Drosophila melanogaster, gene-poor chromatin is associated with the nuclear lamina, and genes near it are silent and marked by repressive chromatin modifications (75). In C. elegans, down-regulation of lamin A or a reduction in repressive chromatin markings, detached genes from the nuclear periphery; detachment also increased the expression of some of these genes (76, 77). Depletion of lamin A alters genome dynamics by inducing fast and normal diffusion in place of slow anomalous diffusion (78). Furthermore, in mammalian cells, reduction in lamin A lead to altered nuclear telomere distribution (79) and gene relocalization that may allow for, previously inhibited, gene activation (80). A study in rabbit of the position of casein milk protein genes (*CSN*) in mammary epithelial cells during lactation compared to hepatocytes, showed *CSN* looped out of its CT to be positioned in euchromatic regions in mammary cells, but remained at the periphery in hepatocytes; a control gene not involved in lactation occupied a similar position relative to its CT in both cell types (81). Tethering genes to the inner nuclear membrane in mouse fibroblasts resulted in transcriptional repression (82). Expression of the murine *β-globin* locus

increased with its relocation from the nuclear periphery to interior (83). With increased transcription, *CFTR* moved from the nuclear periphery to the interior; however, altering its nuclear location did not change its transcriptional status (84). In embryonic stem cells, the *MASH1* gene is transcriptionally repressed and located at the nuclear periphery; upon neural induction, *MASH1* transcription was up-regulated and it relocated to the nuclear interior (85).

There has also been evidence against the nuclear periphery being repressive and the centre being transcriptionally active. For example, artificially tethering chromatin regions to the nuclear envelope down-regulated certain genes, but not all (86, 87). Also, nascent RNA was found to be produced throughout the entire nucleus (88). It has been hypothesized that the nuclear interior may be important in acquiring a higher transcriptional rate, rather than initiating the event itself (89).

1.2. Telomeres

1.2.1. Telomere Structure and the Shelterin Complex

Telomeres are nucleoprotein structures at the ends of chromosomes. Human telomeres are composed of repeats of the DNA sequence 5′(TTAGGG)n3′, measuring between 5 and 15 kb in length (90, 91). Telomeres also have a G-rich DNA strand overhang at the 3′-end, measuring between 35 and 600 nucleotides (92, 93). This G-overhang folds back on itself forming a telomere loop (T-loop) (94, 95), and then evades

into the double-stranded DNA forming a D-loop (96). This folding structure protects telomeres by suppressing recombination and inhibiting telomerase (97).

Telomeric and subtelomeric regions are characterized by repressed heterochromatin with epigenetic markings such as trimethylation of histone H3 at lysine K9 (H3Km3) and histone H4 at lysine K20 (H4K20m3) (98, 99), and subtelomeric DNA methylation (100). It has been suggested that telomere elongation is regulated by the telomere's epigenetic status, with heterochromatic markings as a negative regulator of telomere length. For example, cells deficient for histone lysine *N*-methyltransferases caused the loss of H3K9m3 and H4K20m3 and exhibited very long telomeres (98, 99). Telomere repeat-containing RNAs (TERRAs) are also negative regulators of telomere length (101, 102). TERRAs are long, non-coding telomere RNA transcripts that originate from subtelomeres and contain telomeric repeats in RNA form (102). It has been proposed that TERRAs stimulate telomerase to be recruited to the shortest telomere from which they were transcribed (103). It has also been suggested that TERRAs bind hnRNPA1, releasing hnRNPA1 from telomeric DNA; this allows tripeptidyl peptidase 1 (TPP1)/protection of telomere-1 (POT1) to bind and recruit telomerase to the site (104, 105).

Shelterin is a protein complex bound to telomeres, and is important in their maintenance and protection. The six human telomeric proteins in the shelterin complex are telomere repeat factor-1 and -2 (TRF1 and TRF2), POT1, TRF1-interacting protein 2 (TIN2), the human ortholog of the yeast Repressor/Activator Protein 1 (RAP1) and TPP1.

TRF1 and TRF2 bind to the telomeric double-stranded DNA (106), and POT1 binds to the single-stranded G-overhang (107). TPP1 and POT1 form a heterodimer that is connected to TRF1 and TRF2 via TIN2 (108). RAP1 interacts with TRF2 (108).

TRF1 and TRF2 are negative regulators of telomere length (109, 110). Homozygous deletion of TRF1, TRF2 or TIN2 led to embryonic lethality in mice (111, 112). Many of the shelterin proteins have been implicated in repressing DNA damage responses (DDRs) at telomeres. TRF2 has been associated with the ataxia telangiectasia mutated- (ATM-) mediated non-homologous end-joining (NHEJ) pathway: mouse embryonic fibroblasts (MEFs) deficient in TRF2 exhibited end-to-end fusions mediated by the NHEJ pathway (112). POT1 has been shown to protect telomeres from ataxia telangiectasia and Rad3-related- (ATR-) dependent DDRs, and RAP1 has been implicated in repressing homologous recombination at telomeres (113). Both POT1 and TPP1 regulate telomerase-dependent telomere elongation (114-117). TPP1 recruits telomerase to telomeres. TPP1 null MEFs and mice show decreased binding of telomerase and shortened telomeres (118). As the central component of the shelterin complex, TIN2 helps facilitate rolls of other shelterin proteins such as inhibition of ATM-mediated DDRs and telomerase recruitment (119). Mutations in TIN2 and POT1 have been identified in human disease. Dyskeratosis congenita is characterized by a triad of dystrophic nails, skin hyperpigmentation and oral leukoplakia; bone marrow failure and aplastic anemia are often fatal in patients with this disease (120). Patients with dyskeratosis congenita have missense mutations in TIN2, which are thought to contribute to the shortened telomeres found in these patients (121). Recurrent somatic mutations in

POT1 were identified in 3.5% of a cohort of patients with chronic lymphocytic leukemia; cell lines with mutated *POT1* showed an increase sister chromatid fusions consistent with *POT1*-mutation mediated telomere uncapping (122).

The shelterin complex also works with the hCST complex to maintain telomere homeostasis. hCST is a telomere end-binding complex composed of STN1, TEN1 and CTC1 (123, 124). hCST binds to guanine-rich single-stranded telomeric DNA (123). The roles of hCST include protecting telomeres from eliciting DDRs, and acting as a terminator of telomerase by binding to the 3′ overhang generated by telomerase (125, 126). It has been proposed that the hCST and shelterin complexes compete to bind to the 3′ overhang as depleting the TPPI/POT1 heterodimer increased the association of hCST with the telomere (126).

1.2.2. Telomerase and Telomere Elongation

Telomere length is dynamic. Because DNA polymerases can only replicate DNA in a 5′ to 3′ direction, the lagging strand is built in a backstitching manner with RNA primers. After the final RNA primer is removed, a portion of the 3′ end of the lagging strand is incompletely replicated, termed the end replication problem (127, 128). This causes telomeres to shorten with each cycle of cell division and limits the number of possible DNA replication rounds. The stage at which cells enter replicative senescence due to critically short telomeres is called the Hayflick limit (129). Cells that escape replicative senescence have inactivated cell cycle checkpoint proteins, such as p53 and

Rb1 (130, 131). These cells continue to divide, resulting in dysfunctional telomeres and genomic instability, until they reach a second proliferative block or crisis (132, 133). Cells can evade crisis by activating telomerase (132, 134), which elongates and protects critically short telomeres called t-stumps (135). Telomerase is an enzyme that recognizes the unique telomere sequence at the ends of chromosomes, and elongates the 3′ end to avoid telomere attrition. However, telomerase is insufficient to compensate for the telomere length lost with cell division and is absent in most normal human somatic cells (136); therefore, telomere shortening is associated with age in most tissues (137, 138).

Telomerase is a ribonucleoprotein complex. It consists of a telomerase reverse transcriptase (TERT) and a telomerase RNA component (TERC). TERC is a template for the addition of telomere sequence repeats to the 3′ end (139). TERT expression is high in stem cells and in approximately 85% of cancer cells, but low or undetectable in somatic cells (140-142). The deletion of TERT or TERC in mice led to telomere shortening, genomic instability and aging phenotypes (143, 144). Mice with a competent p53 pathway and no telomerase activity were resistant to cancer (145-148). The overexpression of TERT in mice caused an increased incidence of cancers (149, 150); however, the overexpression of TERT in tumor-resistant mice with enhanced p53, p16 and p19 expression, greatly increased the lifespan of the mice (151). Mutations in the TERT and TERC components of telomerase have also been linked to human disease such as dyskeratosis congenita (120, 140), aplastic anemia (152) and idiopathic pulmonary fibrosis (153).

Although telomerase is the mechanism by which telomeres are elongated in the majority of cancers, alternative methods exist in the remaining tumors (141). Ten to 15% of tumors employ alternative lengthening of telomeres (ALT) methods, which use recombination to amplify or rearrange previously existing telomeric sequences (154-157). The ALT mechanism is most common in mesenchymal tumors (158-160). ALT is repressed in normal cells by telomeric proteins such as the shelterin proteins TRF2 and POT1 (161, 162). ALT-positive tumors have unique features such as the presence of telomeres of heterogeneous lengths (163), extrachromosomal telomeric DNA termed T-circles (164), circular single-stranded DNA rich in cytosine and guanine termed C- or G-circles (165, 166), and ALT-associated promyelocytic leukemia nuclear bodies (APBs) (167, 168).

Most tumors express either telomerase or ALT. However, with experimental manipulation *in vitro*, both mechanisms can occur within the same cell. For example, expression of telomerase in some ALT cell lines resulted in telomerase-mediated elongation of telomeres along with the presence of ALT characteristics (169-171). Contrastingly, studies have shown telomerase expression inhibited ALT characteristics (172) or that the ALT mechanism suppressed telomerase activity (173). *In vivo* studies have identified a subset of tumors that express both telomerase activity and ALT characteristics (174-176); however it is unknown whether these findings reflect the presence of both mechanisms in individual cells, or rather that it reflects tumor mosaicism with certain subpopulations of cells exhibiting ALT and others telomerase.

1.2.3. Telomere Dysfunction and Genomic Instability

Telomere dysfunction is thought to contribute to genomic instability and tumorigenesis (177-181). When telomeres become critically short, for example from the high rate of proliferation in a preneoplastic cell, or uncapped, such as from shelterin defects, they can trigger a DDR (182). In cells with competent tumor suppressor pathways, cell cycle arrest and apoptosis, or senescence, is induced (131, 183). In cells that have lost natural cell cycle checkpoints and do not undergo senescence, the chromosome end is then recognized as a DNA double-strand break (DSB) and a repair mechanism is employed (130, 131). Activation of homologous repair leads to terminal deletions, whereas NHEJ causes end-to-end fusions of sister chromatids or of different chromosomes (184). These fusions generate breakage-fusion-bridge (BFB) cycles as the fused chromatids form a bridge during anaphase, which breaks during cell division (185). This results in the uneven distribution of DNA to daughter cells with chromosome deletions and amplifications. The BFB cycle often repeats leading to complex genomic rearrangements such as dicentrics, rings, translocations and double-minute chromosomes; this genomic instability can be preceded and propagated by changes in the 3D telomere organization of the cells (46, 186). The cycle terminates when the cell enters crisis and undergoes cell death or when chromosomes acquire a new telomere through telomere healing mechanisms such as telomerase and/or ALT.

Other mechanisms that have been proposed to link telomere dysfunction with genomic instability include the resemblance of telomeres to fragile sites and the

susceptibility of telomeres to genotoxicity. Telomeres have similarities with fragile sites due to their complex folding structure and heterochromatic status. As fragile sites cause replication forks to stall and are often sites of DNA breaks (187), telomeres have been proposed as probable sites for the initiation of genomic instability (113). The role of TRF1 in suppressing the ATR-mediated DDR is essential in preventing DNA breaks from stalled replication forks (188). Because guanine triplets are particularly susceptible to oxidative damage, telomeres have a high risk of single-strand DNA breaks (189, 190). Telomeres are also sensitive to DNA damage from ultraviolet (UV) radiation because they are pyrimidine-rich. It was found that after UV radiation, telomeres had sevenfold more cyclobutane pyrimidine dimers than the rest of the genome (191).

1.2.4. Methods to Study Telomeres

Many methods have been employed to measure telomere length. They can be divided into two main categories: firstly, those that measure average telomere length, such as telomere restriction fragment (TRF) analysis and quantitative polymerase chain reaction (Q-PCR); secondly, those that measure the length of individual telomeres, including single telomere length analysis (STELA), quantitative FISH (Q-FISH) and 3D telomere FISH.

TRF involves the digestion of genomic DNA by restriction enzymes and subsequent Southern blot analysis where the gel is labeled with a probe that labels telomeric DNA (192). The average length of the telomeres in the DNA sample can be

determined from the smear size and intensity. This method is advantageous because it allows for the comparison of telomere lengths between studies; however, it requires a large amount of DNA. To measure telomere length with Q-PCR, telomeric sequences of DNA are amplified with specific primers along with a reference gene sequence (193, 194). This allows for the average length of the telomeres in the DNA samples to be determined by comparing the ratio of telomeric copies to those of the reference gene. Although Q-PCR requires a small DNA sample, the results cannot be compared amongst studies, and the distribution of telomere lengths cannot be determined.

STELA can measure individual telomeres because it uses specific primers for the subtelomere region of a specific chromosome telomere (195). It uses this primer, along with a primer that anchors to the 3′ end of telomeres, in ligation-mediated PCR. Following Southern blot analysis and labeling with a specific telomeric probe, the length of the telomere of interest can be determined. The main disadvantage to this method is that not all telomeres can be measured due to the lack of specificity of the telomeric sequences. STELA can only be used to measure the telomeres on chromosome arms Xp, Yp, 2p, 11q, 12q and 17p (196). Telomere lengths can be measured at a cellular and chromosomal level using Q-FISH with a flurochrome-labeled telomeric probe (197, 198), the most common being a peptidic nucleic acid (PNA) probe. This method allows for the visualization and measurement of all the telomeres individually in metaphase preparation. The telomere length is measured as a mean of relative fluorescent units (RFU) that correlates with telomere size in kilobases (197, 199-202). The disadvantage of telomere Q-FISH is that high quality metaphase spreads are necessary. The Mai laboratory

extended the method of Q-FISH from two-dimensional (2D) metaphases to labeling telomeres in 3D nuclei (203). Briefly, samples undergo a 3D fixation procedure (204) to preserve the nuclear architecture of the cells, and then are hybridized with a telomere PNA probe to label all telomeres. 3D image acquisition and deconvolution (205) are employed to generate a 3D rendering of the sample in which each telomere can be visualized within the interphase nucleus. Using TeloView software (203) multiple telomere parameters can be measured: the number of telomeres, the length of each telomere in RFU, the number of telomeric aggregates, the distance of each telomere to the nuclear centre and nuclear periphery, the spherical nature of the telomere distribution (termed the *a/c* ratio), and the nuclear volume. Telomeric aggregates are telomeres in close proximity to each, which cannot be further resolved as separate entities at an optical resolution of 200 nm (203); they can represent either end-to-end-fused chromosomes and/or telomeres that are in close vicinity (206). The main disadvantage of examining 3D telomere organization is that it is time consuming. Consequently, the Mai laboratory developed TeloScan (207). TeloScan is an automated high-throughput scanning, acquisition and analysis system that has significantly reduced sample processing time.

1.2.5. Variations in Telomere Length

Telomere length has been shown to vary with many conditions such as tissue type, age, genetic background, environment and tumorigenesis. Early findings showed that telomeres were longer in fetal liver than in cord blood and bone marrow (208), and longer in cerebral cortex and myocardium than liver and renal cortex (209). Telomeres

are generally longer in females than males (210, 211), although not at birth (212). Studies of monozygotic and dizygotic twins found that telomere length was genetically determined as average telomere length had 78% heritability (213) and lengths of individual telomeres of homologous chromosomes were identical in monozygotic, but not dizygotic twins (214). Telomere length has also been negatively correlated with obesity (215), smoking (215) and psychological stress (216, 217). Telomeres shorten with age by nine to 147 bp per year (209, 210, 218); exceptions to this include cerebral cortex, myocardium and spermatozoa, which all showed no shortening of telomere length with age (209, 219). Meta-analyses have shown inverse associations between leukocyte telomere length and cardiovascular disease (220), type 2 diabetes (221) and cancer (222, 223).

Depending on the type of cancer, telomere length has been negatively, positively or not associated with patient outcomes. Studies of leukocyte telomere length in breast cancer have shown mixed results: three studies found shorter telomeres in patients with breast cancer than healthy controls (224-226); two studies showed longer telomeres were associated with an increased risk of breast cancer (227, 228); two studies found no association of telomere length with breast cancer (229, 230). In colorectal cancer, studies of mean leukocyte telomere length from blood samples showed no association between telomere length and cancer risk (231-233). Telomeres were significantly shorter in the patient populations than healthy controls in studies of esophageal cancer (234, 235), gastric cancer (236, 237) and head and neck cancer (238). Two studies of telomere length in peripheral blood leukocytes from patients with lung cancer found shorter

telomeres in lung cancer cases than healthy controls, and an increased risk of lung cancer in individuals with shorter, compared to longer, telomeres (238, 239); however, a study of telomere length in morning sputum found no association of telomere length with lung cancer (240). Strong associations were identified between telomere length of surrogate tissues and ovarian (241), renal (238, 242) and bladder (238, 243, 244) cancers. The mixed results in breast and lung cancer may be due to different methodologies of telomere length measurement, the variability of the average telomere length parameter in a cohort of patients, prospective versus retrospective analyses and/or the use of different surrogate and control cell types. A prospective, population-based study of almost 800 individuals that were cancer-free at enrollment, found that the hazard ratio for incident cancers, and mortality in those that developed cancer, was highest in those with shortest telomere lengths (245).

In addition to differences in telomere length between tissues, it can also vary between chromosomes within the same cell (197). Studies have shown telomeres on chromosome arms 17p, 19p and 20q are the shortest, and those on chromosome arms 5p, 3p, 4q and 1p are the longest (200, 201, 246, 247). Variation in telomere length of homologous chromosome arms has also been shown (199, 248). Longer telomeres have been found on the arms of the active compared to the inactive X chromosome (248). Chromosome-specific telomere length changes have also been identified in cancer. For example, short telomeres on chromosome arms 17p and 12q are associated with an increased risk of esophageal cancer (235), and short telomeres on chromosome arm 9p are associated with increased risk of breast cancer (226). It has also been suggested that

chromosome-specific protective factors may lead to the lengthening of specific telomeres important to the tumor's pathogenesis (247, 249). In chronic myeloid leukemia (CML), chromosome arms 18p and Xp have the longest telomeres, which differs from the longest telomeres in healthy control patients (247).

1.2.6. 3D Telomere Organization

3D nuclear telomere organization has been studied by the Mai lab in many cell types and cancers using TeloView software (203). Telomeres are organized in a cell cycle dependent manner, with the formation of a telomere disk in late G2 (250, 251). MYC overexpression induced the formation of telomeric aggregates in Ba/F3 and PreB cells in a cyclic appearance that was directly linked to the duration of MYC deregulation (46). Epstein-Barr virus infection of human B cells also induced changes in 3D telomere organization, but in the absence of telomere shortening (252).

Typical differences between normal and tumor cells include altered numbers of telomeres, changes in telomere length, and the presence of telomeric aggregates. Chuang *et al.* (2004) described the altered 3D telomere organization and formation of telomeric aggregates in the RAJI Burkitt lymphoma cell line and in a primary human head and neck squamous cell carcinoma (250). The transition from mono-nucleated Hodgkin cells to multi-nucleated Reed-Sternberg cells can be monitored by changes in 3D telomere organization, with an increase in nuclear volume, very short telomeres and telomeric aggregates (253-255). Unique 3D telomere profiles are also associated with recurrent

compared to non-recurrent Hodgkin's lymphoma patients at diagnosis (256). Telomere profiles based on telomere number and size, and frequency of telomeric aggregates, identified previously unknown patient subgroups in glioblastoma that corresponded with patient survival (257). Mouse models of endometrial carcinoma (258) and melanoma (259) found changes in telomere length, and telomere distribution in the nucleus, to be early events in malignant transformation. A model of progression from myelodysplastic syndromes (MDS) to acute myeloid leukemia (AML) was defined based on distinctive telomere profiles (260). Subpopulations of circulating tumor cells were identified by telomere organization within the same patient with either melanoma, prostate, colon or breast cancer (261). Unique telomere profiles based on telomere signal intensities, telomeric aggregates, nuclear volume and overall telomere distribution, characterized patients with multiple myeloma, the precursor stage monoclonal gammopathy of undetermined significance (MGUS), and patients that relapsed (262). These telomere parameters also distinguished CML patients in the chronic phase from their profile at diagnosis (263). A study of a mouse model of follicular thyroid cancer found altered telomeric signatures in mice as young as one month of age (264).

1.3. MYC

1.3.1. MYC's Role in Cancer Initiation and Maintenance

MYC is a proto-oncogene that largely functions as a transcription factor. Its expression is tightly regulated in non-cancerous cells (265). MYC is activated in over

half of human cancers through multiple mechanisms including chromosomal translocation, gene amplification, increased RNA or protein stability, viral insertion, and oncogenic and epigenetic events (266-270). MYC activation results in the hallmark features of cancer: sustained proliferation and growth, angiogenesis, changes in tumor microenvironment and cellular metabolism, and avoidance of host immune responses (268, 271, 272). Tumor survival often becomes dependent on high levels of MYC, termed MYC addiction. These findings have led MYC to be proposed as a necessary event in tumor initiation (273).

Usually MYC activation cannot induce tumorigenesis alone. MYC overexpression in normal human cells leads to proliferative arrest, senescence and apoptosis due to protective checkpoints (274-276). MYC overexpression also results in DNA replication, but alone it cannot cause cellular division (277); this leads to polyploidy (278) and DNA breakage (279). Therefore, to initiate tumorigenesis MYC cooperates with many other oncogenic events. For example, events that evade cell-cycle checkpoints, such as overexpression of BCL-2 or loss of p53, allow MYC to induce proliferation and malignant transformation (280, 281). In experimental mouse models, MYC suppression after conditional activation has reversed tumorigenesis for a variety of cancer types (282-287). In some cases although remission was initially observed, it was followed by tumor recurrence with reactivated MYC expression, illustrating MYC addiction (288).

1.3.2. MYC Regulates Cell Growth and Metabolism

Multiple growth-promoting signal transduction pathways, such as MEK-ERK and NOTCH, converge on MYC highlighting one of its primary functions: cell growth regulation (289, 290). MYC binds to proximal gene promoter sequences, relieving paused RNA polymerases and initiating transcriptional elongation (291). Although it was proposed that MYC amplifies expression of all genes without specificity (292, 293), this does not account for MYC's ability to repress certain genes (294). Also, simply amplifying genes already expressed in a resting cell would not alter the ratio of growth-promoting versus growth-arresting signals (295). Therefore, it is thought that MYC alters the transcriptome in favor of growth-promoting genes while suppressing growth-arresting genes (294, 296, 297).

MYC activation not only promotes cell growth but also induces synthesis of the cellular components necessary for this growth. MYC directly regulates genes involved in glucose and glutamine metabolism (298, 299). MYC is also involved in ribosome and mitochondrial biogenesis (300, 301). Furthermore, MYC plays a role in activating genes involved in nucleotide and lipid biosynthesis (302-304). These processes push cells into S phase and MYC directly triggers cell-cycle progression by activating cyclin D and CDK4 (305, 306). MYC also activates the E2F transcription factor, which in turn activates genes involved in DNA replication (307).

1.3.3. MYC and DNA Damage and Repair

MYC has the ability to mediate DNA damage. Brief MYC expression in normal human fibroblasts caused DNA breaks due to reactive oxygen species (ROS) (308, 309). A further study showed that MYC-overexpressing cell lines had an increase in ROS (310). It was proposed that the increase in cellular metabolism from MYC activation caused a rise in ROS (309, 311). Also, genes that protect ROS are MYC transcriptional targets (312, 313). MYC can cause DNA damage independent of ROS production (314). MYC induction in normal human foreskin fibroblasts cultured in normal (10%) serum and murine lymphocytes *in vivo* caused ROS-independent DSBs; however, MYC induction in the same fibroblasts cultured in low (0.05%) serum and ambient oxygen saturation cause ROS-associated single-stranded breaks (314).

Replication stress from MYC overexpression may lead to an increase in DNA damage accumulated during S phase (315). MYC overrides cell cycle checkpoints (276) and uncouples DNA replication from mitosis (316), both which can lead to polyploidy and endoreduplication (316-318). MYC also induces DNA damage at early replication and common fragile sites (319). Furthermore, MYC can interfere with DNA break repair. The NHEJ pathway is directly suppressed by MYC causing inhibition of DSB repair and VDJ recombination (320). Homologous recombination is inhibited through MYC regulation of RAD51 (321).

1.3.4. MYC Induces Genomic Instability

Initial studies of MYC-mediated genomic instability occurred when a relationship between MYC and gene amplification, cellular replication, replication stress was not known (322). The first gene discovered to demonstrate a link between MYC and genomic instability was *dihydrofolate reductase* (*DHFR*), which had an increased copy number with MYC overexpression *in vitro*, in transgenic mice and human cancer tissues (278, 323-326). *DHFR* amplification occurred intrachromosomally, extrachromosomally, with and without locus rearrangements and in extrachromosomal elements (EEs) (278, 325, 327, 328). Further studies identified more amplified genes as a result of MYC overexpression (329-336); many of these genes are involved in DNA synthesis and cell cycle progression suggesting that cells harboring such amplifications may have a proliferative advantage (337).

MYC deregulation was found to be associated with illegitimate recombination and long-range chromosomal rearrangements, but not point mutations (338). These events can lead to chromosomal translocations, deletions and inversions (322). MYC-induced EEs were found to be transcriptionally active and to carry MYC targets of locus-specific genomic instability (339). Not only does MYC alter single loci, but it also induces chromosomal instability including centromere and telomere fusions, chromosome and chromatid breaks, ring chromosomes, translocations, deletions and inversions, aneuploidy and Robertsonian chromosomes (259, 276, 311, 312, 338, 340-344). Notably, *MYC box II* mutants were able to induce structural and numerical

aberrations, gene amplification and EEs, but telomere fusions were not observed (345-347).

1.3.5. MYC and Apoptosis

Although MYC is a strong driver of proliferation, it paradoxically is a potent apoptotic agent. The initial observation that an increase in apoptosis occurred after MYC overexpression in pre-malignant but not cancerous cells (348) led to the discovery that tumor cells acquire mechanisms that allow them to evade apoptotic signals. Soon after it was shown that the cell environment and the level or kinetic pattern of MYC, rather than the gene sequence, were key to determining the response to MYC: either proliferation or apoptosis (349).

Often cancers with elevated MYC levels also have elevated levels of BCL-2, a pro-survival agent (350, 351); this has led to the hypothesis that tumors evade the apoptotic effects of MYC because they concurrently overexpress a pro-survival protein. In support of this, *Bcl-2* knockout in *MYC* transgenic mice induces massive apoptosis (352). Additionally, MYC activation of BAG-1, a pro-survival agent, was found to be a critical event in evading MYC's apoptotic effect (353). MYC activation induces the p53 pathway, which enforces the apoptotic potential of MYC; therefore a mechanism for MYC to circumvent activation of the pro-apoptotic pathway is through loss of p53 function, either through mutations in p53 or p14ARF, or overexpression of hMDM2 (354). The Eμ-*myc* transgenic mouse model illustrates this: early in the six-month

latency period high levels of apoptosis are observed but tumor formation does not arise until a secondary genetic change that inactivates the p53 pathway (355). MYC-induced apoptosis has also been shown to occur in a p53-independent manner (356-360).

1.3.6. MYC as a Therapeutic Target

MYC is amplified in a wide range of cancers and often correlates with advanced stage, aggressive tumor behavior, poor clinical outcomes and increased chance of relapse (270, 361). This coupled with its essential role in tumor initiation makes MYC an attractive therapeutic target. As MYC is involved in the regulation of many cellular functions, there are concerns that targeting MYC will generate severe undesirable toxicity. Studies found tissue-specific *MYC* loss or down-regulation was tolerated in liver and intestinal tissues; however, compensatory up-regulation of *MYCN* was generated (362, 363). Therefore MYC inhibition may have a narrow therapeutic index.

MYC, and transcription factors in general, has difficult features to pair with traditional binding models for small organic drug molecules (364), making it a currently "undruggable target". Other obstacles include MYC's absence of enzymatic activity, lack of globular function domains, finely tuned post-translation regulatory mechanisms and short half-life (365-368). Many efforts have been made to identify small molecules that can inhibit MYC:MAX binding, but their use has been limited to mechanistic research due to their limited potency (369, 370). However, the development of Omomyc,

which competitively binds MYC, has shown promise in transgenic mouse cancer models (371, 372).

Another approach for targeting MYC has been to inhibit MYC-dependent transcriptional signaling. Studies have tried targeting coactivator proteins critical to MYC-specific initiation and elongation such as the bromodomain and extraterminal (BET) domain family of coactivator proteins (373). Murine models of hematological malignancies have shown promising results of MYC pathway inhibition and down-regulation of *MYC* transcription with BET inhibition (374). Other active areas of MYC-therapeutic research include inhibitors of transcriptional kinases, targeting upstream signal transduction pathways of MYC such as KRAS, and synthetic lethal interactions with MYC (367).

1.4. Mouse PCT

1.4.1. PCT Pathogenesis

Plasma cells are end-stage fully-matured B cells that secrete immunoglobulin (Ig). PCT cells also secrete Ig, mainly IgG or IgA, in mouse tumors (375) but they continuously cycle. Because spontaneous mouse PCTs are rare (376), most studies rely on induction methods. Of note, only BALB/c and NZB mice are genetically susceptible to developing pristane-induced PCTs (377, 378).

PCTs were initially induced by intraperitoneal (IP) insertion of plastic implants (379, 380). IP injections of pristane (2,6,10,14-tetramethylpentadecane) were later found to be the most efficient oil-based plasmacytomagen (381). The peritoneum appears to be the site of PCT development because it has extensive lymphatic drainage and mesothelial surfaces in which inflammatory exudates accumulate during chronic irritation from the plastic implants or pristane (382). The irritation from pristane injections causes a cellular response of macrophages, neutrophils and lymphocytes that phagocytizes small oil droplets and surround larger ones (383-385). This cellular response induces chronic inflammation and the formation of reactive tissue, oil granuloma (OG) on peritoneal surfaces such as omentum (382). The deposits are then covered by mesothelium and angiogenesis of the OG occurs. The inflammatory cells in the OG produce IL-6, which stimulates B cell to plasma cell differentiation (386). IL-6 has also been implicated as a survival and proliferation factor for PCTs (387-389). A further study that illustrated the inability of IL-6 knockout mice to develop pristane-induced PCTs, provided direct evidence for IL-6 as a critical factor in PCT development (390).

MYC deregulation is known to be an indispensible initiating event in PCT pathogenesis (391, 392). B cells are vulnerable to accumulating oncogenic mutations, which may become expressed at B cell to plasma cell differentiation (386). The effects of MYC activation in B cells and plasma cells include increased rates of proliferation and decreased apoptosis (393, 394). It has been proposed that cytokines such as IL-6 selectively stimulate plasma cells that have undergone MYC deregulation to form neoplastic proliferative plasma cell foci (395, 396).

All PCTs have MYC deregulation; however, the mechanism of deregulation, and PCT latency periods, depend on their method of induction. Slow-onset pristane-only induced PCTs have a latency of greater than 300 days (382). MYC deregulation occurs by *MYC/Ig* chromosomal translocations, most commonly involving the *Ig* heavy chain locus (T(12;15)) in over 90% of the tumors. *Ig* enhancers drive constitutive expression of MYC in B cells leading to tumor development (397). Pristane-induced PCTs followed by Abelson murine leukemia virus infection have a shorter latency with a mean of 88 days (382). These PCTs have both MYC and ABL overexpression and display *MYC/Ig* translocations. However, they also demonstrate the non-random chromosome aberration of chromosome 11 trisomy in 61.1% of tumors (398). This finding suggests amplification of genes on chromosome 11 may promote PCT development when overexpression of MYC and ABL is also present (399). Chromosome 11 trisomy was only found in 7.1% of pristane-only induced PCTs (400). Fast-onset PCTs were induced with pristane followed by *v-abl*/*myc* retrovirus infection and had a mean latency of only 45 days (399). There are no *MYC/Ig* translocations as the constitutive retroviral MYC expression suppresses endogenous MYC production (401). These fast-onset PCTs also had the highest frequency of chromosome 11 trisomy, with 90% of tumors displaying this aberration (399).

Further investigations of this chromosome aberration were performed to determine whether the whole, or a particular region of chromosome 11 was duplicated. Studies of F1 mice that had reciprocal translocations (rcpTs) involving chromosome 11

narrowed the duplicated region to cytoband 11E (399). To further define the important region of cytoband 11E, fast-onset PCTs were induced in congenic T38HxBALB/c mice with a rcpT between chromosomes X and 11 (rcpT(X;11)), in which the telomeric 11E band is translocated to the A2 band of chromosome X (402). This mouse model narrowed the trisomic region to cytoband 11E2, most commonly through duplication of the T(X;11) chromosome (402). This mouse model also created a unique opportunity to study the 11E2 region, as the rcpT(X;11) created a tiny T(X;11) translocation chromosome that contains only cytoband 11E2 and part of E1. Using array comparative genomic hybridization (CGH) and expression arrays, six genes were found to be duplicated and overexpressed in fast-onset compared to slow-onset PCTs (Sabine Mai, unpublished results). The six candidate genes were *Aspscr1, Ict1, Kcnj2, Foxk2, Sec14l1,* and *Tbcd*; the function of these genes are glucose transport, mitochondrial function, resting membrane potential regulation, DNA repair, intracellular transport system and nuclear organization, respectively.

1.4.2. Nuclear Disorganization in Mouse PCT

Studies of mouse-derived cell lines and primary mouse PCTs have demonstrated that altered nuclear organization contributes to the accelerated tumorigenesis and unique chromosome aberrations of fast- compared to slow-onset PCTs. The PreB cell line was generated from diploid mouse PreB cells of BALB/c origin that were immortalized with *v-abl* and stably transfected with MYC-estrogen receptor fusion protein (MYCER) vector for conditional expression (334). This cell line shows similar chromosome 11 aberrations

as seen in fast-onset mouse PCTs (403). Conditional expression of MYC in the PreB cell line caused remodeling of the 3D telomere organization, including the formation of telomere aggregates (46). These MYC expressing cells also showed evidence of BFB cycles such as broken chromosomes, non-rcpTs and chromosome fusions (46). Examination of interphase nuclear positions of the chromosome pairs that showed rearrangements in the PreB cell line, illustrated altered nuclear positions and greater overlap of the chromosome pairs, with MYC overexpression (46). MOPC460D is a PCT cell line with *MYC* activation from chromosomal translocation (T(12;15)) (342, 404). PreB and MOPC460D cell lines have altered 3D centromere positions compared to primary mouse lymphocytes (405). It was proposed that the alteration in centromere positions reflects nuclear remodeling during oncogenesis, and may impact the nuclear organization of chromosomes (405). A later study in PreB and MOPC460D cell lines showed that MYC mediated the formation of Robertsonian chromosomes through centromere disorganization and telomere-telomere fusions (342).

To further study the organization of chromosomes in mouse PCTs, software was developed to detect, segment and measure CTs in 3D nuclei that underwent 3D FISH with chromosome paints (406). To examine whether chromosome proximity affected translocation frequency in slow-onset PCTs, this software was used to determine the proximity and overlap of chromosomes 6, 12, 15 and 16; chromosomes 6 and 15, which are involved in 50% of *MYC/Ig* translocations in BALB/cRb6.15 PCTs, were found in close proximity suggesting their nuclear position may contribute to their Robertsonian translocation frequency (406). Using a modified version of this software (Christiaan

Righolt, unpublished results), the position of the 11E2 cytoband on chromosome T(X:11) in PCTs and normal B cells was determined: the T(X;11) chromosome was found in a more central position in fast-onset PCTs compared to slow-onset PCTs and normal B cells from T38HxBALB/c with rcpT(X;11) mice (Alexandra Kuzyk, unpublished results). A more centralized nuclear position of the 11E2 cytoband may grant it access to an accelerated rate of transcription, supporting the previous finding of six overexpressed 11E2 genes in fast-onset PCTs.

1.4.3. Syntenic Regions to Mouse Cytoband 11E2

The syntenic regions to mouse cytoband 11E2 have been associated with tumorigenesis in other species. The syntenic region to mouse 11E2 is 17q25 in human, and 10q32 in rat. Gain of the distal region of rat chromosome 10 (10q32) is observed in rat endometrial adenocarcinomas of different genetic backgrounds (407). Copy number gains including the 17q25.3 region have been found in 65% (13 of 20 tumors) of metastatic prostate cancers (408), 44% (four of nine tumors) of a renal cell carcinoma (409), 6% (five of 87 tumors) of myeloproliferative neoplasms (410) and 90% (118 of 131 tumors) of BRCA1 mutated breast cancers (411). The increased expression of *Survivin*, located on 17q25.3, has been associated with unfavorable outcomes and decreased survival in colorectal cancer (412, 413) and non-small cell lung cancer (414).

The unbalanced gain of chromosome 17q is the most frequent chromosome aberration in human neuroblastoma (415-417). It is found in approximately 50% of

neuroblastomas (415, 418-420) and is a poor prognostic factor (418, 419, 421, 422). Neuroblastomas with numerical chromosome 17 gain had a better prognosis than those with gain of chromosome 17q or no gain (423). All *MYCN* amplified neuroblastomas exhibit chromosome 17q gain and/or 1p loss (418). The most recent study has narrowed the shortest region of gain from the whole 17q arm to an approximately 14 Mb region from the 17q terminus (424). They also found a high density of overexpressed genes associated with survival in the 17q25.3 region (424). The syntenic region to 17q25.3 is gained in mouse and rat neuroblastoma (425). Because of the cross-species association of this cytoband with aggressive tumors, it has been proposed as a potential oncogenic cluster (424, 426).

1.5. Human Neuroblastoma

1.5.1. Incidence, Clinical Presentation, Prognosis of Neuroblastoma

Neuroblastoma is the most common extracranial solid tumor in childhood with over 650 cases diagnosed each year in North America (427, 428). The median age of diagnosis is 19 months with 37% of cases diagnosed in infants and 90% of cases diagnosed in children younger than five years of age (429). There is no racial bias in incidence (430). There is also no support for screening infants for neuroblastoma (431-433).

Neuroblastomas originate in sites where sympathetic nervous system tissue is present, such as the adrenal medulla or paraspinal nerve tissue. Patients with neuroblastoma most commonly present with an abdominal mass. Other signs and symptoms are often due to tumor mass and metastasis, which include bone pain, pancytopenia, fever and paralysis from spinal cord compression. At diagnosis, a tumor biopsy is needed for diagnostic confirmation with pathology and for tumor staging, which includes molecular tests for *MYCN* copy number, DNA index and 11q and 1p LOH.

In 2010 in the United States, the five-year survival rate for patients diagnosed with neuroblastoma at an age younger than one year was 95%, and between ages one to 14 was 68% (434); the five-year overall survival for patients diagnosed over 21 years of age was 46% (435). At diagnosis, approximately 70% of neuroblastomas are metastatic. Prognosis is dependent on multiple factors including age at diagnosis, site of primary tumor, tumor histology and molecular features (436, 437). Infants that are 18 months and younger at diagnosis have a very good prognosis even with advanced disease (429, 438). Although the primary tumor site is not an independent prognostic factor, adrenal primary tumors are associated with more unfavorable prognostic features, such as *MYCN* amplification, than non-adrenal primary tumors (439). Neuroblastomas with favorable histologic features, such as cellular differentiation, have a better prognosis than those with unfavorable histologic features, such as mitotic figures and karyorrhexis (440, 441). Multiple molecular features such as *MYCN* amplification (442, 443), segmental chromosome aberrations (418, 421, 444-448), *ALK* mutations (449, 450) and telomere length aberrations (451-453), have all been associated with unfavorable outcomes in

neuroblastoma. Neuroblastomas have been found to spontaneously regress; although this is most common for stage 4S tumors, spontaneous regression can occur with tumors of all stages (454-456).

1.5.2. Staging and Treatment of Neuroblastoma

The International Neuroblastoma Pathology Classification System or Shimada System is used to prognostically classify neuroblastomas before therapy (440). Tumors are categorized as favorable or unfavorable based on histologic parameters and patient age. The prognostic value of this system has been confirmed in several large patient cohort studies (440, 441, 457). The Shimada System is described in Table 1-1.

Table 1-1. Shimada Classification System for Neuroblastoma

Shimada Classification	Age (Years)	Histologic Features
Favorable	<1.5	Poorly differentiated or differentiating & low or intermediate MKI[a] tumor
	1.5 - 5	Differentiating & low MKI tumor
Unfavorable	<1.5	a) Undifferentiated tumor b) High MKI tumor
	1.5 - 5	a) Undifferentiated or poorly differentiated tumor b) Intermediate or high MKI tumor
	≥5	All tumors

[a]Mitosis-karyorrhexis index

The International Neuroblastoma Staging System (INSS) is used worldwide to stage neuroblastomas postoperatively (458). Stage 1 tumors are localized, completely resected with or without microscopic residual disease, and ipsilateral lymph nodes are

tumor-negative. Stage 2A tumors are localized, incompletely resected, and ipsilateral lymph nodes are tumor-negative. Stage 2B tumors are localized, completely or incompletely resected, and ipsilateral lymph nodes are tumor-positive. Stage 3 tumors are either unresectable and cross midline with or without lymph node involvement, or localized with contralateral lymph node involvement. Stage 4 tumors have dissemination to distant lymph nodes, bone, bone marrow, liver, skin and/or other organs. Stage 4S tumors are localized as defined in Stages 1 or 2, with dissemination to skin, liver and/or bone marrow, in infants younger than 12 months.

Due to advances in the understanding of neuroblastoma, the Children's Oncology Group (COG) developed a risk classification system for neuroblastomas that incorporates INSS staging and Shimada classification (459). The COG risk classification system is described in Table 1-2.

Table 1-2. COG Risk Stratification System for Neuroblastoma

Risk Group	INSS Stage	Age at Diagnosis	*MYCN* Status	Shimada Classification	DNA Ploidy
Low	1	0-21y	Any	Any	Any
	2A/2B	<365d	Any	Any	Any
		≥365d - 21y	Non-amplified	Any	-
		≥365d - 21y	Amplified	Favorable	-
	4S	<365d	Non-amplified	Favorable	>1
Intermediate	3	<365d	Non-amplified	Any	Any
		>365d - 21y	Non-amplified	Favorable	-
	4	<548d	Non-amplified	Any	Any
	4S	<365d	Non-amplified	Any	1
		<365d	Non-amplified	Unfavorable	Any
High	2A/2B	≥365d - 21y	Amplified	Unfavorable	-
	3	<365d	Amplified	Any	Any
		≥365d - 21y	Non-amplified	Unfavorable	-
		≥365d - 21y	Amplified	Any	-
	4	<365d	Amplified	Any	Any
		≥548d - 21y	Any	Any	-
	4S	<365d	Amplified	Any	Any

The management for neuroblastoma is generally dependent on the tumor's risk category. For low risk tumors, the treatment is usually surgery followed by observation and chemotherapy for symptomatic disease (460). Perinatal neuroblastomas found in the adrenal glands are observed without biopsy (461). Intermediate risk tumors usually receive chemotherapy, except in infants surgery can be followed with observation (462-464). High risk neuroblastomas have a complicated treatment regimen including chemotherapy, surgery, stem cell transplant and radiation therapy (465-468). Current induction chemotherapy regimens are suboptimal as about one-third of patients with high risk disease do not respond to first-line induction therapies (469). Common induction regimes include cisplatin or/or carboplatin, cyclophosphamide, etoposide, vincristine and

doxorubicin (470). To improve response rates, new agents such as Topotecan have been added to the regimen (471). Patients that reach a first remission also receive 13-*cis*-Retinoic acid (468). To treat minimal residual disease and increase induction phase response clinical trials with immunotherapy agents are ongoing (470).

1.5.3. The Effects of *MYCN* Amplification and MYCN Expression in Neuroblastoma

MYCN is part of the *MYC* family of proto-oncogene transcription factors. Although *MYC* is ubiquitous and highly expressed in proliferating cells during development and adult tissues, *MYCN* is only expressed during development in pre-B, kidney, forebrain and intestinal cells (472). *MYCN* plays an essential role in brain development by driving proliferation of granule neuron precursors (473) and its deletion is embryonically lethal (474, 475). *MYCN* along with mutant *HRAS* was found to transform rat embryo fibroblasts into foci that developed in to tumors in rats (476). Furthermore, transgenic mice that overexpress MYCN in neuroectodermal cells were found to develop neuroblastoma (477).

Twenty-five to 30% of neuroblastomas display *MYCN* amplification (457). *MYCN* amplification is a strong indicator of advanced tumor stage and poor clinical outcomes (442, 443, 478). Because of this, *MYCN* amplification is determined in all new neuroblastoma diagnoses, and those who test positive receive more aggressive treatment (479, 480). High MYCN protein expression is associated with *MYCN* amplification (481). MYCN expression can also occur without *MYCN* amplification and is a poor

prognostic factor in neuroblastoma (481-484). Furthermore, in addition to *MYCN* amplified tumors, a subset of *MYCN* non-amplified tumors were found to be associated with high expression of a MYC core target gene signature that predicts poor neuroblastoma prognosis; this subset of tumors was also associated with indicators of poor prognosis such as older patient age and advanced clinical stage (485).

It has been proposed that activation of the PI3K/AKT pathway in neuroblastoma may stabilize MYCN, as GSK3β, which phosphorylates MYCN decreasing its stability, is inactivated by AKT (486, 487). These findings led to the suggestion of PI3K inhibitors as potential therapeutic agents in neuroblastoma. A study that identified the H2A/H2B histone chaperone FACT as a driver of MYCN transcription and protein stability, also found that chemical inhibition of FACT impaired neuroblastoma formation in mice; therefore, it was proposed that FACT may also be a therapeutic target in neuroblastoma (488).

MYCN is involved in many cellular processes including proliferation, apoptosis, metastasis, pluripotency and angiogenesis (489, 490). Increased expression of MYCN in a neuroblastoma cell line was associated with an increase in the rate of DNA synthesis and proliferation by shortening the G1 phase (491). A role for MYCN in invasion and metastasis was proposed as a decrease in MYCN expression in a neuroblastoma cell line led to increased tumor cell attachment, decreased tumor cell motility and decreased proteolytic ability (492). Lentivirus vector-mediated silencing of MYCN induced differentiation and apoptosis in neuroblastoma cell lines and reduced tumor growth in

nude mice (493). The identification of embryonic stem cell-related factors as putative MYCN targets by expression microarray was further validated by studies of MYCN overexpression in a neuroblastoma cell line: expression of lif, klf2, klf4 and lin28b was closely correlated with MYCN expression (494). MYCN overexpression was also found to down-regulate leukemia inhibitory factor, which is a modulator of endothelial cell proliferation, suggesting a role of MYCN in angiogenesis (495). A genome-wide gene expression analysis of neuroblastoma tumors and cell lines identified differentially regulated genes with *MYCN* expression to be known oncogenes (*NCYM* and *RAB20*), genes associated with neural differentiation (*PTN, FMNL, DNER, CLU, GDA, NCRAM, ECEL1* and *SNPH*), and cell proliferation (*CDCA7, CENPE* and *CDC2L2*) (496).

1.5.4. Structural Chromosome Aberrations and Gene Expression Profiles in Neuroblastoma

Neuroblastoma has several recurrent structural chromosome aberrations that relate to disease prognosis. *MYCN* amplification occurs through the gain of chromosome region 2p24 as intrachromosomal homogeneously staining regions or extrachromosomal double minutes (497-499) and is a strong predictor of aggressive disease (443). LOH at 1p36 was found in 23% of neuroblastomas, and was associated with *MYCN* amplification and decreased progression-free survival in low and intermediate risk disease (444). Allelic loss of 1p was also found to be associated with decreased three-year survival in patients with Stage 3 and 4 disease (500). LOH at 11q23 was identified in 34% of tumors, and unbalanced 11q LOH, defined as loss of 11q with retention of 11p, was

found in 49% of tumors with 11q23 LOH; unbalanced 11q LOH was associated with decreased event-free survival in the entire cohort, and 11q23 LOH was associated with decreased progression-free survival in low and intermediate risk disease (444). Gain of chromosome arm 17q, from 17q21-qter, is the most frequent chromosome abnormality in neuroblastoma, found in 53.7% of tumors; the gain is associated with *MYCN* amplification, 1p deletion, adverse outcomes and decreased five-year overall survival (418).

Multiple studies used CGH and array-CGH to identify subgroups of neuroblastomas based on genomic profiles that correlated with patient outcomes (422, 446, 501-507); the principal conclusion of this work was that tumors with segmental chromosome aberrations have a worse prognosis than those with whole chromosome losses and gains. Although many of these studies suggested using CGH to profile neuroblastomas at diagnosis to determine prognosis, it has not been adopted as a standard of practice.

The lack of clinically translatable findings from CGH experiments led investigations of neuroblastoma in a new direction: expression profiling. A study by Hiyama *et al.* (2004) found favorable tumors to be associated with genes involved in neuronal differentiation and apoptosis; unfavorable tumors were associated with *MYCN, hTERT, NME1* and genes involved in cell cycle regulation (508). All studies found that their unique gene signature, ranging from 19 to 200 genes, was capable of significantly stratifying their patient cohort into higher- and lower-risk groups (508-512). The general

recommendation from these studies was to implement gene expression profiling of neuroblastomas at diagnosis to improve patient stratification and personalize treatment options; however, similar to genomic profiling, gene expression profiling has not been adopted as a routine clinical tool. The lack of clinical translation of the CGH and expression profiling results may be due to the inconsistency of the identified signatures.

1.5.5. Telomere Length and Maintenance in Neuroblastoma

Segmental and numerical chromosome aberrations in neuroblastoma have been proposed to be a result of telomere dysfunction (451). Previous studies of telomere length in neuroblastomas have found conflicting results. Long telomere length has been proposed as a poor prognostic factor (452, 453); conversely, short telomeres have also been suggested as an indication of poor prognosis (513). Lundberg *et al*. (2011) found two groups of neuroblastomas to have poor clinical outcomes: firstly, those with *MYCN* amplification, which showed decreased or unchanged telomere length; secondly those without *MYCN* amplification that had increased telomere length (451). Contrastingly, this study also found that tumors without *MYCN* amplification and decreased or unchanged telomere length, had excellent clinical outcomes (451). Onitake *et al.* (2009) found *MYCN* amplified tumors to have short telomeres (453). A study of average telomere length in neuroblastoma found one third of tumors to have two subpopulations of cells with different telomere lengths; tumors with predominately short or predominately long telomeres had the same overall survival as tumors with

homogeneously short or long telomeres, respectively (175). This study also found tumors with long telomeres to have lower event-free survival than those with short telomeres.

Both telomerase and ALT have been proposed to play a role in telomere length regulation in neuroblastoma. Neuroblastomas with high telomerase expression are clinically aggressive and have poor outcomes (514, 515). High telomerase expression is also associated with *MYCN* amplified tumors (453). Of 40 neuroblastoma cell lines, four lacked telomerase activity, had elongated telomeres and lacked *MYCN* amplification, suggesting they had an ALT-based telomere maintenance mechanism (516). A study found that neuroblastomas without *MYCN* amplification but with poor survival and increased telomere length, to also have APBs; this suggests the presence of an ALT mechanism in these tumors (451). A study of 102 neuroblastomas detected hTERT expression in 99 tumors and the ALT mechanism in 60 tumors, 20 of which also had hTERT expression; tumors with both ALT mechanism and telomerase had significantly reduced overall survival compared to solely the presence of ALT or high hTERT expression (175).

1.6. Thesis Rationale, Hypotheses and Objectives

1.6.1. Rationale

Nuclear disorganization is a feature of cancer cells. 3D telomere organization has been found to be altered in cancer cells compared to normal cells (203). 3D telomere

organization has also been able to distinguish multiple myeloma from its precursor stage (262), subgroups of glioblastoma with differing patient survival (257), and recurrent compared to non-recurrent Hodgkin's lymphomas at diagnosis (517). Mouse PCT is a unique model of cancer because it has different latency periods depending on the method of induction (382, 399). This allows an aggressive (fast-onset PCT) and non-aggressive (slow-onset PCT) form of the same tumor to be studied. Therefore we examined whether there are differences in the 3D telomere organization of fast- compared to slow-onset PCTs, and normal mouse lymphocytes. This study is described in Chapter 3.

It has been proposed that tumors have chromosome-specific protective mechanisms that maintain or lengthen the telomeres of specific chromosomes, which contain key regions to the pathogenesis of the cancer (247, 249). However, the link between uniquely lengthened telomeres on a chromosome that is important to tumorigenesis has not been identified. The sole chromosome aberration found in fast-onset mouse PCT is the duplication of cytoband 11E2 (402). Fast-onset PCTs induced in T38HxBALB/c with rcpT(X;11) mice have a tiny T(X;11) translocation chromosome that contains only cytoband 11E2 (402). This creates a unique opportunity to study the 11E2 region, which is necessary for fast-onset PCT development. Therefore we examined whether the T(X;11) chromosome has chromosome-specific protected telomeres. This study is also described in Chapter 3.

The syntenic region to mouse cytoband 11E2 is human cytoband 17q25. The most frequent chromosome aberration in neuroblastoma is the gain of chromosome arm

17q (415-417), which is a poor prognostic indicator (418, 419, 421, 422). *MYCN* amplification and high MYCN expression are also predictors of poor prognosis in neuroblastoma (442, 443). As cytoband 11E2 is duplicated in aggressive fast-onset mouse PCTs, we investigated whether copy number of cytoband 17q25 is increased in aggressive *MYCN* amplified, and high MYCN-expressing, neuroblastoma patient samples. This study is described in Chapter 4.

The location of chromosomes in the interphase nucleus is non-random (36-38, 518) and influences gene transcription with the nuclear interior associated with higher rates of transcription compared to the periphery (73, 84, 85). The position of CTs has been found to be altered with tumorigenesis (36, 46-49). Cytoband 11E2 was found in a more central nuclear location in fast- compared to slow-onset PCTs (Alexandra Kuzyk, unpublished results). This supports our finding of six genes on cytoband 11E2 being exclusively overexpressed in fast-onset PCTs (Sabine Mai, unpublished results). We studied whether cytoband 17q25 was associated with a more central nuclear location in *MYCN* amplified compared to non-amplified neuroblastoma patient samples. We also investigated whether MYCN overexpression could influence the nuclear position of cytoband 17q25 in two neuroblastoma cell lines. This study is also described in Chapter 4.

Studies of telomere length in neuroblastoma have been inconclusive as to whether short or long telomeres are associated with poor patient prognosis (451-453). 3D telomere organization has been illustrated as a diagnostic and prognostic biomarker in

multiple cancers (254, 257, 260). We investigated whether 3D telomere organization could identify subgroups of neuroblastomas with unique clinical characteristics. We then compared the groups identified by telomere analysis with current classification systems used to predict neuroblastoma prognosis. We also investigated whether MYCN overexpression could alter telomere organization in two neuroblastoma cell lines. This study is described in Chapter 5.

1.6.2. Hypothesis

We hypothesize that there is a close functional relationship between MYCC (and MYCN) expression and the 3D nuclear organization of telomeres and chromosomal sub-regions in mouse plasmacytoma and human neuroblastoma.

Sub-hypotheses:

1. Fast- and slow-onset mouse PCTs, and normal mouse lymphocytes, have unique 3D telomere organization.
2. Cytoband 11E2 exhibits chromosome-specific protected telomeres in fast-onset mouse PCTs.
3. Cytoband 17q25 has an increased copy number in *MYCN* amplified compared to non-amplified neuroblastomas.
4. The nuclear location of cytoband 17q25 is altered and driven by MYCN in *MYCN* amplified compared to non-amplified neuroblastomas.
5. 3D telomere organization in neuroblastoma identifies clinically relevant tumor subgroups and is altered by MYCN overexpression.

1.6.3. Objectives

The objectives of this thesis are:

1. To determine the 3D telomere organization of fast- and slow-onset PCTs, and normal mouse lymphocytes.
2. To determine the telomere length of chromosome T(X;11) in fast-onset PCTs.
3. To determine the copy number of cytoband 17q25 in *MYCN* amplified compared to non-amplified neuroblastomas.
4. To determine the nuclear location of cytoband 17q25 in *MYCN* amplified compared to non-amplified neuroblastomas and the relationship of 17q25 nuclear location to MYCN expression.
5. To determine the 3D telomere organization of a cohort of neuroblastomas and the relationship of telomere organization to MYCN expression.

Chapter 2:

Selected Telomere Length Changes and Aberrant Three-dimensional Nuclear Telomere Organization during Mouse Plasmacytomas

Part of this chapter was published in:

Kuzyk A[1] and Mai S[1]. (2012). Selected telomere length changes and aberrant three-dimensional nuclear telomere organization during fast-onset mouse plasmacytomas. *Neoplasia*. **14**(4): 344 – 51.

[1]Manitoba Institute of Cell Biology, Department of Biochemistry and Medical Genetics, The University of Manitoba, CancerCare Manitoba, Winnipeg, Manitoba, Canada

Running Title: Telomeres in Mouse Plasmacytoma

Key Words: telomere, 3D nucleus, genomic instability, mouse plasmacytoma

Contributions: Alexandra Kuzyk contributed to study design, performed the research, analyzed the data and wrote the manuscript. Sabine Mai designed the study and critically reviewed the manuscript.

2.1. Abstract

Mouse PCT can develop within 45 days when induced by a v-*abl/myc* replication-deficient retrovirus, in contrast to within 300 days when induced with pristane only. Fast-onset PCT development is always associated with trisomy of cytoband E2 of mouse chromosome 11. Trisomy of 11E2 was identified as the sole aberration in all fast-onset mouse PCTs in [T38HxBALB/c]N congenic mice, with a rcpT between chromosome X and 11 (rcpT(X;11)). Using this mouse model, we have now examined the overall and individual telomere lengths in fast- and slow-onset PCTs compared with normal B cells using 3D Q-FISH of telomeres. We found fast-onset PCTs to have a significantly different 3D telomere profile, compared with slow-onset PCTs and primary B cells of wild-type littermates with and without rcpT(X;11) ($P < 0.0001$ for all comparisons). Our data also indicate that in fast-onset PCTs the T(X;11) chromosome carrying 11E2 is the only chromosome with telomere lengthening ($P = 4 \times 10^{-16}$). This trend is not seen for the T(X;11) chromosome in control [T38HxBALB/c]N mice with the rcpT(X;11). This finding supports the concept of individual telomere lengthening of chromosomes that are functionally important for the tumorigenic process.

2.2. Introduction

Telomeres are DNA-protein structures at the ends of mammalian linear chromosomes. Telomeres shorten with each cycle of cell division (128, 519), and once they reach a critically short length, in a primary cell, this cell will normally undergo

senescence (137, 520, 521). Therefore, rapidly dividing cells, such as stem and tumor cells, or cells surviving “crisis”, often activate telomere lengthening mechanisms to ensure their replicative potential (522-525). Approximately 85% of tumor cells use telomerase, a reverse transcriptase with an RNA template, to add telomeric repeats to the 3′ end of parental DNA (526, 527). However, not all tumor cells with elevated telomerase have long telomeres (135). Approximately 15% of tumor cells use the alternative lengthening of telomeres mechanisms to lengthen telomeres through cycles of homologous recombination (156, 159, 528, 529).

Telomere regulation plays a critical role in genome instability and tumorigenesis (530-532). Critically short telomeres and uncapped telomeres can trigger a series of events that lead to genomic instability and include dynamic chromosome structure and number abnormalities (533, 534). Dysfunctional telomeres can cause the fusion of sister chromatids, or the fusion of neighboring chromosomes, leading to the formation of anaphase bridges (535). These bridges break as the centromeres are pulled apart (so-called BFB cycles), which results in unbalanced translocations and terminal deletions in the daughter cells (523). The repetitive nature of such aberrant genome remodeling cycles creates ongoing rearrangements, aneuploidy and polyploidy, all of which are commonly found in tumor cells, especially in tumors with complex karyotypes and high levels of cell-to-cell heterogeneity (46, 49, 113, 186, 536). However, these cycles will end if a new telomere is acquired, usually through the cell's activation of telomere lengthening pathways.

Most cancer studies reported in the literature show mean telomere shortening (537-539), but few studies have measured individual telomere lengths. Quantitation of telomere length using a telomeric PNA probe was done for the first time in 1996 by Lansdorp *et al*. (197). Chromosome-specific features were proposed to control telomere length because particular telomere lengths were associated with specific chromosomes (200). Telomeres on specific chromosome arms were also found to have interallelic differences through the use of STELA, a polymerase chain reaction-based technique (195, 196). Chromosome-specific telomere length changes have been identified in esophageal cancer (235), CML (247, 249), and breast cancer (226). These findings in tumor cells have led to the hypothesis that there may be chromosome-specific protective factors leading to lengthening of certain telomeres on chromosomes "key" to the pathogenesis of the cancer (247, 249); however, the connection between a chromosome known to be critical for tumorigenesis and uniquely lengthened telomeres has yet to be made.

Mouse PCT is a B-cell lineage tumor and the mouse model for human Burkitt lymphoma because they both result from *MYC* activating chromosomal translocations (391) and are cytogenetically identical. Slow-onset mouse PCTs are induced with solely IP injections of pristane, harbor *MYC/Ig* translocations and develop within 300 days. Fast-onset mouse PCTs, which can develop within 45 days, are induced with v-*abl/myc*, which generates constitutive retroviral MYC expression in infected preB lymphocytes (399). A characteristic of these tumors is the presence of chromosome 11 aberrations, which are the only chromosomal change in fast-onset PCTs (399). The generation of a

mouse model with a rcpT between chromosomes 11 and X, congenic [T38HxBALB/c]N with rcpT(X;11) mice, allowed us to narrow down the affected region on chromosome 11. This rcpT generates a very small T(X;11) translocation chromosome with only cytoband E2 and part of E1 (Figure 2-1). The chromosome 11 aberration found in all fast-onset PCTs was determined to be trisomy of the 11E2 cytoband, which contains all the genes necessary for the accelerated tumorigenesis of these tumors (402).

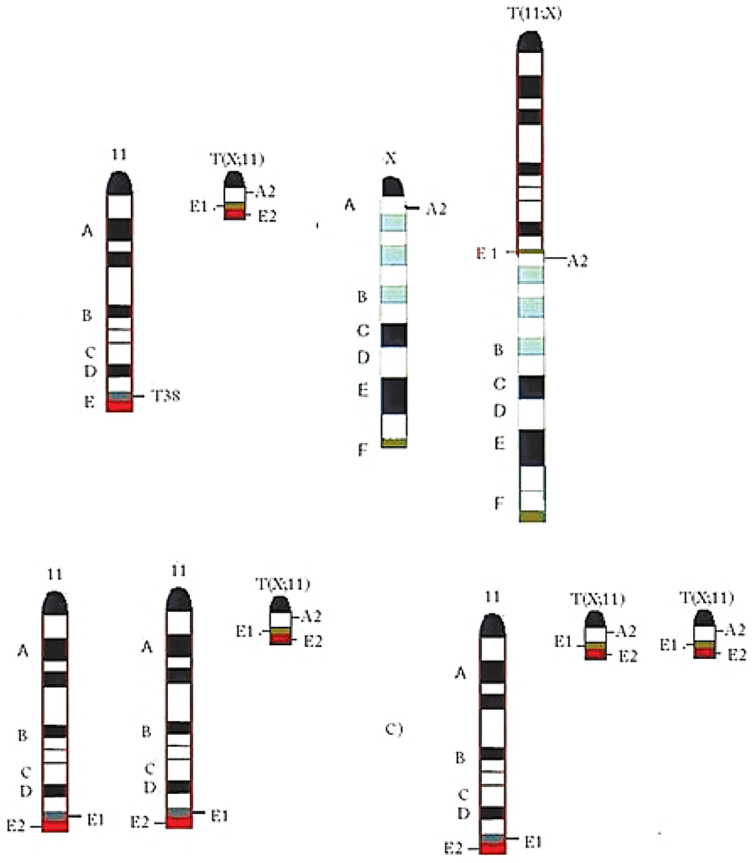

Figure 2-1. Graphical Illustration of the Chromosomal Constitution of Chromosomes 11 in the [T38HxBALB/c]N Backcross Generation Mouse.

Chromosome 11 with the breakpoint T38H in the telomeric cytoband 11E1 (brown),

whereas the breakpoint in Chr X is located in the centromeric A2 band. The cytoband 11E2 is red. The reciprocally translocated T(11;X) chromosome resulted from the fusion of the ABCD bands of Chr 11 proximal to the T38H breakpoint with the centromeric A2 band of Chr X. The T(X;11) chromosome was generated by the translocation of the X-derived A2 subband onto the 11E1 cytoband of Chr 11. The final, definitive version of this figure has been published in Wiener *et al.* (2010) (402) SAGE Publications Ltd. All rights reserved. © http://online.sagepub.com.proxy1.lib.umanitoba.ca.

We examined for the first time in mouse PCT, whether telomere dysfunction has a role in this tumor's development. We analyzed both the 3D telomere organization and potential 2D telomere length changes in the [T38HxBALB/c]N mouse model, which could have been difficult because of the long telomeres in inbred mice (537, 540, 541). However, we present the consistent finding, in both 2D and 3D experiments, of more very short telomeres in the fast-onset PCT cells compared with the control [T38HxBALB/c]N mice, with or without the rcpT(X;11) translocation. Compared to the wild-type mice, fast-onset PCTs had significantly greater numbers of telomeres and telomeric aggregates per cell, percentage of cells with aggregates and nuclear volume. Fast-onset PCTs also have a significantly different 3D telomere organization than slow-onset PCTs, with more telomeric aggregates ($P < 0.0001$). Our unique rcpT mouse model allows us to study the metaphase telomere length of the T(X;11) translocation chromosome for chromosome-specific telomere length changes that may indicate a protective mechanism. We find the T(X;11) translocation chromosome, which carries the 11E2 band critical for fast-onset PCT development (402), has significantly longer

telomeres in the fast-onset PCT compared with the wild-type rcpT(X:11) mice. Therefore, we demonstrate, for the first time, a connection between a chromosome key to a tumor's development and chromosome-specific telomere lengthening. This finding may provide significant support for a chromosome-specific protective mechanism used by tumor cells.

2.3. Materials and Methods

2.3.1. Cell Harvest, Culture, and Fixation

Primary lymphocytes were harvested from the spleens of congenic [T38HxBALB/c]N wild-type and [T38HxBALB/c]N with rcpT (X;11) mice (402). Primary PCT cells were harvested from the ascites of fast- and slow-onset PCT mice (382). All procedures were done in accordance with Animal Protocol 11-019 as approved by Central Animal Care Services, University of Manitoba (Winnipeg, Manitoba, Canada). For metaphase preparation of wild-type [T38HxBALB/c]N mice, with or without rcpT(X;11), lymphocytes were cultured short term (48–72 hours) in RPMI 1640 with 10% fetal bovine serum, 1% l-glutamine, 1% sodium pyruvate, 1% penicillin-streptomycin, and 0.1% β-mercaptoethanol (Invitrogen/Gibco, Burlington, Ontario, Canada) with lipopolysaccharide at a concentration of 10 μg/ml at 37°C in a humidified atmosphere and 5% CO2. Cells were maintained at a density of around 10^6 cells/ml.

2.3.2. 2D Chromosome and 3D Nuclei Fixation

Primary cells from the mice or cell culture were spun down at 200g for 10 minutes at room temperature. For 3D fixation (46, 250, 345), the pellet was resuspended in 5 ml of 0.075 M KCl for 10 minutes at room temperature and then overlaid with 1 ml of fresh 3:1 methanol-to-acetic acid fixative and inverted gently. Twice more, the cells were spun down at 200*g* for 10 minutes at room temperature and resuspended in 2 ml of fixative. Thirty microliters of this solution was gently placed on a slide, and the remainder was stored at -20°C. For 2D fixation, the initial pellet was resuspended in 5 ml of 0.075 M KCl for 30 minutes at room temperature, spun down at 200g for 10 minutes at room temperature and then the pellet underwent drop fixation with 3:1 methanol-to-acetic acid fixative (542). For statistical significance, at least 20 metaphases with non-overlapping chromosomes and 30 nuclei were examined in three independent experiments for each mouse type (46, 49).

2.3.3. Telomere Q-FISH

Telomere Q-FISH was performed on both 2D metaphases and 3D interphase nuclei with a PNA probe for telomeres purchased from DAKO (Glostrup, Denmark). In brief for the 2D telomere hybridization, the slides were fixed in fresh 3.7% formaldehyde/1 x phosphate-buffered saline (PBS), washed in 1x PBS, followed by a pepsin/HCl treatment and a second fixation. After ethanol dehydrations, the telomere PNA probe was applied, sealed onto the slide with rubber cement, and underwent a 3-minute denaturation at 80°C and 2-hour hybridization at 30°C using a Hybrite (Vysis; Abbott Diagnostics, Des Plains, IL). Then the slides were washed in 70% formamide/10

mM Tris at pH 7.4, 1x PBS, 0.1x SSC at 55°C, and 2x SSC/0.05% Tween 20. The cells were then counterstained with 4′6′-diamidino-2-phenylindole (DAPI), dehydrated, and mounted in Vectashield (Vector Laboratories, Burlington, Ontario, Canada). For the 3D telomere hybridization, briefly, the slides were fixed in 3.7% formaldehyde/1x PBS, incubated in 0.5% Triton X, followed by an hour incubation in glycerol and freeze-thaw treatment with liquid nitrogen. After 1x PBS washed and a HCl incubation, the slides were equilibrated in 70% formamide/2x SSC at pH 7.0. Then the slides underwent the same denaturation and hybridization, subsequent washes, staining, and mounting procedure as in the 2D fixation protocol.

In 3D, very short telomeres are defined as signals at a relative fluorescent intensity from 0 to 5,000 and short telomeres are defined as signals at a relative fluorescent intensity from 5,000 to 20,000. In 2D, very short telomeres are defined as signals at a relative fluorescent intensity from 0 to 30,000 and short telomeres are defined as signals at a relative fluorescent intensity from 30,000 to 50,000.

Telomeric aggregates are telomeres that are found in close proximity and cannot be further resolved as separate entities at an optical resolution of 200 nm (203). The *a/c* ratio is a measure of the spherical nature of the telomere distribution, with higher ratio indicating more cells in the G2/M phase and a higher overall level of cell proliferation (203, 250).

2.3.4. Image Acquisition

2D and 3D imaging and acquisition were performed using an AxioImager Z2 microscope (Carl Zeiss, Toronto, Canada), an AxioCam HR charge-coupled device (Carl Zeiss), and Zeiss AxioVision 4.8 software (Carl Zeiss). A 63x/1.4 oil objective lens (Carl Zeiss) was used with a DAPI filter, for detection of nuclear DNA staining, and a cyanine 3 filter, for detection of the telomere PNA probe signals. All metaphases images were taken at the same exposure time, and tricolor beads were used for standardization; the same protocol was used for all imaging of all interphase nuclei. For 3D imaging, 80 *z* stacks at 200 nm each, with *x, y* = 102 nm, *z* = 200 nm were acquired. The acquired images were deconvolved using the constrained iterative algorithm (205). To quantitatively analyze the metaphase telomere signals, Case Data Manager 4.0 software (Applied Spectral Imaging, Migdal HaEmek, Israel) for PC was used. TeloView software (203) was used to quantitatively analyze the 3D interphase telomere signals.

2.3.5. Statistical Analysis

Statistical analysis was done to compare the number of interphase telomeric signals at a certain intensity, using bins at an interval of 1000, from 0 to 225,000. An analysis was also done on the number of metaphase telomere signals at a certain intensity, using bins at an interval of 5000, from 0 to 195,000. Using a $\chi 2$ test, the telomere signal distribution was compared between the fast- and slow-onset PCTs and the wild-type mice, with and without rcpT(X;11). Analyses were done with both one threshold set at the 50th percentile or median, and two thresholds set at the 25^{th} and 75^{th}

percentiles. $\chi 2$ analysis was also used to compare the percentage of very short telomeres between the mouse types. Analysis of variance (ANOVA) with Tukey's multiple comparison test, was used to compare the number of telomeres, number of telomeric aggregates, percentage of aggregates, *a/c* ratio and nuclear volume between mouse types. $P < 0.01$ is considered significant.

Statistical analysis was also done to compare the telomere length of translocation chromosome T(X;11) to the telomere length of all other chromosomes. This was done using a Kolmogorov-Smirnov test in both the fast-onset PCT and the [T38HxBALB/c]N with rcpT(X;11) wild-type mice. $P < 0.001$ is considered significant.

2.4. Results

2.4.1. 3D Telomere Organization

To investigate the 3D telomere organization in wild-type mice, with or without rcpT(X;11), and in fast- and slow-onset PCTs, 3D Q-FISH was performed with a telomere PNA probe. This approach preserves the 3D nuclear architecture of the cells and specifically labels interphase telomeres in the whole cell population. After acquisition and constrained iterative deconvolution, all 3D interphase nuclei were analyzed with TeloView to determine the number of telomeric signals per cell and their intensity. The signal intensity correlates to the length of the telomere (202). The number of telomeric

aggregates per cell, the percentage of cells with aggregates, the *a/c* ratio and the nuclear volume of each cell were also determined.

Figure 2-2 (A – D) shows a representative example of the 3D telomere organization in a primary lymphocyte interphase nucleus from the [T38HxBALB/c]N wild-type and [T38HxBALB/c]N with rcpT(X;11) control mice and a primary plasmacytoma cell nucleus from the fast- and slow-onset PCT mice. The telomeric signals were visibly smaller in the fast-onset PCT nuclei than in controls and slow-onset PCTs. The results from three independent experiments for each mouse type were combined, and the telomeric profiles of the three mice were compared. Figure 2-2 E is a scatterplot that illustrates the number of telomere signals at a specific intensity. The distribution of telomeres is shown for intensities in the range of 0 to 140,000. As expected, 3D nuclei of the wild-type mice, whether carrying the rcpT(X;11) or not, have a similar telomere profile and are not significantly different, $P = 0.4$ (as determined by a $\chi 2$ test with $P < 0.01$ considered significant). The fast-onset PCT nuclei have many more low-intensity or very short telomeres (Materials and Methods), and their telomere profile is significantly different from both wild-type mice, with or without rcpT(X;11) ($P < 0.0001$ for both comparisons), and slow-onset PCTs ($P < 0.01$).

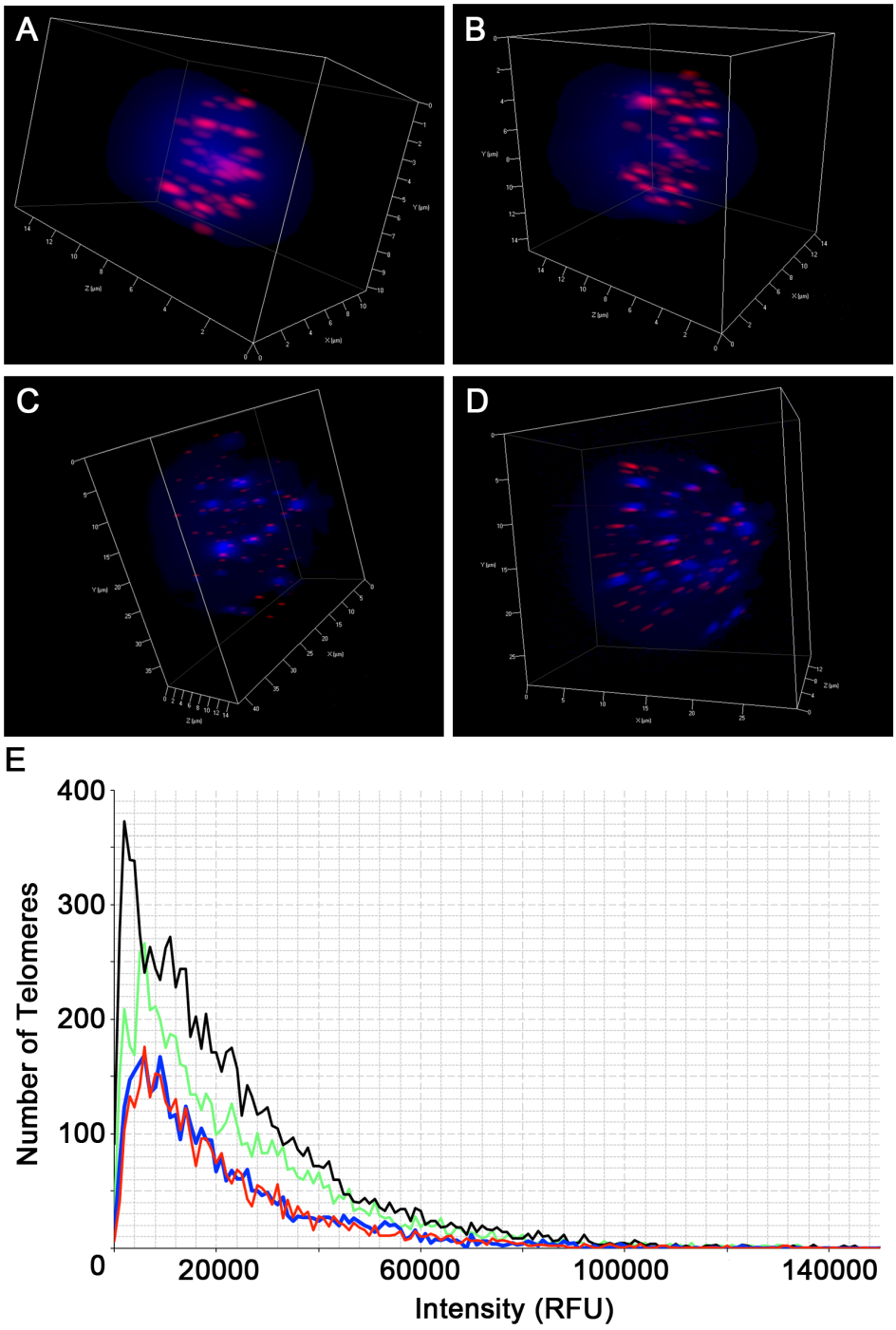

Figure 2-2. 3D Telomere Organization in Interphase Nuclei of PCT and Wild-type Mice. (A) Primary lymphocyte nucleus from the [T38HxBALB/c]N wild-type mouse. (B) Primary lymphocyte nucleus from the [T38HxBALB/c]N with rcpT(X;11) mouse.

(C) Plasmacytoma cell nucleus from the fast-onset PCT mouse. (D) Plasmacytoma cell nucleus from the slow-onset PCT mouse. (E) Comparison of the telomeric profile of the four mouse types. The intensity correlates to the telomere length. The fast-onset PCT nuclei (black) have more very short telomeres and a significantly different telomere length distribution than the slow-onset PCT (green) ($P < 0.01$), [T38HxBALB/c]N wild-type (red) and the [T38HxBALB/c]N with rcpT(X;11) (blue) mice ($P < 0.0001$ for both comparisons).

There was a significant difference amongst the four mouse types for each measured telomere parameter (Table 2-1) ($P < 0.0001$). Fast-onset PCTs had the highest number of telomeres per cell (89.50), followed by slow-onset PCTs (64.14). The wild-type mice had the lowest number of telomeres per cell (37.27 and 38.79), and in a pair-wise comparison, there was no significant difference between the two types of wild-type mice. Fast-onset PCTs had the highest number of aggregates per cell (11.14), followed by slow-onset PCTs (6.71). The wild-type mice had the lowest number of aggregates per cell (4.46 and 4.27), and in a pair-wise comparison, there was no significant difference between the two types of wild-type mice. In both fast- and slow-onset PCTs, 100% of cells contained telomeric aggregates; both types of control mice had a similar percentage of cells with aggregates (94% and 92%). The *a/c* ratio was significantly greater in the fast- and slow-onset PCTs (3.15 and 2.12, respectively; $P < 0.0001$ for all comparisons), compared to the *a/c* ratio in the control mice (1.30 and 1.31). The nuclear volume was also significantly greater in the fast- and slow-onset PCTs (1072 μ^3 and 1404 μ^3; $P <$

0.0001 for all comparisons), compared to the nuclear volume in the control mice (392.5 μ^3 and 443.1 μ^3).

Table 2-1. Statistical Analysis of Telomere Parameters by Mouse Type

	[T38HxBALB/c]N Wild-type	[T38HxBALB/c]N with rcpT(X;11)	Fast-onset PCT	Slow-onset PCT	*P*-value Between Subgroups[a]
Average Number of Telomeres per Cell	37.27	38.79	89.5	64.14	<0.0001
Average Number of Aggregates per Cell	4.46	4.27	11.14	6.71	<0.0001
Average Percentage of Cells with Aggregates (%)	94	92	100	100	<0.0001
Average *a/c* Ratio	1.3	1.31	3.15	2.12	<0.0001
Average Nuclear Volume (μm^3)	392.5	443.1	1072	1404	<0.0001

[a] *P*-value determined by one-way ANOVA

2.4.2. 2D Telomere Length

To determine the length of individual telomeres on all chromosomes in wild-type mice, with or without rcpT(X;11), and in fast-onset PCTs of the same mice, 2D Q-FISH was done with a telomere PNA probe. This method hybridizes metaphases with a specific probe for labeling all telomeric signals. After acquisition, all metaphase spreads were

analyzed with Case Data Manager 4.0 to determine the intensity of each telomere signal, which correlates to the length of the telomere (202).

Figure 2-3 (A – C) illustrates an example of the telomeric signals in a metaphase spread from the [T38HxBALB/c]N wild-type and [T38HxBALB/c]N with rcpT(X;11) control mice and in fast-onset PCTs. As indicated with a circle, the small T(X;11) translocation chromosome is easy to identify based on size alone (see also Figure 2-1). The results from three independent experiments for each mouse type were combined, and the telomere lengths of the three mice were compared. Figure 2-3 D is a scatterplot that illustrates the percentage of telomere signals at a specific intensity. The distribution of telomeres is shown for intensities in the range of 0 to 160,000. As in the 3D interphase study, chromosomes from wild-type mice, with or without rcpT(X;11), have a similar distribution of telomere lengths and are not significantly different, $P = 1.0$ (as determined by a $\chi 2$ test with $P < 0.01$ considered significant). The chromosomes of fast-onset PCTs have more lower intensity or very short telomeres (see Materials and Methods), and their telomere length distribution is significantly different from [T38HxBALB/c]N mice, carrying rcpT(X;11) or not ($P < 0.0001$ for both mouse types).

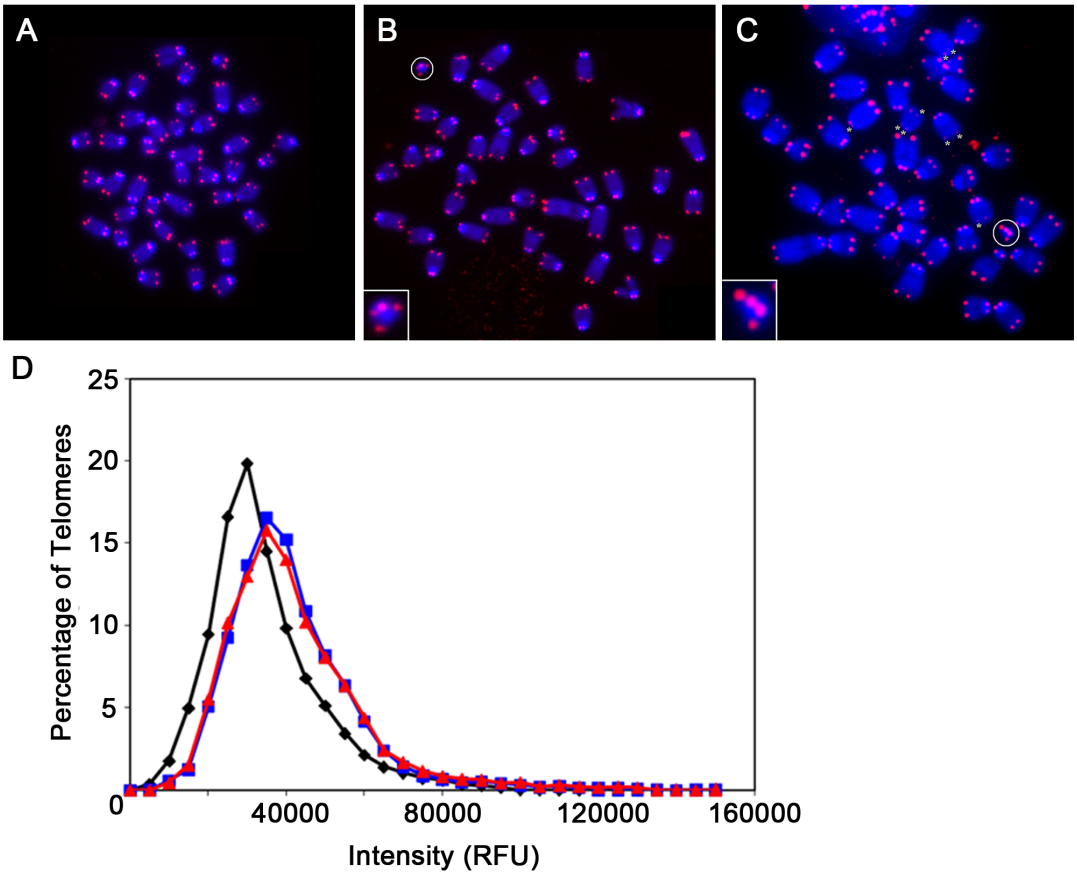

Figure 2-3. 2D Telomere Length in Metaphase Chromosomes of PCT and Wild-type Mice. (A) Metaphase spread from the [T38HxBALB/c]N wild-type mouse. (B) Metaphase spread from the [T38HxBALB/c]N with rcpT(X;11) mouse. The translocation chromosome T(X;11) is circled and enlarged. (C) Metaphase spread from the fast-onset PCT mouse. The translocation chromosome T(X;11) is circled and enlarged. Very short telomeres are marked with an asterisk. (D) Comparison of the telomeric length distribution of the three mouse types. The intensity correlates to the telomere length. The fast-onset PCT nuclei (black) have more very short telomeres and a significantly different telomere profile than the [T38HxBALB/c]N wild-type (red) and the [T38HxBALB/c]N with rcpT(X;11) (blue) mouse ($P < 0.0001$ for both mouse types).

The graphs in Figure 2-4 (A and B) compare the telomere length of translocation chromosome T(X;11) to the telomere length of the rest of the chromosomes for the [T38HxBALB/c]N with rcpT(X;11) (Figure 2-4 A) and fast-onset PCT mice (Figure 2-4 B). In the tumor-free control mouse, [T38HxBALB/c]N with rcpT(X;11), the telomeres of the T(X;11) translocation chromosome do not have a significantly different length from those of the rest of the chromosomes, $P = 0.006$ (as determined by a Kolmogorov-Smirnov test with $P < 0.001$ considered significant). However, in the fast-onset PCT mouse, the telomeres of the T(X;11) translocation chromosome, carrying 11E2, are significantly longer than those of the rest of the chromosomes ($P = 4 \times 10^{-16}$).

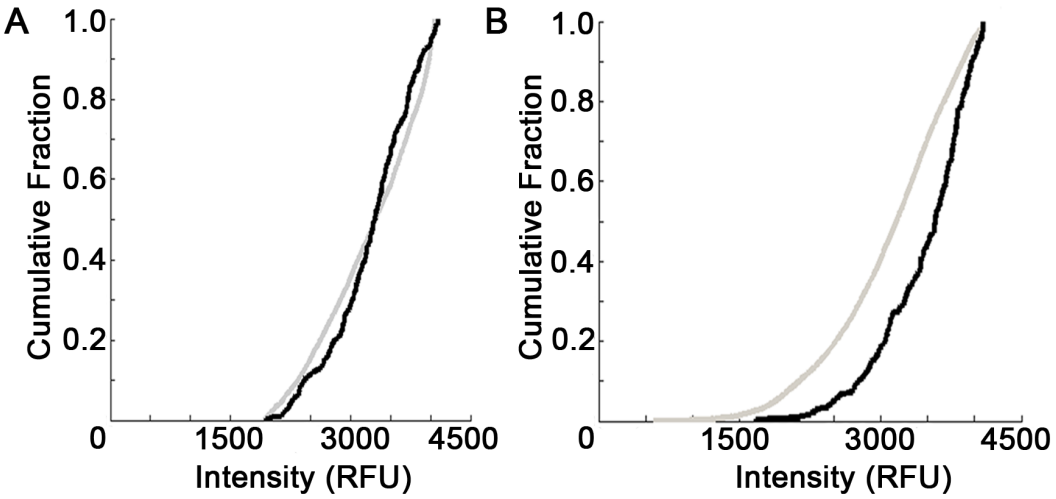

Figure 2-4. Comparison of the Length of the T(X;11) Translocation Chromosome in PCT and Wild-type Mice. (A) In the [T38HxBALB/c]N with rcpT(X;11) mouse, telomeres of the T(X;11) translocation chromosome (black) are not significantly longer than those of the other chromosomes (gray) ($P = 0.006$). (B) In the fast-onset PCT mouse, the telomeres of the T(X;11) translocation chromosome (black) are significantly longer than the other chromosomes (gray) ($P = 4 \times 10^{-16}$).

2.5. Discussion

Although short telomeres are a common finding in many tumor cells, 3D telomere organization and telomere length have not been previously examined in mouse PCT. Our mouse model offers a unique opportunity to study chromosome-specific telomere length regulation because its rcpT places only the genes necessary for accelerated tumorigenesis on a single easily identifiable chromosome, the T(X:11) translocation chromosome (402). Because we also studied control wild-type mice, with and without the rcpT(X;11) translocation, we are able to make conclusions about tumor-specific telomere changes.

Inbred mice can pose a problem for telomere studies because they normally have long telomeres (540, 541). When comparing generations of telomerase knockout mice, significant decreases in telomere size were not seen until generation six (537). However, we present similar results regarding significant alterations in telomere length within the identical mouse strain/generation. Using two complementary approaches, 2D and 3D telomere Q-FISH, we identified significant telomere length changes during PCT development. With a 3D interphase nuclei study, features of every cell can be analyzed, whereas only metaphases can be examined in a 2D study. Also, multiple telomeres parameters in addition to telomere length can be measured with 3D compared to 2D telomere FISH. Therefore, a 3D analysis is more exact and provides more information, and although it is complemented by the results of a 2D study, it cannot be replaced by solely a 2D analysis.

We found that the 3D interphase nuclei of fast-onset PCT mice had visibly and significantly shorter telomeres compared with the slow-onset PCT and wild-type mice, with or without the rcpT(X;11) translocation ($P < 0.0001$; Figure 2-2). There was a significant difference in the distribution of telomere lengths between the fast- and slow-onset PCTs ($P < 0.01$), and between the PCT and wild-type mice ($P < 0.0001$ for both comparisons). PCT mice had a significantly greater number of telomeres and telomeric aggregates per cell, and percentage of cells with aggregates ($P < 0.0001$). Telomeric aggregates have been found in greater numbers in tumor cells and also in increasing number with tumor progression (254, 260, 262). We also determined that there were more short telomeres on the metaphase chromosomes of fast-onset PCT mice than wild-type mice, with a significantly difference in their telomere length distribution ($P < 0.0001$ for both wild-type mice; Figure 2-3). By examining the telomeres of the T(X;11) translocation chromosome compared with all other telomeres, we identified that T(X;11) telomeres were significantly longer than telomeres on all other chromosomes in the fast-onset PCT cells ($P = 4$ x 10-16), but this finding was not illustrated in the wild-type mice with rcpT(X;11) ($P = 0.006$; Figure 2-4).

It is now apparent that gene expression depends on more than the underlying DNA sequence. Therefore, it is important to study the nuclear architecture of cells, such as telomeres, because this may lead to new diagnostic and treatment options. Multiple studies have identified changes in the 3D telomere organization in disease states (186, 207, 250, 254, 257, 543). For example, MDS and AML are part of the same disease spectrum because some cases of MDS will transform into AML, but they have unique

telomere profiles (260). Unique 3D telomeric signatures have been identified for normal versus tumor cells, which can aid in the diagnosis of patients (207).

Our findings in fast-onset mouse PCTs identify a tumor for which there is a unique 3D telomere profile compared with control cells (Figure 2-2 E). More short telomeres were observed in the fast-onset PCT mouse compared with the control mice. This is consistent with our mouse model because a fast-developing tumor, with 45 days of latency period, exhibits a high rate of cell division and consequently displays enhanced telomere shortening, as we observed in this study. Also the *a/c* ratio was highest in fast-onset PCTs, indicating more cells at the G2/M boundary and therefore an overall higher level of cell proliferation.

Telomerase and alternative lengthening of telomeres, the mechanisms by which tumor cells lengthen telomeres to avoid cell senescence from critically short telomeres, are well described. However, chromosome-specific telomere alterations are not as well understood. In 2009, Samassekou *et al*. identified chromosome arms in CML that consistently had longer telomeres (18p, Xp, 1p, and 14p) and ones that consistently had shorter telomeres (20q, 21p, 21q, and 9q) than the rest of the chromosomes (247). In their most recent study, Samassekou *et al*. found that Xp and 5p had significantly longer telomeres at a higher frequency in CML than in healthy cells (249). They propose that the presence of only one X chromosome may drive the cell to protect it from telomere shortening. They also suggest that because the gene encoding the reverse transcriptase component of telomerase is located on 5p, the cell may lengthen its telomeres to regulate

the gene. These findings have led them to propose that tumor cells may protect key genes responsible for their tumorigenesis through a chromosome-specific telomere lengthening mechanism.

Our study supports this hypothesis and goes one step further to prove its potential validity. In fast-onset PCTs, the T(X;11) translocation chromosome contains all the genes necessary for the tumor's accelerated development in cytoband 11E2 (402), and the trisomy of 11E2 represents the only aberration; therefore, it is probably the most important chromosome to protect. Our findings indicate that the T(X;11) translocation chromosome has significantly longer telomeres than all other chromosomes in the fast-onset PCT cells but not in B cells of the tumor-free [T38HxBALB/c]N mice with rcpT (X:11). Therefore, these findings illustrate a chromosome-specific protective mechanism and suggest a functional tumor-dependent requirement for this selective protection. A deeper understanding of the mechanism behind telomere-specific protection is needed. The multiple possibilities include: maintenance of a specific telomere length while all others are shortened; lengthening of a specific telomere after all telomeres were initially shortened; or lengthening of a specific telomere without change in the length of other telomeres. Whether the selective-protection functions via special binding of shelterin proteins or a chromosome-specific ALT or telomerase mechanism, is also not known.

Mouse PCT is cytogenetically identical to human Burkitt lymphoma and therefore is an excellent mouse model of the cancer. The genes within mouse chromosome 11E2 are syntenic to rat chromosome 10q32 (544) and human chromosome 17q25 (545). This

region is duplicated, translocated and amplified in many lymphoid and non-lymphoid tumor types such as human AML, neuroblastoma, breast, ovarian, and thyroid cancers (424, 545-548). Therefore, the chromosome-specific telomere length increase observed on translocation chromosome T(X;11) in fast-onset mouse PCT may also occur on the human chromosome 17 due to the functional relevance of 17q25 for tumor development and warrants further investigation in an independent study.

To examine whether telomere dysfunction has an important role in mouse PCT, we used the techniques of 2D and 3D telomere Q-FISH to study the tumorigenic changes associated with mouse PCT in interphase telomere organization and metaphase telomere length. We found selective telomere lengthening and aberrant 3D telomere organization in the fast-onset PCTs. Therefore, we provide significant support for a chromosome-specific protective mechanism that has a functional tumor-dependent requirement for its selective protection.

2.6. Acknowledgements

The authors thank Ludger Klewes for his assistance with mouse cell harvest and Mary Cheang for her assistance with statistical analysis.

Prologue to Chapter 3 and 4

After examining the 3D nuclear chromosome territory and telomere organization in a mouse PCT model, we wanted to continue studying nuclear disorganization but in a human cancer context. We choose to use human neuroblastoma for multiple reasons. Firstly, we had access to neuroblastoma patient samples at our home institution and there was potential to obtain a neuroblastoma tumor microarray from COG. We also had access to multiple neuroblastoma cell lines for mechanistic studies. Secondly, both PCT and neuroblastoma have clear aggressive and non-aggressive forms: fast- and slow-onset PCT, and *MYCN* amplified and non-amplified neuroblastoma. Therefore our goal of determining differences in nuclear organization between aggressive and non-aggressive forms of a cancer could be carried forward from our mouse model to the human context.

Lastly, there are multiple similarities in the pathogenesis of PCT and neuroblastoma. First of all, both tumors have additional copies of the same chromosome region. The sole aberration in fast- compared to slow-onset PCT is the duplication of cytoband 11E2. The human syntenic region to mouse cytoband 11E2 is 17q25; cytoband 17q25 is found on chromosome arm 17q, which is the most frequent chromosome aberration in neuroblastoma and an independent predictor of poor prognosis. Secondly, both cancers have deregulation of the *MYC* family of oncogenes: MYC in PCT and MYCN in neuroblastoma.

Our studies of 3D chromosome and telomere organization in neuroblastoma are described in Chapters 3 and 4, respectively.

Chapter 3:

MYCN Overexpression is Associated with Unbalanced Copy Number Gain, Altered Nuclear Location and Overexpression of Chromosome Arm 17q Genes in Neuroblastoma Tumors and Cell Lines

This chapter was published in:

Kuzyk A[1], Booth S[1], Righolt C[1], Mathur S[1], Gartner J[2] and Mai S[1]. (2015). MYCN overexpression is associated with unbalanced copy number gain, altered nuclear location and overexpression of chromosome arm 17q genes in neuroblastoma tumors and cell lines. *Genes Chr Cancer.* **54**(10): 616 – 628.

[1]Manitoba Institute of Cell Biology, Department of Biochemistry and Medical Genetics, The University of Manitoba, CancerCare Manitoba, Winnipeg, Manitoba, Canada

[2]Deparment of Pathology, The University of Manitoba, Health Sciences Centre, Winnipeg, Manitoba, Canada

Running Title: MYCN and chromosome arm 17q gain in neuroblastoma

Key Words: MYCN, neuroblastoma, chromosome 17, nuclear architecture

Contributions: Alexandra Kuzyk contributed to study design, obtained ethics approval, performed the research, analyzed the data and wrote the manuscript. Samuel Booth

contributed to data analysis by imaging and determining chromosome 17 copy number in half the patient samples. Christiaan Righolt contributed to software design for data analysis. Shubha Mathur contributed to the research by performing multicolor banding (mBANDing) of one cell line. John Gartner provided the patient samples and their clinical characteristics, and critically reviewed the manuscript. Sabine Mai designed the study and critically reviewed the manuscript.

3.1. Abstract

MYCN amplification and MYCN overexpression are poor prognostic factors in neuroblastoma. Tumors with unbalanced chromosome arm 17q gain are often associated with *MYCN* amplification; however, the relationship between chromosome 17 copy number status and MYCN expression is not known. We investigated the relationship between MYCN expression and chromosome 17 copy number, nuclear location, and gene expression. By performing dual-colored FISH on 16 primary neuroblastomas we found that those with unbalanced gain of 17q have high MYCN expression, whereas those with no gain have medium expression and those with numerical gain have low expression ($P < 0.0001$). We also found the nuclear location of 17q correlates with chromosome 17 copy number status: copies in tumors with unbalanced gain and no gain of chromosome 17 occupy a more central location than those in tumors with balanced gain ($P < 0.0001$). We show that a more central nuclear location of 17q coincides with increased expression of genes found within this chromosome arm. To further understand the association between MYCN expression and chromosome 17, we overexpressed MYCN in two low-expressing

MYCN cell lines, SHEP and GIMEN. We found that both cell lines had an unbalanced gain of chromosome 17q, a more central nuclear location of the region and increased expression of the 17q genes. Therefore, this study indicates, for the first time, a functional relationship between MYCN overexpression and the gain of 17q in neuroblastoma.

3.2. Introduction

Neuroblastoma is characterized by both clinical and molecular heterogeneity (436, 549). To determine prognosis and patient management, COG uses a combination of factors, including the age at diagnosis, disease stage, histological grade, ploidy and *MYCN* amplification (447). Because this panel still yields inconsistent results, more reliable prognostic biomarkers are needed. Nuclear organization is important in regulating DNA replication, transcription, and the maintenance of DNA structure. Nuclear disorganization is a feature of cancer cells, including the altered location of chromosomes and parts thereof, and has been proposed as a biomarker for disease classification and progression (49, 254, 260, 262). To our knowledge, nuclear disorganization has not been examined in neuroblastoma.

MYCN amplification occurs in 25 - 30% of neuroblastomas (457) and is a powerful biomarker used to predict poor prognosis and tumor aggressiveness (442, 443). Multiple studies have reported MYCN protein overexpression also as a poor prognostic factor in neuroblastomas (481-484), except one study of solely Stage 3 and 4 single-copy

MYCN tumors that found no significant difference in four-year survival between neuroblastomas with high compared with low MYCN expression (550). Valentijn *et al.* (2012) found a 157-gene signature that predicts poor clinical outcome and is associated with all *MYCN* amplified neuroblastomas, as well as a group of neuroblastomas without *MYCN* amplification but with moderate MYCN immunostaining (485).

The unbalanced gain of 17q is the most frequent chromosome aberration in neuroblastoma (415-417) and is an independent prognostic factor of poor outcome (418, 419, 421, 422). Theissen *et al*. (2014) found that neuroblastomas with numerical gain of chromosome 17 have a better prognosis compared with those with partial or no gain (423), a distinction not made in previous studies (551). Tumors with partial or no gain of chromosome 17 also had very similar gene expression profiles (423). These findings suggest that although neuroblastomas with no gain of chromosome 17 are genetically distinct from those with partial chromosome 17 gain, these types of tumors may share similar oncogene regulation, such as MYCN, resulting in similar gene expression profiles and prognosis. In accordance with this hypothesis, a study by Godfried *et al*. (2002) found that two genes on chromosome arm 17q, *NM23-H1* and *NM23-H2*, were up-regulated after MYCN transfection in the low MYCN-expressing SHEP-2 neuroblastoma cell line (552).

The aim of our study was to determine the relationship between MYCN expression and unbalanced, numerical and no gain of chromosome 17. We also examined whether the nuclear location of the 17q region correlated with 17q copy

number status. We used immunofluorescence quantification and found that neuroblastomas with an unbalanced gain of 17q have high MYCN expression, those with no gain of chromosome 17 have medium expression, and tumors with numerical chromosome 17 gain have low expression. We also found a more central nuclear location of 17q in neuroblastomas with unbalanced gain and no gain of chromosome 17 compared with those tumors with numerical gain of chromosome 17. We showed that altered nuclear location and unbalanced gain of 17q are induced with MYCN overexpression in low MYCN-expressing cell lines, suggesting for the first time, a functional relationship between MYCN and chromosome 17 copy number status in neuroblastoma.

3.3. Materials and Methods

3.3.1. Cell Lines and Patient Samples

Established neuroblastoma cell lines SHEP and GIMEN were a gift to our laboratory from Manfred Schwab (The German Cancer Research Center, Heidelberg, Germany). Cells were cultured in RPMI 1640 with 10% fetal bovine serum, 1% l-glutamine, 1% sodium pyruvate, and 1% penicillin-streptomycin (Life Technologies Inc., Burlington, Ontario, Canada) at 37°C in a humidified atmosphere and 5% CO2. Tissue sections of 16 formalin-fixed paraffin-embedded primary human neuroblastomas and patient-matched lymph nodes, 5 μm in thickness, were obtained from the Health Sciences Centre (Winnipeg, Manitoba, Canada). Tumor areas were identified through examination

of haematoxylin and eosin stained sections. The experimenters were blinded as to the *MYCN* amplification status of the cases, with the key held by the pathologist until after the experiments and measurements were complete. This study was approved by Pathology Access Committee for Tissue (12-0048), Health Science Centre Research Impact committee (2012:187), CancerCare Manitoba Research Resource Impact Committee (92-2012), and Research Ethics Board (H2012:391).

3.3.2. MYCN Transfection of SHEP and GIMEN Neuroblastoma Cell Lines

MYCN pUHD 10-3, a gift to our laboratory from Manfred Schwab, contains the entire *MYCN* coding sequence under the control of an hCMV minimal promoter. For transfection, approximately $6x10^5$ SHEP and $2x10^5$ GIMEN cells were seeded per well in a 6-well plate and grown to near confluence. Twenty-four hours post-seeding, cells were co-transfected with TransIT-X2 (MIR6004, Mirus Bio LLC, Madison, WI) and pmaxGFP (Lonza, Allendale, NJ) in a ratio of reagent:vector DNA of 2:1, as per the company's protocol. Cells were cultured in the absence of serum for the first 12 h. At 15 h post-transfection, the transfection efficiency was 40%, and the cells were sterile sorted by GFP expression. Cells were put back into culture and harvested at 72 h for immunofluorescence, metaphase spreads and 3D nuclei fixation.

3.3.3. Metaphase Spread Preparation and 3D Nucleus Fixation

The cells were harvested from the cultures of SHEP and GIMEN and underwent 2D and 3D fixation to prepare metaphases and nuclei for immunofluorescence and FISH experiments. The 2D chromosome fixation was performed according to our published protocol (553). The 3D nuclei fixation was performed according to the protocol published by Solovei *et al*. (2002) (204).

3.3.4. Immunofluorescence

SHEP and GIMEN cells were cultured on glass coverslips, fixed with 3.7% formaldehyde for 10 min, washed three times in 1 x PBS, permeabilized with 0.2% TritonX-100 for 12 min, and then washed three times in PBS. Blocking was performed for five min in immunofluorescence buffer (PBS plus 1% bovine serum albumin and 2% fetal calf serum) before applying primary antibodies (dilutions described below) and incubating at 4°C overnight. Blocking was performed in immunofluorescence buffer before applying secondary antibodies and incubating at room temperature for one hour, shaking. After washing three times with PBS, the cells were counterstained with DAPI and mounted in Vectashield (Vector Laboratories, Burlington, Ontario, Canada). The antibodies were diluted as follows: MYCN, a gift to our laboratory from Manfred Schwab and is described in Wenzel *et al*. (1991) (554), 1/2000; ASPSCR1 (WH0079058M1, Sigma-Aldrich Canada Co., Oakville, Ontario, Canada) 1/50; FOXK2 (SAB2100846, Sigma-Aldrich Canada Co.) 1/100; TBCD (14867-1-AP, Proteintech Group Inc., Chicago, IL) 1/50; Cy3 goat anti-mouse IgG secondary antibody (A10521, Life Technologies Inc.) 1/1000; Alexa Fluor 488 goat anti-rabbit IgG secondary antibody

(A-11008, Life Technologies Inc.) 1/1000. Neuroblastoma tissue samples were immunofluorescently stained for MYCN, ASPSCR1, FOXK2 and TBCD according to the protocol described by Robertson and Isacke (2011) (555) with the same dilutions described for the cell lines.

The slides were imaged using an AxioImager Z2 microscope (Carl Zeiss, Toronto, Ontario, Canada), an AxioCam HR charge-coupled device (Carl Zeiss) with a 63x/1.4 oil objective lens (Carl Zeiss) and DAPI, Cy3 and FITC filters. Exposure times were kept constant between cell lines and between tissue samples to allow for quantitative immunofluorescence comparison and analysis of protein expression between samples. The acquired images were quantitatively analyzed using Zeiss AxioVision 4.8 software (Carl Zeiss), specifically the "Outline Spline tool", to determine the average signal intensity of the antibodies for at least 30 cells per experimental replicate for the cell lines and at least 100 cells in each tissue sample. After subtracting the background intensity, we used the following ranges to classify MYCN expression in the tissue samples: low = < 2000 relative fluorescence units (RFU), medium = 2000 – 4999 RFU, and high = ≥ 5000 RFU for MYCN. ASPSCR1, FOXK2, and TBCD expression and MYCN expression in the cell lines were categorized as high, medium, or low by visual inspection. Throughout this paper, expression refers to expression of the protein.

3.3.5. 2D and 3D FISH

Metaphases and nuclei from the neuroblastoma cell lines underwent FISH with chromosome band 17q25.3 and 17p11.2 probes (G100160R-8 and G10020G-8, Agilent Technologies Inc., Santa Clara, CA) according to the product instructions. Neuroblastoma tissue samples underwent FISH with the probes as described in the protocol by Chin *et al*. (2003) (556).

Image acquisition was performed as described above using DAPI, Cy3 and FITC filters. For 3D images, 60 - 80 *z*-stacks for cell lines and 40 *z*-stacks for tissue at 200 nm each, with $\Delta x = \Delta y$ = 106 nm and Δz = 200 nm, were acquired. The acquired 3D images were deconvolved using a constrained iterative algorithm (205). The copy number of 17q25.3 and 17p11.2 signals in the neuroblastoma cell line metaphases were determined visually from at least 20 metaphases with non-overlapping chromosomes from three consecutive passages. A modified version of TeloView (203), implemented using the DIPimage toolbox for Matlab (www.diplib.org), was used to analyze the copy number of 17q25.3 and 17p11.2 and the radial distance of each signal in at least 30 non-overlapping intact interphase nuclei from three consecutive passages in neuroblastoma cell lines, or 100 in each tissue sample. The program detected the volume of the 3D nuclei automatically using an isodata threshold (557) and the signals were detected by TeloView as described previously (203). The relative radial position of each signal within its nucleus was determined by an algorithm that calculated the relative radial position as the ratio of two quantities: the distance between the signal and the center of mass of its nucleus to the radius of the nucleus. To perform this computation robustly, the nucleus was first approximated by an ellipsoid (using the moment of inertia tensor) and then

normalized to a sphere. Chromosome 17 copy number status was defined as numerical gain with equal gain of at least one additional copy of 17q25.3 and 17p11.2, as unbalanced gain with additional gained copies of 17q25.3 compared with 17p11.2, and as no gain with no additional copies of 17q25.3 or 17p11.2, relative to genome ploidy.

3.3.6. mBANDing

Metaphases from the SHEP and GIMEN neuroblastoma cell lines underwent mBANDing with chromosome 17 Xcyte mBAND paint (Metasystems Group Inc., Boston, MA) according to the product instructions. The paint labels chromosome 17 with three different fluorochromes: pseudo-colored cyan at the 17p end, magenta for the interstitial region and green at the 17q end (Supplementary Fig. 3-1 A). The slides were imaged with an Axioplan 2 microscope (Carl Zeiss) equipped with a 63x/1.4 oil objective lens (Carl Zeiss), the ISIS-FISH imaging system 5.0 SR 3 (Metasystems Group Inc.), a DAPI filter to detect nuclear staining and DEAC, Cy3, and FITC filters to detect the tri-color mBANDed chromosome 17. At least 20 metaphases with non-overlapping chromosomes from three consecutive passages were evaluated for the structural arrangement of chromosome 17.

3.3.7. Western Blotting

Western blot analysis was conducted on whole cell lysates obtained from approximately $1x10^6$ asynchronously growing SHEP and GIMEN cell lines before and 72

h post-transfection of MYCN. Cells were lysed at 4°C in radioimmunoprecipitation assay buffer containing protease inhibitor. Cell debris was cleared by centrifugation. Lysates were resolved on a 4 - 20% gradient SDS-polyacrylamide gel and transferred to a 0.45 μm polyvinylidene difluoride membrane. Membranes were blocked with 5% nonfat milk for one hour at room temperature and incubated overnight at 4°C with MYCN antibody in a dilution of 1/1000. Membranes were washed in triplicate with tris-buffered saline and 1% Tween 20 at 10 min intervals and incubated at room temperature with secondary antibodies. Membranes were repeatedly washed as described above and incubated with SuperSignal West Dura chemiluminescent substrate (Thermo Fisher Scientific, Rockford, IL) prior to X-ray film exposure.

3.3.8. Statistical Analysis

Statistical analyses were performed using GraphPad's Prism 6 software (La Jolla, CA). The ordinary multiple comparisons Tukey test was used to compare the MYCN expression levels, and nuclear location of 17q25 and 17p11 signals, with chromosome 17 copy number status. For this test, family-wise significance and confidence levels were set at 0.05 and $P < 0.001$ was considered significant. A two-tailed unpaired student *t*-test was performed with the confidence interval set at 95% and $P < 0.001$ considered significant, to compare the nuclear location of 17q25 and 17p11 signals pre and post MYCN-transfection in the SHEP and GIMEN cell lines.

3.4. Results

3.4.1. MYCN Expression in Neuroblastoma Patient Samples

To determine the correlation between MYCN expression level and chromosome 17 copy number status in neuroblastoma, we performed dual-colored FISH for a chromosome band on both the 17q and 17p arm followed by MYCN immunofluorescence on 16 neuroblastoma patient samples and four patient-matched lymph node tissue samples. Lymph node tissue was used as a control for this study because there is no expression of MYCN, or *MYCN* amplification, in adult lymphoid tissues (472). A summary of clinical patient characteristics can be found in Table 3-1.

Table 3-1. Clinical Characteristics of Manitoba Neuroblastoma Patients Samples

Patient #	*MYCN* Amplif-ication Status	Tumor Stage	Age at Diagnosis (Years)	Histologic Grade	5-Year Survival	1p LOH[d]	Unbalan-ced 11qLOH	Ploidy
1	Non-amplified	2B	1	Fav[b]	Alive	Not done	Not done	1.26
2	Non-amplified	1	2	Fav	Alive	Not done	Not done	1.62
3[a]	Non-amplified	1	17 days	Fav	Alive	No	No	1.52
4	Non-amplified	1	5	Fav	Alive	No	No	1.55
5	Non-amplified	1	6	Fav	N/A[c]	Not done	Not done	Unsatis-factory
6[a]	Non-amplified	4	1	Fav	N/A	No	No	1.397
7	Amplified	4	2	Unfav	Alive	Not done	Not done	1.46
8	Amplified	4	1	Unfav	Deceased	Not done	Not done	1
9	Amplified	4	3	Unfav	Deceased	Yes	Yes	1.958
10	Amplified	4	6	Unfav	Deceased	Not done	Not done	Not done
11	Amplified	4	1	Fav	N/A	Not done	Not done	1
12[a]	Non-amplified	4	4	Unfav	Alive	Not done	Not done	2.03
13	Non-amplified	4	2	Unfav	Alive	Not done	Not done	1.24
14	Non-amplified	4	3	Unfav	Deceased	No	Yes	1
15[a]	Non-amplified	4	3	Unfav	N/A	No	Yes	1.127
16	Non-amplified	4	1	Unfav	N/A	No	No	1

[a]Cases in which patient-matched lymph node tissue was available.
[b]Favorable
[c]Case was diagnosed less than 5-years ago
[d]Loss of heterozygosity

Of the stage four neuroblastomas examined, 7/11 (64%) had unbalanced 17q gain and 4/11 (36%) had no gain of chromosome 17. All stage one and two neuroblastomas had numerical chromosome 17 gain. The lymph node tissues had no gain of chromosome 17. *MYCN* amplified neuroblastomas had unbalanced 17q gain, whereas in *MYCN* non-amplified tumors 5/11 (45%) had numerical chromosome 17 gain, 4/11 (36%) had no gain, and 2/11 (18%) had unbalanced gain of 17q. The five-year survival was 100% for neuroblastomas with numerical gain, 75% for those with no gain, and 57% for those with unbalanced gain. An example of neuroblastomas with unbalanced, no gain, and numerical gain of chromosome 17, as determined by FISH, can be seen in Figure 3-1 A – F.

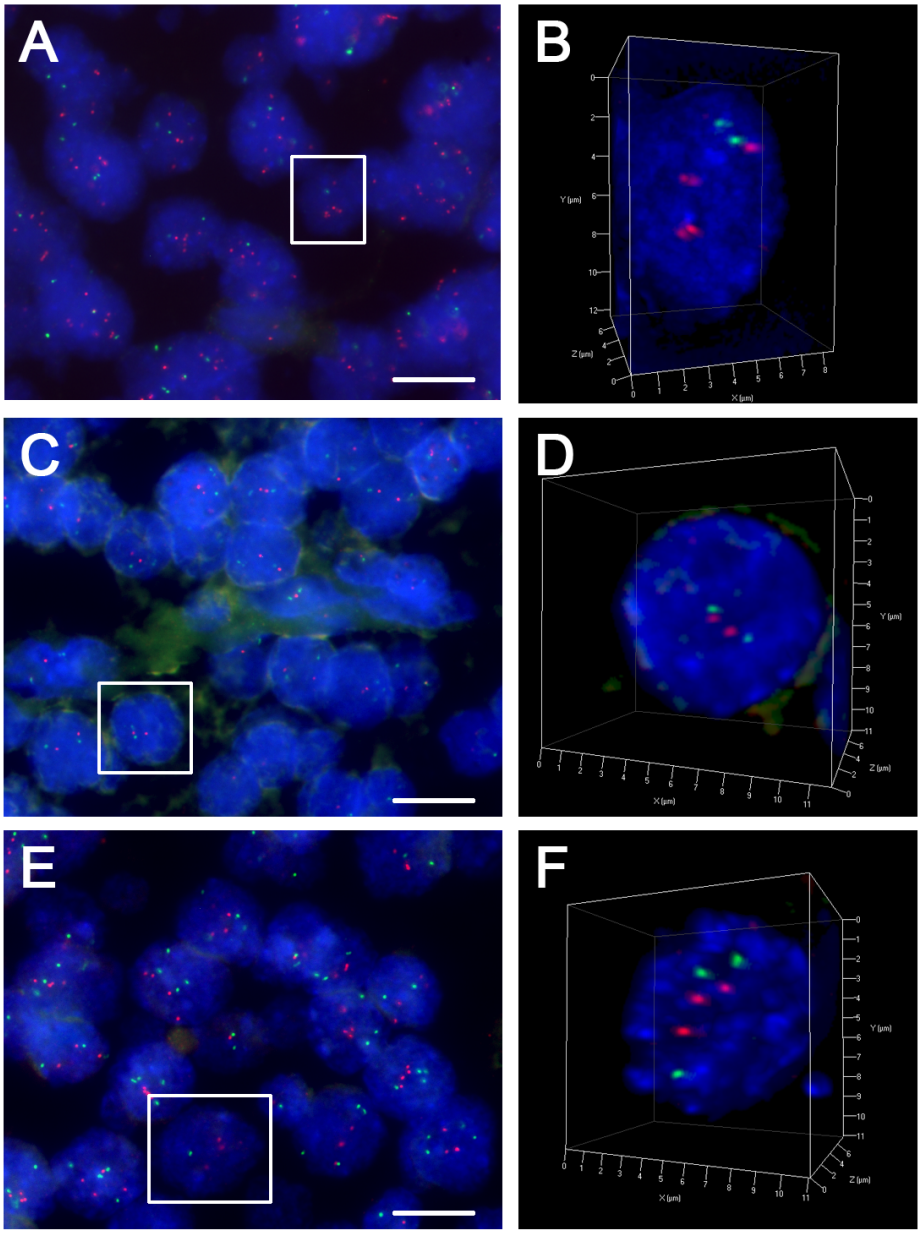

Figure 3-1. 3D Chromosome Band 17q25 and 17p11 FISH in Neuroblastoma Tissue Samples. The nuclei are counterstained with DAPI (blue) with cytoband 17q25 in red and cytoband 17p11 in green. Images of multiple cells in 2D and 3D rendering of individual representative nuclei (outlined in white in the overview) of a neuroblastoma with (A – B) unbalanced gain, (C – D) no gain, and (E – F) numerical gain of chromosome 17. Scale bars represent 5 µm.

Neuroblastomas with unbalanced gain of chromosome 17 had significantly higher MYCN expression, with an average of 6216 RFU (Fig. 3-2 A), compared with those with no gain, with an average of 2673 RFU (Fig. 3-2 B) ($P < 0.0001$). Neuroblastomas with numerical chromosome 17 gain had significantly lower MYCN expression, with an average of 595 RFU (Fig. 3-2 C), compared with both neuroblastomas with unbalanced 17q and no gain ($P < 0.0001$ for both). The lymph node tissues had significantly lower MYCN expression than tumor tissue (Fig. 3-2 D) ($P < 0.001$). A summary of the MYCN expression data in all patient samples can be found in Table 3-2.

Table 3-2. Immunofluorescence of MYCN, ASPSCR1, FOXK2 and TBCD in Neuroblastoma Patient Samples

Patient #	Chromosome 17 Copy Number Status	MYCN Expression Level	Average MYCN Intensity (RFU[b])	ASPSCR1 Expression Level	FOXK2 Expression Level	TBCD Expression Level
1	Numerical gain	Low	227	Low	Low	Low
2	Numerical gain	Low	1164	Low	Low	Low
3	Numerical gain	Low	325	Low	Low	Low
3 LN[a]	No gain	Low	115	Low	Low	Low
4	Numerical gain	Low	1129	Low	Low	Low
5	Numerical gain	Low	132	Low	Low	Low
6	Unbalanced gain	Low	1995	Low	Medium	Low
6 LN	No gain	Low	121	Low	Low	Low
7	Unbalanced gain	High	8758	Medium	High	High
8	Unbalanced gain	High	9277	High	Medium	High
9	Unbalanced gain	High	7390	High	High	High
10	Unbalanced gain	High	7483	High	High	High
11	Unbalanced gain	High	6099	High	High	Medium
12	Unbalanced gain	Medium	2510	Medium	High	Medium
12 LN	No gain	Low	123	Low	Low	Low
13	No gain	Medium	2506	Medium	High	Medium
14	No gain	Medium	3331	Medium	Low	Medium
15	No gain	Medium	2344	Medium	Medium	Medium
15 LN	No gain	Low	101	Low	Low	Low
16	No gain	Medium	2512	Low	Medium	Low

[a]Relative fluorescence units
[b]Lymph node

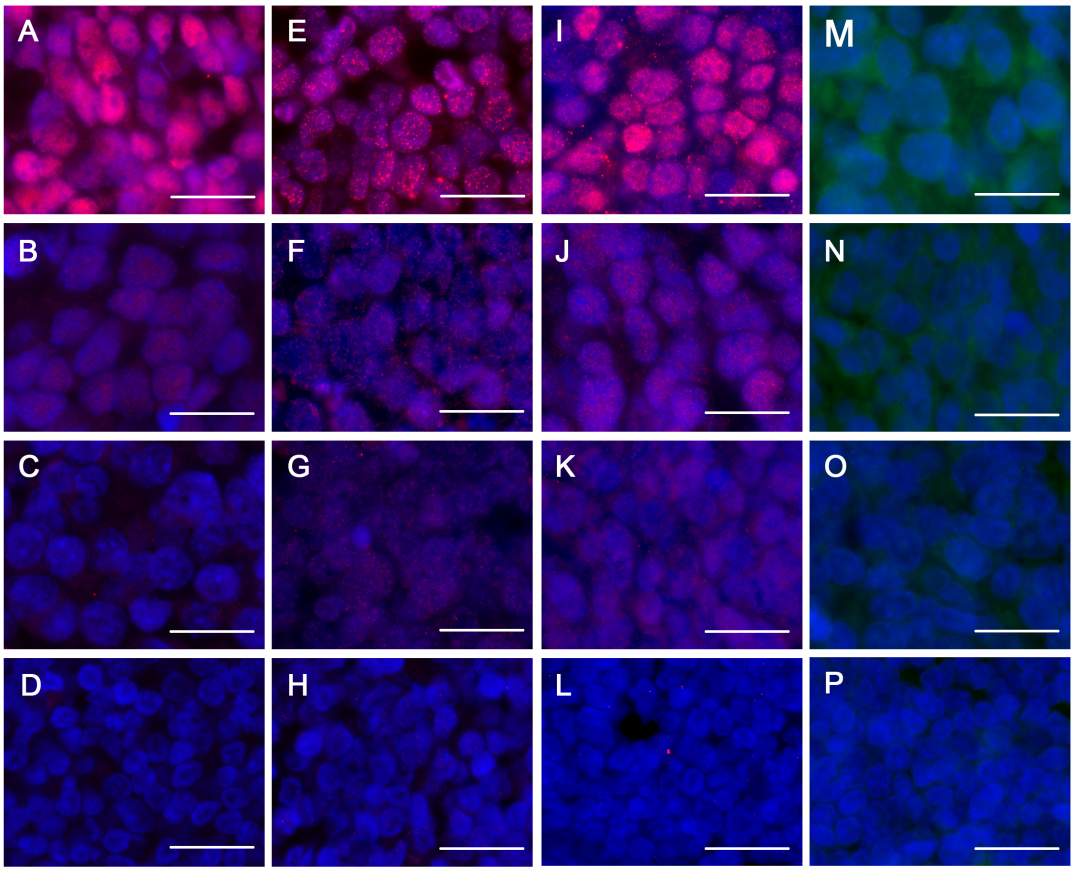

Figure 3-2. Immunofluorescence of MYCN, ASPSCR1, FOXK2 and TBCD in Neuroblastoma Tissue Samples. High, medium, low, and lymph node expression of (A – D) MYCN, (E – H) ASPSCR1, (I – L) FOXK2, and (M – P) TBCD. The nuclei are counterstained with DAPI (blue); the protein expression is red (MYCN, ASPSCR1, FOXK2) or green (TBCD). Exposure times were kept constant between tissue samples. Scale bars represent 10 μm.

We conclude that the 16 patients showed a correlation between MYCN expression and chromosome 17 status: high expression in tumors with unbalanced gain,

medium expression in tumors with no gain, and low expression in tumors with numerical gain. MYCN expression also correlates with tumor stage and five-year survival as neuroblastomas with either unbalanced or no chromosome 17 gain have a high MYCN expression, more advanced stage and poorer five-year survival compared with those with numerical gain of chromosome 17.

3.4.2. Nuclear Location of 17q in Neuroblastoma Patient Samples

To determine the correlation between the nuclear location of chromosome 17 and its copy number status, we used a modified version of TeloView to analyze the neuroblastoma patient samples that had undergone dual-colored 17q/17p FISH. This program determines the distance of each signal from the nuclear center as a percentage of the nuclear radius. A signal in the central shell of the nucleus has a radial distance of < 33.34%; a signal in the middle shell has a radial distance of 33.34 – 66.67%; a signal in the peripheral shell has a radial distance of > 66.67%.

Neuroblastomas with an unbalanced gain of chromosome 17q had an average 17q radial distance of 40.45% (range 2.02 – 99.72%), with the majority of signals found in the central shell of the nucleus (46.13%) (Fig. 3-1 A – B). The average radial distance of 17p was 58.19% (range 8.57 – 99.85%), and the majority of signals were found in the peripheral and middle shells of the nucleus (41.23 and 48.87%, respectively; Table 3-3). This distribution suggests that unbalanced copies of 17q have a more central nuclear location than those found on whole copies of chromosome 17. Neuroblastomas with

numerical gain of chromosome 17 had an average 17q radial distance of 62.59% (range 12.82 – 99.84%), with the majority of signals found in the peripheral shell of the nucleus (48.93%) (Fig. 3-1 E – F). The average radial distance of 17p was 63.64% (range 11.67 – 99.57%), and the majority of signals were also found in the peripheral shell of the nucleus (48.87%: Table 3-3). This distribution suggests that the whole copies of chromosome 17 have a peripheral location in the nucleus. Neuroblastomas with no gain of chromosome 17 had an average 17q radial distance of 43.61% (range 2.39 – 89.95%), with the majority of signals found in the middle shell of the nucleus (55.83%) (Fig. 3-1 C – D). The average radial distance of 17p was 45.14% (range 2.69 – 32.06%), and the majority of signals were also found in the middle shell of the nucleus (51.91%; Table 3-3). This distribution suggests that the majority of the whole copies of chromosome 17 are located in the middle shell of the nucleus. These results demonstrate that the whole copies of chromosome 17 in tumors with no gain have a more central nuclear location than those with numerical gain ($P < 0.0001$). A summary of the radial distances of 17p and 17q in the neuroblastoma patient samples can be found in Table 3-3.

Table 3-3. Results of 17q and 17p FISH in Neuroblastoma Patient Samples

Patient #	Average Radial Distance 17q (%)	Average Radial Distance 17p (%)	Range Radial Distance 17q (%)	Range Radial Distance 17p (%)	17q in Central Shell (%)	17p in Central Shell (%)	17q in Middle Shell (%)	17p in Middle Shell (%)	17q in Peripheral Shell (%)	17p in Peripheral Shell (%)
1	66.88	65.35	20.13 - 99.38	11.67 - 99.57	7.33	8.94	34.03	36.87	58.64	54.19
2	63.7	63.96	19.10 - 99.65	14.68 - 99.30	9.95	8.45	41.86	44.98	48.19	46.58
3	60.51	61.13	18.17 - 99.75	18.86 - 99.61	15.06	13.32	39.1	41.08	45.84	45.6
4	59.71	62.8	18.71 - 99.69	19.01 - 99.67	16.41	10.88	38.67	41.28	44.92	47.84
5	63.22	66.04	12.82 - 99.84	11.84 - 99.95	10.92	7.27	39.32	40.85	49.76	51.88
6	44.65	62.2	2.28 - 98.63	19.85 - 99.28	39.57	1.66	38.58	59.94	21.85	38.4
7	42.02	56.01	3.35 - 99.72	11.58 - 98.62	45.66	8.98	37.17	64.07	17.17	26.95
8	41.01	56.65	3.55 - 95.85	18.16 - 99.85	45.17	5.03	38.07	67.34	16.76	27.64
9	35.51	56.92	2.02 - 89.82	11.45 - 99.74	52.23	5.1	37.17	65.31	10.59	29.59
10	42.26	63.32	2.46 - 97.82	14.08 - 99.04	43.14	4.42	37.48	50.44	19.38	45.13
11	39.19	53.88	3.52 - 98.99	20.18 - 99.83	48.75	5.82	41.5	76.19	9.75	17.99
12	38.06	56.43	3.71 - 98.42	8.57 - 97.60	49.28	5.72	37.96	69.7	12.76	24.58
13	40.74	44.35	2.39 - 89.95	2.69 - 89.61	39.22	37.56	49.51	43.9	11.27	18.54
14	47.05	47.17	6.02 - 87.16	5.60 - 90.96	21.76	25.91	66.84	61.66	11.4	12.44
15	48.83	45.59	3.49 - 88.47	6.80- 88.94	23.53	32	54.9	50	21.57	18
16	37.78	43.45	8.30 - 89.95	4.62 - 89.95	42.35	33.51	52.55	52.13	5.1	14.36

To determine whether the nuclear location of 17q correlated with expression of genes in this chromosome arm, we performed immunofluorescence for ASPSCR1, FOXK2 and TBCD on the neuroblastoma patient samples. A summary of these findings can be found in Table 3-2. Regarding ASPSCR1, 4/7 (57%) of the neuroblastomas with unbalanced gains had high expression, 3/4 (75%) with no gain had medium expression, and 5/5 (100%) with numerical gain had low expression (Fig. 3-2 E – G). Regarding FOXK2, 5/7 (71%) of neuroblastomas with unbalanced gains had high expression, 3/4 (75%) with no gain had medium or high expression, and 5/5 (100%) with numerical gain had low expression (Fig. 3-2 I – K). Regarding TBCD, 4/7 (57%) of neuroblastomas with unbalanced gains had high expression, 3/4 (75%) with no gain had medium expression, and 5/5 (100%) with numerical gain had low expression (Fig. 3-2 M – O).

Neuroblastomas with unbalanced gain of 17q are associated with the highest protein expression of genes found on 17q and the most central nuclear location of 17q

(Fig. 3-1 B). Neuroblastomas with no gain of chromosome 17 have higher expression of these genes than neuroblastomas with numerical gain of chromosome 17. The neuroblastomas with no gain of chromosome 17 have a more central nuclear location of the 17q region than those with numerical gain (Fig. 3-1 D and F). As the nuclear center is associated with greater rates of transcription than the periphery (46, 67, 84, 86, 558), this may explain the higher expression of 17q genes seen in the neuroblastomas with no gain, compared with those with numerical gain of chromosome 17.

3.4.3. Unbalanced Gain of 17q with MYCN Transfection in Neuroblastoma Cell Lines

To determine whether there is a causal relationship between MYCN expression and chromosome 17 copy number status in neuroblastoma, we transfected two low MYCN expressing cell lines with a MYCN expression vector and analyzed the cells for changes in chromosome 17 copy number, nuclear location, and gene expression. Both cell lines were co-transfected with MYCN and GFP vectors. At 15 h post-transfection, the cells were sterile sorted by GFP expression to enrich for a population that over-expressed MYCN. Western blotting confirmed the increased expression of MYCN in both the SHEP and GIMEN cell lines after MYCN transfection (Fig. 3-4 Q). FISH and immunofluorescence experiments were conducted on the sorted cell populations.

The SHEP neuroblastoma cell line has two whole copies of chromosome 17 and partial gain of the 17q21 – qter region through translocation to chromosome 22 (Fig. 3-3 A) (559). The copy number of chromosome 17 was verified by mBANDing, which

reveals two whole copies of chromosome 17 (Supplementary Fig. 3-1 C1 and C2) and one partial copy comprised of the 17q terminal region (Supplementary Fig. 3-1 C3). Seventy-two hours after MYCN transfection and overexpression (Fig. 3-4 E) we found that 8/60 (13%) of metaphases from the SHEP cell line (15/98 (15%) of nuclei) had additional unbalanced gain of chromosome 17q, with four copies of 17q25 and two of 17p11 (Fig. 3-3 C). The GIMEN neuroblastoma cell line has four copies of chromosome 17 (Fig. 3-3 E). The copy number of chromosome 17 was verified by mBANDing, which revealed four partial copies of chromosome 17 comprised of the interstitial and 17q end region (Supplementary Fig. 3-1 E1 – E4) and two partial copies comprised of two copies of the 17p terminal region (Supplementary Fig. 3-1 E5 and E6). We found that 72 h after MYCN transfection and overexpression (Fig. 3-4 M) 55/60 (92%) of metaphases (81/92 (88%) of nuclei) had an unbalanced gain of chromosome 17, with six copies of 17q25 and four of 17p11 (Fig. 3-3 G). These findings suggest that MYCN overexpression can drive an unbalanced gain of chromosome 17.

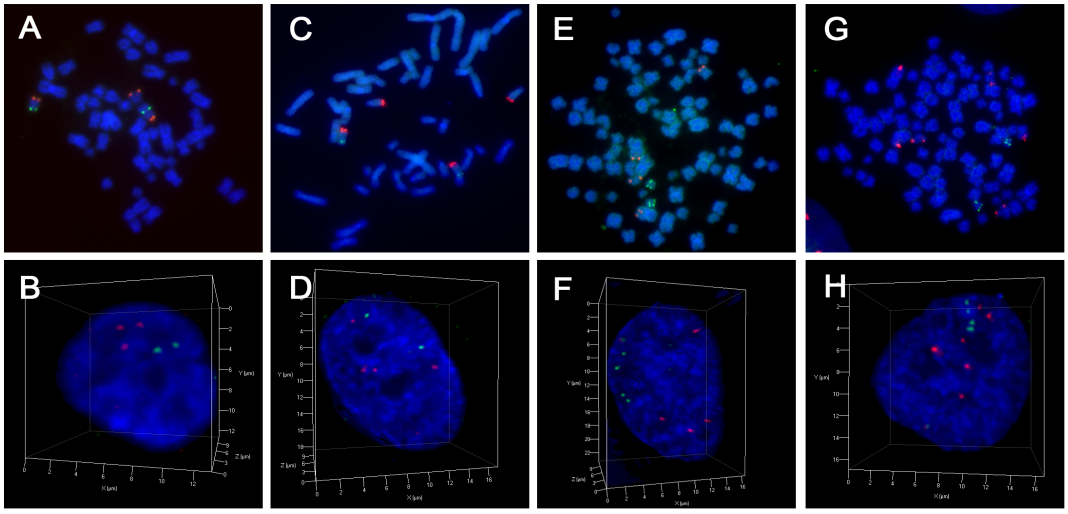

Figure 3-3. Chromosome Band 17q25 and 17p11 FISH in Neuroblastoma Cell Lines. (A – B) Metaphase spread and 3D nucleus of a (A – B) SHEP cell pre-MYCN transfection illustrating three copies of 17q and two copies of 17p (C – D), SHEP cell post-MYCN transfection illustrating four copies of 17q and two copies of 17p (E – F), GIMEN cell pre-MYCN transfection illustrating four copies of each 17q and 17p and (G – H), GIMEN cell post-transfection illustrating six copies of 17q and four of 17p. Cytoband 17q25 is labeled in red and 17p11 in green. The DNA is counterstained with DAPI (blue).

Before MYCN transfection, the SHEP cell line had an average 17q radial distance of 68.46% (range 24.51 – 99.35%), with the majority of signals found in the peripheral shell of the nucleus (50.89%) (Fig. 3-3 B). The average radial distance of 17p was 72.23% (range 31.11 – 99.94%), and the majority of signals were also found in the peripheral shell of the nucleus (63.68%) (Table 3-4). After MYCN transfection, the SHEP cell line had an average 17q radial distance of 49.98% (range 1.55 – 96.94%), with

the majority of signals found in the middle shell of the nucleus (51.68%) (Fig. 3-3 D). The average radial distance of 17p was 59.27% (range 15.54 – 99.97%), and the majority of signals were also found in the middle shell of the nucleus (56.91%) (Table 3-4). Before MYCN transfection, the GIMEN cell line had an average 17q radial distance of 64.16% (range 10.02 – 99.81%), with the majority of signals found in the middle and peripheral shells of the nucleus (45.03 and 46.69%) (Fig. 3-3 F). The average radial distance of 17p was 64.73 % (range 9.79 – 99.16%), and the majority of signals were also found in the peripheral shell of the nucleus (50.42%) (Table 3-4). After MYCN transfection, the GIMEN cell line had an average 17q radial distance of 45.55% (range 1.31 – 99.74%), with the majority of signals found in the central shell of the nucleus (42.44%) (Fig. 3-3 H). The average radial distance of 17p was 56.21% (range 3.99 – 99.24%), and the majority of signals were found in the middle shell of the nucleus (57.62%) (Table 3-4). Overall these results demonstrate that after MYCN transfection, the 17q region had a more central nuclear location than pre-MYCN transfection in both cell lines ($P < 0.0001$ for both). These changes in distribution after transfection suggest that increased expression of MYCN causes movement of the 17q region towards the center of the nucleus. The findings in the GIMEN cell line suggest that it is the unbalanced copies of 17q that move, rather than the whole copies of chromosome 17. A summary of the radial distances of 17p and 17q pre and post-transfection in the SHEP and GIMEN cell lines can be found in Table 3-4.

Table 3-4. Results of 17q and 17p FISH in Neuroblastoma Cell Lines

Cell line	Average Radial Distance 17q (%)	Average Radial Distance 17p (%)	Range Radial Distance 17q (%)	Range Radial Distance 17p (%)	17q in Central Shell (%)	17p in Central Shell (%)	17q in Middle Shell (%)	17p in Middle Shell (%)	17q in Peripheral Shell (%)	17p in Peripheral Shell (%)
SHEP Pre-transfection	68.46	72.23	4.51 - 99.3	1.11 - 99.9	1.78	0.53	47.33	35.79	50.89	63.68
SHEP Post-transfection	49.98	59.27	.55 - 96.9	5.54 - 99.9	25.5	7.18	51.68	56.91	22.82	35.91
GIMEN Pre-transfection	64.16	64.73	0.02 - 99.8	.79 - 99.1	8.29	8.22	45.03	41.36	46.69	50.42
GIMEN Post-transfection	45.55	56.21	.31 - 99.7	.99 - 99.2	42.44	12.5	39.13	57.62	18.43	29.88

With MYCN overexpression in the SHEP cell line the expression of ASPSCR1 (Fig. 3-4 B and F), FOXK2 (Fig. 3-4 C and G) and TBCD (Fig. 3-4 D and H) increased from low to medium. With MYCN overexpression in the GIMEN cell line, ASPSCR1 expression increased from low to medium (Fig. 3-4 J and N), and FOXK2 and TBCD expression increased from low to high (Fig. 3-4 K – P). As discussed above, this may be due to the more central nuclear location of these genes post- compared with pre-transfection.

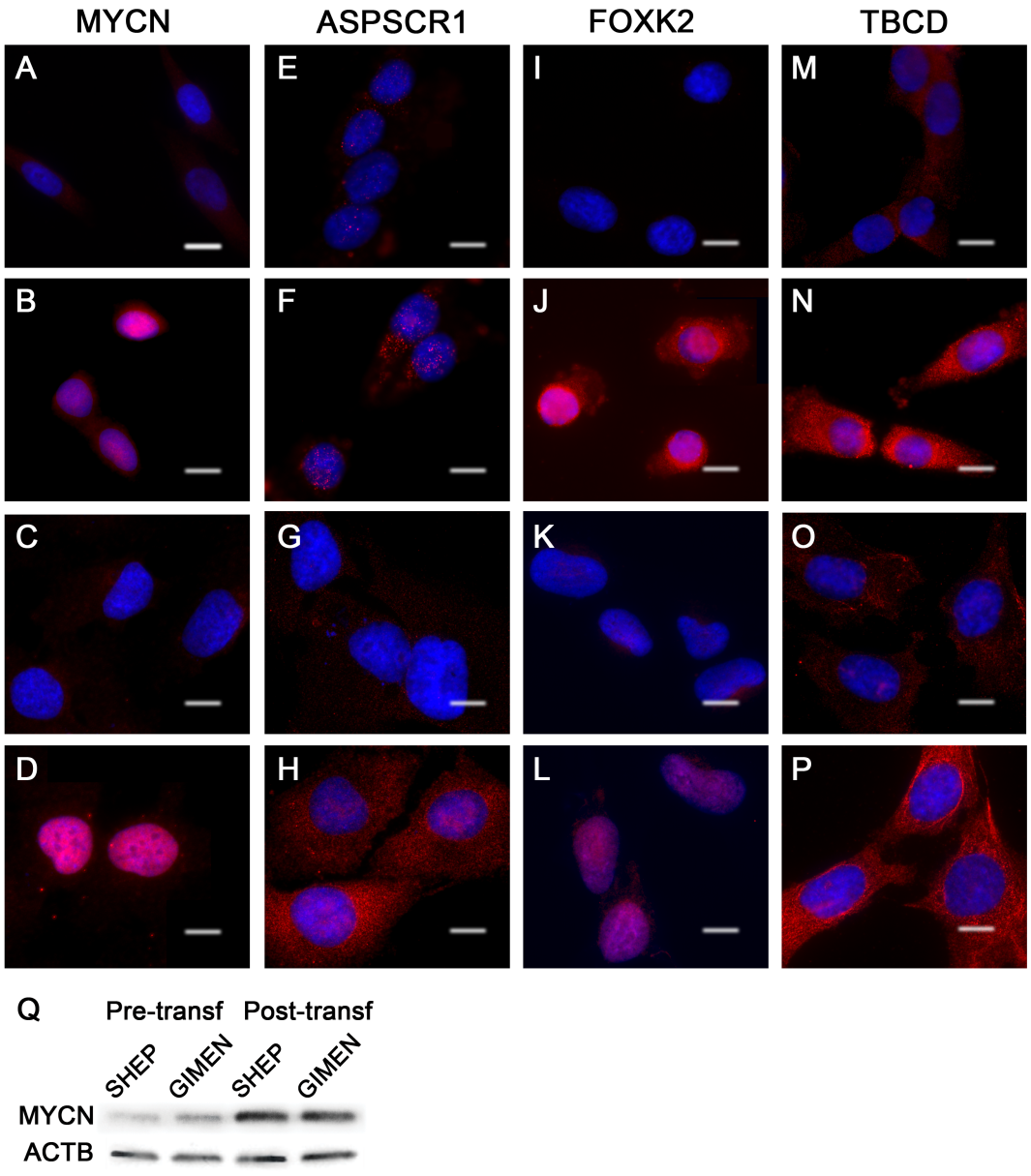

Figure 3-4. MYCN, ASPSCR1, FOXK2 and TBCD Expression in Neuroblastoma Cell Lines Pre- and Post-MYCN Transfection. In horizontal order, expression of MYCN, ASPSCR1, FOXK2, and TBCD in (A – D) SHEP cells pre-MYCN transfection, (E – H) SHEP cells post-MYCN transfection, (I – L) GIMEN cells pre-MYCN transfection, and (M – P) GIMEN cells post-MYCN transfection. (Q) Western blot

analysis confirms the increased expression of MYCN in the SHEP and GIMEN cell lines after MYCN transfection. Scale bars represent 5 μm.

3.5. Discussion

In this study we found a correlation between MYCN expression and the copy number status of chromosome 17 in neuroblastoma. By investigating 16 primary neuroblastomas with dual-colored FISH, we found that neuroblastomas with unbalanced gain of 17q have high MYCN expression, those with no gain of chromosome 17 have medium expression, and neuroblastomas with numerical gain have low expression. We also found that the nuclear location of chromosome 17 correlates with chromosome 17 copy number status. Primary neuroblastomas with unbalanced gain of chromosome 17 have the majority of 17q signals in the central shell of the nucleus, whereas those with no gain have the majority in the middle shell of the nucleus, and those with numerical gain have the majority in the peripheral shell of the nucleus. Using tissue immunofluorescence, we found that expression of genes in the 17q region are highest in neuroblastomas with unbalanced gain, followed by those with no gain of chromosome 17, and tumors with numerical gain have the lowest expression. To gain an understanding of the association between MYCN expression levels and 17q copy number status we overexpressed MYCN in two low-expressing MYCN cell lines, SHEP and GIMEN. We demonstrated that MYCN transfection promotes unbalanced gains of 17q, more central nuclear location of the 17q region, and increased expression of genes in the 17q region.

This finding indicates, for the first time, a functional relationship between MYCN overexpression and the gain of chromosome arm 17q in neuroblastoma.

Unbalanced 17q gain has been found to be more common in the very aggressive *MYCN* amplified neuroblastomas compared with *MYCN* non-amplified tumors (418, 419, 421, 422). Previous studies have, however, been confounded by the fact that numerical versus no gain of chromosome 17 was not distinguished in the non-unbalanced gain patient group; this has led to mixed conclusions as to whether the copy number status of chromosome 17 provides any prognostic value in *MYCN* non-amplified patients. Our findings provide further support for the hypothesis that neuroblastomas with numerical gain of chromosome 17 have a better prognosis compared to those with no gain, initially proposed by Theissen *et al*. (2014) (423). In our study, the majority of neuroblastomas with unbalanced gain of 17q are *MYCN* amplified and have high MYCN expression. Intriguingly, we find that neuroblastomas with no gain of chromosome 17 have a medium level of MYCN expression whereas those with numerical gain have low expression ($P < 0.0001$). We therefore propose that MYCN expression correlates with chromosome 17 copy number status and explains why *MYCN* non-amplified with no gain of 17q neuroblastomas have a poor prognosis similar to neuroblastomas that are *MYCN* amplified with unbalanced gain.

As nuclear organization contributes to tumor pathogenesis (560), and because the nuclear center is often considered more transcriptionally active (67, 84, 86, 558), we investigated whether the nuclear location of 17q varied with chromosome 17 copy

number status and might explain the similarities seen in gene expression between neuroblastomas with unbalanced and no gain of chromosome 17 (423). We found that neuroblastomas with unbalanced and no gain of chromosome 17 had a more central nuclear location of 17q than neuroblastomas with numerical gain ($P < 0.0001$). We also found increased expression of genes in these neuroblastomas compared with those with numerical gain. We propose that MYCN, similar to MYC (46), may drive nuclear repositioning of genes and chromosomes towards the centre of the nucleus. This dynamic behavior may grant genes access to transcriptional machinery leading to their increased expression. As there are significant differences in the nuclear location of 17q depending on the level of MYCN expression and tumor stage ($P < 0.0001$), it may provide additional diagnostic and prognostic value for neuroblastomas.

Due to the correlation between *MYCN* amplification and unbalanced 17q gain, a functional relationship between the two has been previously suggested but not shown. For example, Godfried *et al*. (2002) proposed such a relationship for the genes *NM23-H1* and *NM23-H2* after finding increased copy number of these genes in *MYCN* amplified tumors by two color interphase FISH in tissue samples (552). We further investigated our, and previous groups', correlative findings in neuroblastoma patient samples for a causative mechanism through MYCN overexpression in low MYCN-expressing cell lines. We found that post-MYCN transfection, both SHEP and GIMEN cell lines had unbalanced gains of 17q compared with their chromosome 17 karyotype pre-transfection. We also found that MYCN transfection caused more central nuclear location of the 17q region and increased expression of genes in this region in both cell lines. For the first

time, we show a functional relationship between MYCN and 17q gain in neuroblastoma. In conclusion, we propose that the mechanism for chromosome 17 copy number status in neuroblastomas begins with MYCN expression driving a central nuclear repositioning of the 17q region. This leads to overexpression of genes in this region and subsequent tumor progression. In a subset of neuroblastomas, excessive overexpression of MYCN leads to the unbalanced gain of 17q in addition to its altered nuclear location. This genetic change leads to excessive overexpression of genes in this region and aggressive tumor progression and evolution in these cells.

3.6. Acknowledgements

This work was supported by a CIHR operating grant to Sabine Mai (MOP-123379) and a CIHR studentship to Alexandra Kuzyk.

3.7. Supplementary Figure

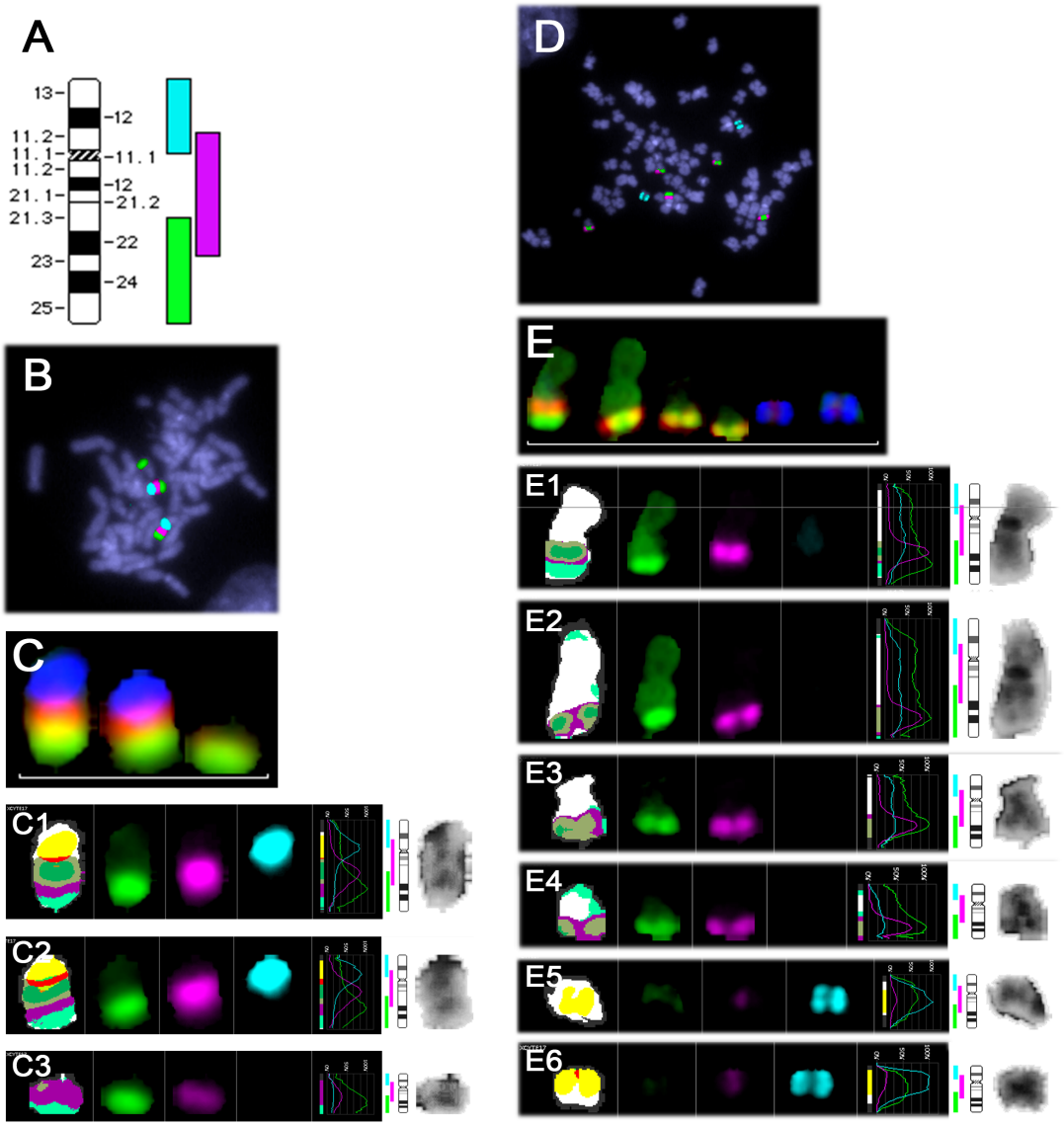

Supplementary Figure 3-1. mBAND of Chromosome 17 in Neuroblastoma Cell Lines. (A) The labeling scheme of the chromosome 17 mBAND probe. The 17p end is pseudo-colored in blue, the interstitial region in magenta, and the 17q end in green. (B) Metaphase spread of the SHEP cell line that has undergone mBAND FISH of chromosome 17. (C) mBAND patterns of chromosome 17 in the SHEP cell line show

two whole copies of chromosome 17 characterized by blue, magenta, and green staining (C1 – C2), and one partial copy of chromosome 17 characterized by green staining corresponding to the 17q terminal region (C3). (D) Metaphase spread of the GIMEN cell line that has undergone mBAND FISH of chromosome 17. (E) mBAND patterns of chromosome 17 in the GIMEN cell line show four partial copies of chromosome 17 characterized by green and magenta staining corresponding to the interstitial and 17q terminal region (E1 – E4), and two partial copies of chromosome 17 characterized by blue staining corresponding to two copies of the 17p terminal region (E5 – E6).

Chapter 4:

Identification of Neuroblastoma Subgroups Based on Three-dimensional Telomere Organization

This chapter is in submission for publication:

Kuzyk A[1], Gartner J[2] and Mai S[1]

[11]Manitoba Institute of Cell Biology/The Research Institute of Oncology and Hematology, Department of Biochemistry and Medical Genetics, Faculty of Health Sciences, University of Manitoba, Winnipeg, Manitoba, Canada

[2]Deparment of Pathology and Immunology, Faculty of Health Sciences, University of Manitoba, Winnipeg, Manitoba, Canada

Running Title: 3D telomere organization in neuroblastoma

Key Words: telomere, neuroblastoma, 3D FISH, nuclear architecture, MYCN

Contributions: Alexandra Kuzyk contributed to study design, obtained ethics approval, applied for the neuroblastoma tumor microarray from COG, performed the research, analyzed the data and wrote the manuscript. John Gartner provided the Manitoba patient samples and their clinical characteristics, and critically reviewed the manuscript. Sabine Mai designed the study and critically reviewed the manuscript.

4.1. Abstract

Using 3D telomere quantitative fluorescence *in situ* hybridization, we determined the 3D telomere organization of 74 neuroblastoma tissue samples. Hierarchical cluster analysis of the measured telomere parameters identified three subgroups from our patient cohort. These subgroups have unique telomere profiles based on telomere length and nuclear architecture. Subgroups with higher levels of telomere dysfunction were comprised of tumors with greater numbers of telomeres, telomeric aggregates and short telomeres ($P < 0.0001$). Tumors with greater telomere dysfunction were associated with unfavorable tumor characteristics (greater age at diagnosis, unfavorable histology, higher stage of disease, *MYCN* amplification and higher MYCN expression) and poor prognostic risk ($P < 0.001$). Subgroups with greater telomere dysfunction also had higher intratumor heterogeneity. MYCN overexpression in two neuroblastoma cell lines with constitutively low MYCN expression induced changes in their telomere profile that were consistent with increased telomere dysfunction; this illustrates a functional relationship between MYCN and 3D telomere organization. This study demonstrates the ability to classify neuroblastomas based on the level of telomere dysfunction, which is a novel approach for this cancer.

4.3. Introduction

Neuroblastoma is the most common extra-cranial malignancy in children. This neoplasm is characterized by both clinical and molecular heterogeneity, and the

prognostic risk calculation is multifactorial. The most important parameters predictive of an unfavorable outcome include *MYCN* amplification (442, 443), MYCN protein overexpression (481, 483), age greater than 18 months at diagnosis (561, 562), loss of chromosome arm 1p (421, 447) and 11q (444) and gain of chromosome arm 17q (418).

Neuroblastomas have been subgrouped according to their pattern of chromosomal instability: whereas some tumors exhibit numerical and few or no structural aberrations, others are dominated by structural rearrangements, including intrachromosomal rearrangements (563, 564). Chromosome instability has been linked to telomere length aberrations in many cancers, including neuroblastoma (451, 564). However, there have been conflicting findings on whether an increase, decrease or unchanging telomere length is associated with a better outcome (451-453). These inconclusive results may be due to the methods employed to measure telomere length, wherein only the average telomere length for each cell was determined.

Nuclear architecture is key to cellular function (66), and changes in nuclear architecture contribute to the pathogenesis and progression of cancer (565). Our laboratory developed a method of analyzing the interphase nuclear organization of telomeres as a novel and more in-depth approach to study telomere length and telomere dysfunction in disease (203). Our method uses 3D Q-FISH to label all telomeres in interphase nuclei while preserving the nuclear architecture of the sample. Our software measures multiple telomere parameters for each cell including the number of telomeres, the length of each telomere, the number of telomeric aggregates, the nuclear volume and

the spatial organization of the telomeres (203, 250). These measurements create a telomere profile unique to an individual sample. Increases in the number of telomeres, telomeric aggregates and short telomeres are frequently associated with tumor compared to non-tumor cells, aggressive forms of disease, and poor patient outcomes (250, 254, 260, 262).

In this study we examined for the first time, the 3D telomere organization in 74 archived neuroblastoma tissue samples. Using hierarchical cluster analysis of the measured telomere parameters, we identified three tumor subgroups representing unique levels of telomere dysfunction. We found that tumors with greater telomere dysfunction were associated with unfavorable tumor characteristics including *MYCN* amplification and higher MYCN expression. To test the hypothesis that high levels of MYCN present in a subgroup of patients (11/74) leads to increased telomere dysfunction, we overexpressed MYCN in two neuroblastoma cell lines with constitutively low MYCN expression. This induced changes in the telomere parameters similar to those seen in high MYCN-expressing neuroblastoma tissue samples, demonstrating a functional relationship between MYCN expression and 3D telomere dysfunction.

4.3. Materials and Methods

4.3.1. Patient Samples

A total of 74 primary neuroblastoma tissue samples, 5 μm in thickness, were obtained from the Health Sciences Centre (Winnipeg, Manitoba, Canada) (n = 16) and Children's Oncology Group (COG) (n = 58). All of the tumor samples were derived from untreated patients. Haematoxylin and eosin stained sections were used to identify tumor areas. The experimenters were blinded to the tumor characteristics and outcome data until after the experiments and measurements were complete. After decoding this information, it was discovered that only 31 out of the 74 patients had clinical follow-up and therefore survival analyses for the whole cohort was not feasible. Available survival information is shown Supplementary Table 4-7.

Patients were classified according to the International Neuroblastoma Staging System (INSS) (458) and divided into clinical-genetic risk groups using the COG risk scoring system (447). The *MYCN* amplification status was determined by FISH for the COG samples. The *MYCN* amplification status of the Manitoban samples were provided to us by the Health Sciences Centre (Winnipeg, Manitoba, Canada). MYCN protein expression was determined for all samples by tissue immunofluorescence. Tumor characteristics of the study cohort are shown in Table 4-1.

Table 4-1 Neuroblastoma Cohort Characteristics

	Cases (n)
Stage	
1	13
2	11
3	8
4	30
4S	11
Unknown	1
Histology	
Favorable	28
Unfavorable	35
Unknown	11
Age at Diagnosis	
<18 months	41
>18 months	33
MYCN Amplification	
No	63
Yes	11
MYCN Expression	
Low	43
Medium	20
High	11
COG Risk Score	
Low	36
Intermediate	8
High	28
Unknown	2

4.3.2. Cell Lines

The established neuroblastoma cell lines SHEP and GIMEN were a gift from Manfred Schwab (The German Cancer Research Center, Heidelberg, Germany). The cells were cultured in RPMI 1640 with 10% fetal bovine serum with 1% l-glutamine, 1% sodium pyruvate, and 1% penicillin-streptomycin (Life Technologies Inc., Burlington, Ontario, Canada) at 37°C in a humidified atmosphere and 5% CO_2.

4.3.3. MYCN Transfection of SHEP and GIMEN Neuroblastoma Cell Lines

SHEP and GIMEN cell lines were transfected with *MYCN* pUHD 10-3, a gift from Manfred Schwab (The German Cancer Research Center, Heidelberg, Germany), which contains the entire *MYCN* coding sequence under the control of an hCMV minimal promoter. Before transfection, $6x10^5$ SHEP and $2x10^5$ GIMEN cells were seeded per well and grown to near confluence. Twenty-four hours post-seeding, cells were co-transfected with TransIT-X2 (MIR6004, Mirus Bio LLC, Madison, WI) and pmaxGFP (Lonza, Allendale, NJ) in a ratio of reagent:vector DNA of 2:1, as per the company's protocol. Cells were cultured in the absence of serum for the first 12 h. The transfection efficiency was 40% at 15 h when the cells were sterile sorted by GFP expression. The sorted transfected cells were put back into culture and harvested at 72 h for 3D nuclei fixation. Mock-transfected cells were used as a control.

4.3.4. 3D Nuclei Fixation

Cells were harvested from the cultures of SHEP and GIMEN and underwent 3D fixation to prepare nuclei for Q-FISH experiments. 3D nuclear fixation was performed according to the protocol published by Solovei *et al*. (2002) (204).

4.3.5. Immunofluorescence

MYCN immunofluorescence, imaging and analysis were performed on the neuroblastoma tissue samples and SHEP and GIMEN cell lines as previously described (566). The MYCN antibody, a gift from Manfred Schwab, is described in Wenzel et al. (1991), and was used at a titre of 1/2000. The slides were imaged using an AxioImager Z2 microscope (Carl Zeiss, Toronto, Ontario, Canada), an AxioCam HR charge-coupled device (Carl Zeiss) with a 63x/1.4 oil objective lens (Carl Zeiss) and DAPI and Cy3 filters (Carl Zeiss). Cy3 exposure times were kept constant between cell lines and between tissue samples. Thirty cells per experimental replicate were analyzed for the cell lines and 100 cells were analyzed in each tumor sample. We used the following ranges to classify MYCN expression: low as < 2000 relative fluorescence units (RFU), medium as 2000 to 4999 RFU, and high as ≥ 5000 RFU.

4.3.6. 3D Telomere Q-FISH

Nuclei from the neuroblastoma cell lines and 5 μm tissue sections underwent 3D telomere Q-FISH with a telomere probe (DAKO, Glostrup, Denmark). The hybridization and image acquisition was performed according to previously published protocols (517, 567). The slides were imaged using an AxioImager Z2 microscope (Carl Zeiss), an AxioCam HR charge-coupled device (Carl Zeiss) with a 63x/1.4 oil objective lens (Carl Zeiss) and DAPI and Cy3 filters for detection of nuclear DNA staining and telomere probe signals, respectively (Carl Zeiss). Cy3 exposure times were kept constant between

cell lines and between tissue samples, and tricolor beads were used to standardize the bulb strength. Eighty *z*-stacks for cell lines and 40 *z*-stacks for tissue at 200 nm each, with $\Delta x=\Delta y$ = 106 nm and Δz = 200 nm, were acquired and then deconvolved using the constrained iterative algorithm (205). Thirty cells per experimental replicate were analyzed for the cell lines and 100 cells were analyzed in each tumor sample.

The 3D interphase telomere signals were quantitatively analyzed with TeloView software (203) to measure the following parameters in each cell: the number of signals, which corresponds to the number of telomeres (203); the intensity of each signal, which correlates with telomere length (202); the number of telomeric aggregates, which are telomeres in close proximity that cannot be resolved as separate entities at an optical resolution of 200 nm (203); the nuclear volume (203); and the *a/c* ratio, which is a measurement of the spherical nature of the telomere distribution (203). From these measurements the following parameters were calculated: the percentage of cells per patient with aggregates, the number of telomeres per nuclear volume, and the mean telomere intensity (253, 256, 260). With these measurements we generated a 3D telomere profile for each cell, and then combined the data from multiple cells to create an overall profile for each tumor sample and each cell line replicate.

4.3.7. Statistical Analysis

Statistical analysis was conducted using SAS 9.3 (SAS Institute Inc., Cary, NC) software. Hierarchical clustering analysis was used to subgroup the neuroblastoma tissue

samples based on the following telomere parameters: number of telomeres per cell, number of telomeric aggregates per cell, percentage of cells per patient with aggregates, number of telomeres per nuclear volume and *a/c* ratio. To visualize the results of the clustering analysis, a hierarchical tree plot was generated (Supplementary Fig. 4-1). Canonical discriminant analysis was also performed to generate a plot of canonical variable (can) 1 vs. can2. Can1 is a calculated value for each tumor sample based on a linear combination of the clustering variables that has the highest correlation with the clusters. Can2 is the second linear combination of the clustering variables uncorrelated with can1 but also showing correlation with the clusters.

The nested factorial analysis of variance (ANOVA) with Tukey multiple comparisons test was used to compare the telomere parameters between the subgroups. The Chi-square test was employed to compare tumor characteristics amongst the subgroups. Telomere signal intensities were binned at intervals of 1000 and divided into three groups formed by the 25^{th} and 75^{th} percentiles. In tumor samples, telomeres were defined as short with an RFU less than 6000, medium-length with and RFU between 6000 and 11999 and long with an RFU greater than or equal to 12000. In cell lines, telomeres were defined as short with an RFU less than 7000, medium-length with and RFU between 7000 and 16999 and long with an RFU greater than or equal to 17000. The Chi-square test was used to compare the distribution of short, medium and long telomeres. The unpaired t-test was used to compare the telomere parameters of the cell lines after MYCN- and mock-transfection. $P < 0.05$ was considered significant.

4.4. Results

4.4.1. 3D Telomere Organization Identifies Neuroblastoma Subgroups

We investigated the 3D telomere organization in 74 neuroblastoma tissue samples using 3D telomere Q-FISH while blinded to tumor characteristics. After image acquisition and deconvolution (205), 100 nuclear segments from each tumor were analyzed with TeloView software (203) to determine the telomere profile associated with that sample (see Materials and Methods). Hierarchical cluster analysis was used to stratify the study cohort into subgroups based on the 3D telomere parameters.

Cluster analysis revealed three unique subgroups, shown graphically in Figure 4-1 A. The number of neuroblastomas in each subgroup was as follows: 23 in Subgroup I (red), 18 in Subgroup II (blue), and 33 in Subgroup III (green). A tissue overview as well as a nucleus illustrating the telomere hybridization from a representative sample in each of the subgroups is shown in Figure 4-1 B – G. The scatterplot in Figure 4-1 H illustrates the distribution of telomere lengths in each subgroup, with a plot of the number of telomeres found at each relative fluorescence intensity interval measured.

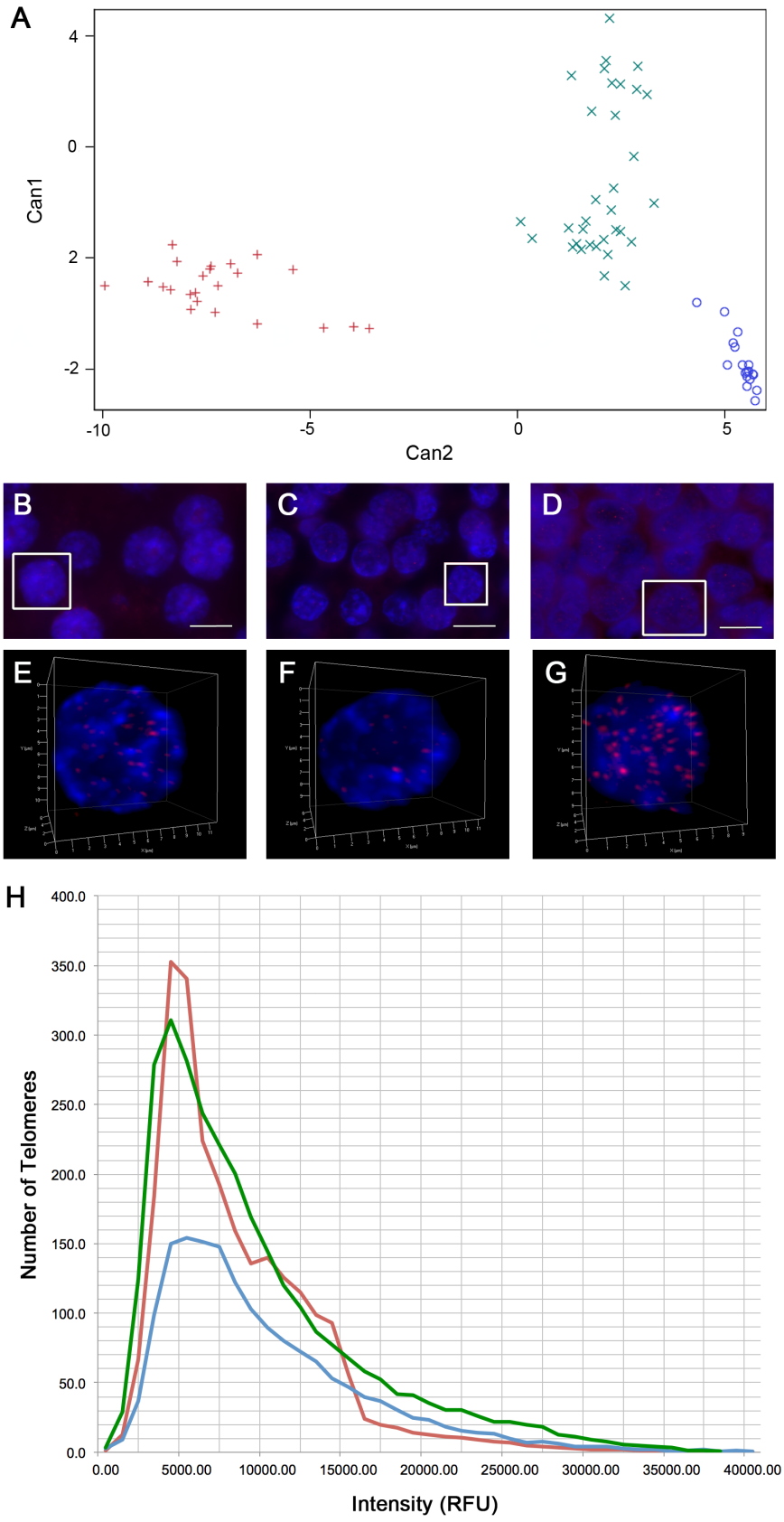
A
4
0
-2
Can1
-10
-5
0
5
Can2
B
C
D
E
F
G
H
400.0
350.0
300.0
250.0
200.0
150.0
100.0
50.0
0.0
Number of Telomeres
0.00
5000.00
10000.00
15000.00
20000.00
25000.00
30000.00
35000.00
40000.00
Intensity (RFU)

Figure 4-1. 3D Telomere Organization of Neuroblastoma Subgroups. Hierarchical cluster analysis based on the measured telomere parameters of the 74 neuroblastoma tissue samples in our study cohort revealed three unique subgroups. Subgroup I (red), Subgroup II (blue) and Subgroup III (green) are illustrated in a graphical representation (A). 3D telomere Q-FISH of the tumors labels all telomeres (red) in the nuclei, counterstained with DAPI (blue). Images of multiple cells in 2D, and 3D renderings of individual representative nuclei (outlined in white in the overview) are illustrated for a neuroblastoma in Subgroup I (B & E), Subgroup II (C & F) and Subgroup III (D & G). Scale bars represent 10 μm. The distribution of telomere lengths in each subgroup are illustrated in a scatterplot (H) of the number of telomeres found at each relative fluorescence intensity interval measured.

Chi-square analysis revealed a significantly different distribution of telomere lengths between the subgroups ($P < 0.0001$). As shown in Table 4-2, there was also a significant difference in the percentage of short, medium and long telomeres per cell ($P < 0.001$ for all comparisons). Subgroups I and III are comprised of neuroblastomas with the greatest percentage of short telomeres per cell (38.7% and 35.9%). Subgroup II contains tumors with the highest percentage of medium-length telomeres (42.92%). Tumors with the highest percentage of long telomeres per cell are found in Subgroup III (31.9%). These findings illustrate that Subgroup III, which has a high percentage of both short and long telomeres, has the most telomere length heterogeneity.

Table 4-2 Statistical Analysis of Telomere Parameters by Neuroblastoma Subgroup

	Subgroup I	Subgroup II	Subgroup III	*P*-value between subgroups[a]
Average number of telomeres per nuclear segment (SD[b])	24.6[c] (3.4)	16.1 (2.3)	29.5 (6.2)	<0.0001
Average number of telomeric aggregates per nuclear segment (SD)	1.1 (0.1)	1.9 (0.1)	3.4 (1.0)	<0.0001
Average percentage of cells per patient with telomeric aggregates (SD, %)	42.4 (6.9)	99.5 (0.7)	90.3 (5.2)	<0.0001
Average nuclear volume (SD, μm^3)	351.30 (71.20)	335.78 (76.76)	318.03 (85.55)	ns[d]
Average number of telomeres per nuclear volume (SD)	0.072 (0.013)	0.060 (0.017)	0.092 (0.029)	<0.0001
Average *a/c r*atio per cell (SD)	2.57 (0.64)	2.18 (0.56)	3.81 (0.87)	<0.0001
Average mean telomere intensity per patient (SD, RFU)	8833.0 (341.7)	10322.6 (649.1)	10118.3 (472.3)	<0.0001
Average percentage of short telomeres per cell (SD, %)	38.7 (4.8)	31.0 (4.9)	35.9 (7.3)	<0.001
Average percentage of medium telomeres per cell (SD, %)	40.0 (3.5)	42.9 (2.7)	32.2 (4.1)	<0.0001
Average percentage of long telomeres per cell (SD, %)	21.4 (2.7)	26.4 (4.3)	31.9 (4.7)	<0.0001

[a] *P*-value determined by one-way ANOVA
[b] Standard deviation
[c] Data range indicated in Supplementary Table 4-6
[d] Not significant

In addition to measuring individual telomere lengths, 3D telomere organization calculates telomere parameters that reflect tumor cell nuclear architecture. Telomeric aggregates are telomeres in close proximity that cannot be resolved as separate entities at a resolution of 200 nm. The subgroups displayed significantly different numbers of telomeric aggregates per cell and percentages of cells per patient with telomeric aggregates ($P < 0.0001$ for both comparisons). Subgroup III was comprised of neuroblastomas with the most telomeric aggregates (3.4), followed by Subgroup II (1.9) and Subgroup I (1.1). The highest percentage of cells with telomeric aggregates was

found in tumors belonging to Subgroup II (99.5%), followed by Subgroup III (90.3%) and Subgroup I (42.4%).

The greatest number of telomeres per cell was observed in the neuroblastomas found in Subgroup III (29.5), followed by Subgroup I (24.6), and Subgroup II (16.1) ($P < 0.0001$). As the nuclear volume is similar for all subgroups, Subgroup III, which has tumors with the most telomeres per cell, exhibits the most dense telomere distribution: the average number of telomeres per nuclear volume is 0.092 for Subgroup III, 0.072 for Subgroup I and 0.060 for Subgroup II. The *a/c* ratio, which measures the spherical nature of the telomere distribution, was also significantly different between the subgroups ($P < 0.0001$). Subgroup III was comprised of tumors with the largest *a/c* ratio (3.81), followed by Subgroup I (2.57), and Subgroup II (2.18).

In summary, the three subgroups contain neuroblastomas with unique telomere profiles based on both telomere length and nuclear organization. The lowest level of telomere dysfunction is seen in Subgroup I, which contains tumors with the fewest telomeric aggregates per nucleus and lowest percentage of cells per patients with telomeric aggregates. Subgroup III illustrates the highest level of telomere dysfunction; it is comprised of tumors with the most telomeres per nucleus, the highest number of telomeric aggregates per nucleus, and a high percentage of short telomeres per cell and cells per patient with telomeric aggregates. A moderate level of telomere dysfunction is seen in Subgroup II, which contains tumors with the least number of telomeres per cell, but has more telomeric aggregates per cell than Subgroup I, and the highest percentage of

cells per patient with telomeric aggregates. Telomere dysfunction has been linked to genomic instability, with higher levels of telomere dysfunction indicating greater genomic instability (186, 560). Therefore, neuroblastomas with the highest level of genomic instability are found Subgroup III, followed by those in Subgroup II, and the tumors in Subgroup I have the lowest level of genomic instability.

Neuroblastomas are known to exhibit intratumor heterogeneity (568), with increasing diversity of telomere length strongly associated with disease progression and mortality (175). Our study supports these findings as we determined that Subgroup III had the greatest standard deviation in all the telomere parameters, except percentage of cells per patient with telomeric aggregates and mean telomere intensity; therefore Subgroup III is comprised of the neuroblastomas with the greatest intratumor heterogeneity. As tumors with the highest level of telomere dysfunction are also found in Subgroup III, our findings illustrate that greater intratumor heterogeneity correlates with higher levels of telomere dysfunction.

4.4.2. Tumor Characteristics in the Neuroblastoma Subgroups

We decoded the neuroblastoma tissue samples to determine the histopathological characteristics of the tumors in each of the three subgroups identified by hierarchical cluster analysis of the 3D telomere parameters. The histology, age at diagnosis, *MYCN* amplification status and MYCN expression level of each sample is summarized in Table

4-3. Chi-square analysis indicated there was an association between the cluster to which a tumor belonged and every tumor characteristic ($P < 0.001$ for all comparisons).

Table 4-3 Histopathological Characteristics and Classification of Neuroblastoma Subgroups

	Subgroup I (n)	Subgroup II (n)	Subgroup III (n)	*P*-value[a]
Histology				
Favorable	13	9	6	0.0005
Unfavorable	4	7	24	
Unknown	6	2	3	
Age at Diagnosis				
<18 months	19	13	9	<0.0001
>18 months	4	5	24	
MYCN Amplification				
No	23	18	22	0.0003
Yes	0	0	11	
MYCN Expression				
Low	23	18	2	<0.0001
Medium	0	0	20	
High	0	0	11	
Stage				
1	9	3	1	
2	7	4	0	
3	2	1	5	<0.0001
4	0	5	25	
4S	5	5	1	
Unknown	0	0	1	
COG Risk Score				
Low	21	13	2	
Intermediate	1	2	5	<0.0001
High	0	3	25	
Unknown	1	0	1	

[a] *P*-value determined by Chi-square test

The majority of neuroblastomas with unfavorable histology and an age of diagnosis of more than 18 months were found in Subgroup III (24/35 and 24/33, respectively), whereas most tumors with favorable histology and an age of diagnosis of less than 18 months were found in Subgroups I and II. All tumors with *MYCN*

amplification and medium or high levels of MYCN expression were found in Subgroup III. Subgroups I and II were comprised of tumors with low MYCN expression and no *MYCN* amplification; however tumors in Subgroup II had a higher average MYCN expression than those in Subgroup I (1281.09 RFU vs. 285.26 RFU, $P < 0.0001$). Our data clearly demonstrates that neuroblastomas with unfavorable histopathological characteristics were found in the subgroups associated with more telomere dysfunction.

Survival analysis of the 31 patients in our cohort with clinical follow-up illustrated that tumors in Subgroup III (green) displayed the largest decrease in survival probability with time, compared to tumors in Subgroup I (red) and Subgroup II (blue) (Supplementary Fig. 4-2); however, this trend was not statistically significant.

4.4.3. 3D Telomere Profiles versus Current Neuroblastoma Classification Systems

After decoding the neuroblastoma cohort, we determined the INSS stage and COG risk score of the tumors in each of the subgroups to gauge their prognosis (summarized in Table 4-3). Chi-square analysis indicated there was an association between the cluster to which a tumor belonged and both INSS stage and COG risk ($P < 0.0001$ for both comparisons).

The majority of neuroblastomas with Stage 1 disease were found in Subgroup I (9/13), which also contained no tumors of Stage 4 disease. Subgroup III was comprised of mainly Stage 4 tumors (25/33). Similar numbers of tumors of all stages were found in

Subgroup II (3 Stage 1, 4 Stage II, 1 Stage 3, 5 Stage 4, 5 Stage 4S). Subgroups I and II were comprised almost solely of low COG risk neuroblastomas (21/23 and 13/18, respectively); however, Subgroup II contained three tumors of high risk. The majority of tumors in Subgroup III were of high COG risk (25/33). Therefore, neuroblastomas of high stage and poor prognostic risk were found in the subgroups with more telomere dysfunction.

4.4.4. Changes in 3D Telomere Organization Following MYCN Transfection in Neuroblastoma Cell Lines

3D telomere profiles that indicated more telomere dysfunction were associated with tumor subgroups with higher MYCN expression. To determine whether there is a functional relationship between MYCN expression and 3D telomere organization, we transfected two neuroblastoma cell lines with constitutive low MYCN expression, SHEP and GIMEN, with a MYCN expression vector. 3D telomere Q-FISH was conducted on transfected cells, and mock-transfected controls, to analyze the nuclei for changes in their telomere profiles. Transfected cells were sorted to ensure that only cells with MYCN overexpression were analyzed (see Materials and Methods). Representative nuclei illustrating the telomere hybridization in the control and MYCN-transfected SHEP and GIMEN cell lines are shown in Figure 4-2 A – D. The scatterplot in Figure 4-2 E illustrates the distribution of telomere lengths from each condition, with a plot of the number of telomeres found at each relative fluorescence intensity interval measured:

SHEP (grey) and GIMEN (black) cell lines after MYCN- (solid lines) and mock- (dashed lines) transfection.

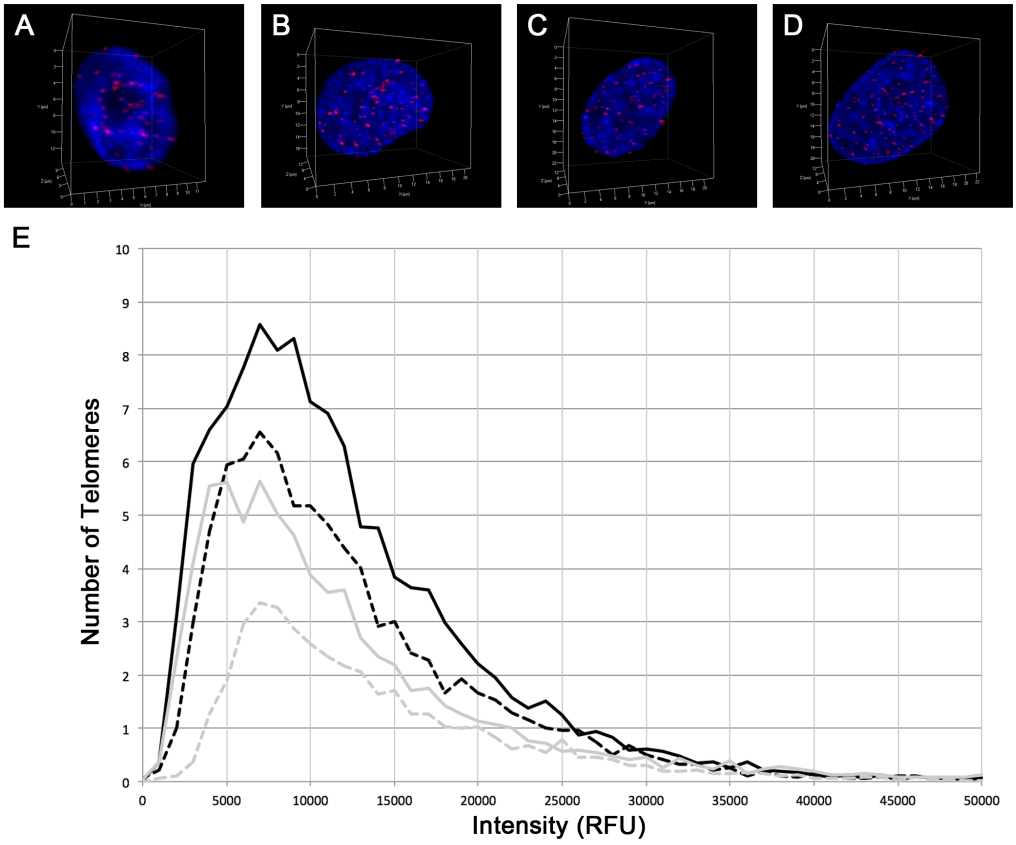

Figure 4-2. 3D Telomere Organization of Neuroblastoma Cell Lines. 3D telomere Q-FISH labels all telomeres (red) in the SHEP neuroblastoma cell line mock- (A) and MYCN-transfection (B) and the GIMEN neuroblastoma cell line mock- (C) and MYCN-transfection (D). Nuclei are counterstained with DAPI (blue). The distribution of telomere lengths for each condition are illustrated in a scatterplot (E) of the number of telomeres found at each relative fluorescence intensity interval measured: SHEP (grey)

and GIMEN (black) cell lines after MYCN- (solid lines) and mock- (dashed lines) transfection.

The average MYCN expression was significantly higher in the post- compared to mock-transfection nuclei for both the SHEP and GIMEN cell lines: 1480.78 vs. 6962.54 RFU in the SHEP cell line ($P < 0.0001$) and 1577.19 vs. 7839.49 RFU in the GIMEN cell line ($P < 0.0001$). As shown in Table 4-4, all telomere parameters were significantly different between the MYCN-transfected and control cells for both cell lines ($P < 0.05$ for all comparisons), except nuclear volume in both cell lines and percentage of long telomeres in the GIMEN cell line. Similar to the results seen in low compared to higher MYCN-expressing tumor samples, increased MYCN expression in the cell lines is associated with an increase in the number of telomeres, number of telomeric aggregates and percent of cells with telomeric aggregates ($P < 0.05$ for all comparisons). For both cell lines there is a significantly different distribution of telomere lengths between the control and MYCN-transfected cells ($P < 0.0001$), with a higher percentage of short telomeres correlated with increased MYCN expression ($P < 0.05$ for both comparisons). An increase in the average number of telomeres per nuclear volume and the *a/c* ratio indicates there is also a different nuclear distribution of the telomeres after MYCN transfection ($P < 0.05$ for all comparisons).

Table 4-4 Statistical Analysis of Telomere Parameters by Neuroblastoma Cell Line

	SHEP control	SHEP MYCN-transfection	GIMEN control	GIMEN MYCN-transfection	*P*-value between SHEP conditions[a]	*P*-value between GIMEN conditions[a]
Average MYCN expression per cell (RFU)	1480.78	6962.54	1577.19	7839.49	<0.0001	<0.0001
Average number of telomeres per nucleus	41.8	74.9	85.7	120.3	<0.0001	<0.01
Average number of aggregates per nucleus	4.9	9.6	10.6	15.1	<0.05	<0.01
Average percentage of cells per replicate with aggregates (%)	71.3	100.0	80.7	100.0	<0.001	<0.01
Average nuclear volume (μm^3)	1053.31	1262.03	1934.85	2225.43	ns[b]	ns
Average number of telomeres per nuclear volume	0.040	0.060	0.044	0.054	<0.05	<0.05
Average *a/c r*atio per cell	3.34	6.34	6.32	11.32	<0.01	<0.05
Average percentage of short telomeres per cell (%)	15.1	30.5	24.7	39.1	<0.001	<0.01
Average percentage of medium telomeres per cell (%)	55.7	47.1	52.2	38.5	<0.05	<0.05
Average percentage of long telomeres per cell (%)	29.3	22.4	23.1	22.4	<0.05	ns

[a] *P*-value determined by unpaired t-test
[b] Not significant

In summary, the increased expression of MYCN in both cell lines following MYCN transfection was associated with altered telomere profiles that indicated increased telomere dysfunction. These findings closely parallel those in the neuroblastoma tissue samples and illustrate a functional relationship between MYCN expression and 3D telomere organization.

4.5. Discussion

Using 3D telomere Q-FISH we determined the telomere profiles of 74 neuroblastoma tissue samples. Statistical hierarchical cluster analysis identified three

patient subgroups based on the measured 3D nuclear telomere parameters. These subgroups had unique levels of telomere dysfunction. We found that tumors with more telomere dysfunction were associated with unfavorable histopathologic characteristics and poor prognosis. Subgroup III, which had the highest level of telomere dysfunction, clearly identified a group of neuroblastomas that are of high risk as the majority are Stage 4, have *MYCN* amplification and high MYCN expression, are greater than 18 months at diagnosis and have unfavorable histology. Although tumors in Subgroups I and II had similar characteristics, Subgroup II had a higher level of telomere dysfunction and may identify neuroblastomas with poorer prognosis; accordingly, Subgroup II contained more tumors of higher stage and COG risk than Subgroup I. Previous studies have also found that telomere profiles can differentiate tumors that are clinically similar. For example, 3D telomere organization identified recurrent compared to non-recurrent Hodgkin's lymphoma patients at diagnosis (256). And previously unknown subgroups of glioblastoma that corresponded with patient survival were discovered using 3D telomere organization (257).

Telomere dysfunction has previously been implicated in neuroblastoma pathogenesis. However, previous studies that determined mean telomere length have been inconclusive as to whether no change, an increase, or a decrease in telomere length is associated with poor patient prognosis (451-453). Our method of 3D telomere analysis determines the length of each individual telomere in addition to mean telomere length. All subgroups had a significantly different distribution of telomere lengths. Interestingly, Subgroups II and III did not have significantly different mean telomere intensities, but

they had unique percentages of short, medium and long telomeres ($P \leq 0.05$ for all comparisons, see Supplementary Tables 4-1 – 4-4). This finding supports using our approach of measuring all individual telomere lengths as it can detect differences that may be overlooked by methods that solely determine mean telomere length.

In addition to measuring telomere length, our method also analyzes the 3D nuclear telomere distribution. The difference in these parameters indicated that each neuroblastoma subgroup had a unique nuclear architecture. The *a/c* ratio measures the spherical nature of the telomere distribution and correlates with the cell cycle (203, 250). A higher ratio indicates more cells at the G2/M boundary; therefore, Subgroup III, which has the largest *a/c* ratio, has the highest level of cellular proliferation. As telomeres shorten with each cell cycle, high rates of proliferation can lead to critically short telomeres (182). Critically short telomeres trigger DNA damage responses and trigger end-to-end fusions of sister chromatids or of different chromosomes (184); subsequently, telomere fusions generate dicentric chromosomes and breakage-fusion-bridge cycles that lead to chromosome rearrangements and ongoing genomic instability (543). Telomeric aggregates can represent telomere fusions (543). Subgroup III also has the highest number of telomeric aggregates.

3D telomere organization reflects genomic reflect genomic stability (186, 560). As the neuroblastoma subgroups had different telomere profiles, they will also have unique levels of genomic instability: subgroups with higher levels of telomere dysfunction will have greater genomic instability. Previously it has been found that

MYCN amplified neuroblastomas have multiple structural chromosome aberrations; however, a subset of high-risk *MYCN* non-amplified tumors harbor more segmental chromosome aberrations including intrachromosomal rearrangements (564) suggesting that these tumors have the most genomic instability. It has also been proposed that these high-risk *MYCN* non-amplified tumors employ the alternative lengthening of telomeres (ALT) mechanism (451), a feature of which is heterogeneous telomere lengths (163). To compare our data with these findings we further examined Subgroup III, which contained tumors with the highest level of genomic instability and highest prognostic risk. We divided Subgroup III into two groups: IIIa, composed of 22 *MYCN* non-amplified tumors, and IIIb, composed of 11 *MYCN* amplified tumors. Subgroup IIIb had tumors with more telomeres and telomeric aggregates per cell than those in IIIa ($P < 0.0001$, see Supplementary Table 4-5); however, the tumors in Subgroup IIIa had more telomeres and telomeric aggregates per cell than both Subgroups I and II. The neuroblastomas in Subgroups IIIa and IIIb also had a significantly different distribution of telomere lengths ($P < 0.0001$); *MYCN* amplified neuroblastomas in IIIb had predominately short telomeres, while *MYCN* non-amplified tumors in IIIa had similar percentages of short, medium-length and long telomeres. Therefore, our results are consistent with the previous findings of a subgroup of high-risk *MYCN* non-amplified neuroblastomas that exhibit a high level of genomic instability and use ALT.

As tissue samples with *MYCN* amplification and higher MYCN expression were associated with more telomere dysfunction, we examined whether MYCN overexpression could reproduce these findings. MYCN transfection in two neuroblastoma cell lines with

constitutive low MYCN expression generated changes in their telomere profiles that were consistent with increased telomere dysfunction. Therefore we suggest that MYCN overexpression in neuroblastoma may cause telomere dysfunction. Previously it has been shown that MYC deregulation alters 3D telomere organization with increases in telomere aberrations and genomic instability (46).

In conclusion, this study demonstrates that 3D telomere organization can be used to subgroup neuroblastomas. Classifying neuroblastomas based on the level of telomere dysfunction is a novel approach for this cancer. Similar to previous studies in acute myeloid leukemia, multiple myeloma, glioblastoma and Hodgkin's lymphoma (254, 257, 260, 262), we found telomere profiles in neuroblastoma to correlate with tumor characteristics and patient prognosis. We propose that 3D telomere organization may be a novel prognostic marker in neuroblastoma and further studies are needed to validate its potential.

4.6. Acknowledgments

The authors would like to thank Mary Cheang for her assistance with statistical analysis. The authors would also like to thank COG for development of the neuroblastoma tumor microarray. This work was supported by CIHR funding received by SM.

4.7. Supplementary Tables

Supplementary Table 4-1 Statistical Analysis of Average Mean Telomere Intensity per Patient[a]

	Subgroup I	Subgroup II	Subgroup III
Subgroup I		≤0.0001	≤0.0001
Subgroup II	≤0.0001		ns[b]
Subgroup III	≤0.0001	ns	

[a]*P*-value determined by one-way ANOVA with Tukey test
[b]Not significant

Supplementary Table 4-2 Statistical Analysis of Percentage of Short Telomeres per Cell[a]

	Subgroup I	Subgroup II	Subgroup III
Subgroup I		≤0.01	ns[b]
Subgroup II	≤0.01		≤0.05
Subgroup III	ns[b]	≤0.05	

[a]*P*-value determined by one-way ANOVA with Tukey test
[b]Not significant

Supplementary Table 4-3 Statistical Analysis of Percentage of Medium Telomeres per Cell[a]

	Subgroup I	Subgroup II	Subgroup III
Subgroup I		≤0.05	≤0.0001
Subgroup II	≤0.05		≤0.0001
Subgroup III	≤0.0001	≤0.0001	

[a]*P*-value determined by one-way ANOVA with Tukey test

Supplementary Table 4-4 Statistical Analysis of Percentage of Long Telomeres per Cell[a]

	Subgroup I	Subgroup II	Subgroup III
Subgroup I		≤0.001	≤0.0001
Subgroup II	≤0.001		≤0.0001
Subgroup III	≤0.0001	≤0.0001	

[a] *P*-value determined by one-way ANOVA with Tukey test

Supplementary Table 4-5 Statistical Analysis of Telomere Parameters in Neuroblastoma Subgroup III

	Subgroup IIIa	Subgroup IIIb	*P*-value between subgroups[a]
Average number of telomeres per nuclear segment	25.8	37.0	<0.0001
Average number of telomeric aggregates per nuclear segment	2.8	4.8	<0.0001
Average percentage of cells per patient with telomeric aggregates (%)	87.9	95.3	<0.0001
Average nuclear volume (μm^3)	302.50	349.10	ns[b]
Average number of telomeres per nuclear volume	0.081	0.114	<0.01
Average *a/c r*atio per cell	3.50	4.43	<0.01
Average mean telomere intensity per patient (RFU)	10158.2	10038.3	ns
Average percentage of short telomeres per cell (%)	32.5	42.5	<0.0001
Average percentage of medium telomeres per cell (%)	33.5	29.8	<0.05
Average percentage of long telomeres per cell (%)	34.0	27.7	<0.0001

[a] *P*-value determined by unpaired t-test
[b] Not significant

Supplementary Table 4-6 Data Range of Telomere Parameters by Neuroblastoma Subgroup

	Subgroup I	Subgroup II	Subgroup III
Average number of telomeres per nuclear segment	15.6 - 29.2	13.7 - 24.6	15.1 - 41.3
Average number of telomeric aggregates per nuclear segment	0.9 - 1.3	1.5 - 2.1	2.2 - 5.3
Average percentage of cells per patient with telomeric aggregates (%)	28.0 - 58.0	98.0 - 100.0	79.0 - 99.0
Average nuclear volume (μm^3)	213.98 - 552.07	227.21 - 499.47	167.07 - 537.50
Average number of telomeres per nuclear volume	0.046 - 0.091	0.034 - 0.095	0.043 - 0.176
Average *a/c r*atio per cell	1.81 - 4.42	1.37 - 3.71	2.55 - 6.61
Average mean telomere intensity per patient (RFU)	8177.9 - 9722.0	9041.8 - 11595.8	8922.5 - 11188.2
Average percentage of short telomeres per cell (%)	30.0 - 47.4	24.9 - 43.4	24.9 - 51.2
Average percentage of medium telomeres per cell (%)	32.0 - 46.7	38.1 - 50.0	21.3 - 39.4
Average percentage of long telomeres per cell (%)	14.2 - 28.7	18.8 - 37.4	18.5 - 40.2

Supplementary Table 4-7 Neuroblastoma Cohort Suvival Data

Patient ID	Number of Follow-up Days	Patient Status at End of Follow-up	Five-year Survival
1	2623	Alive	Yes
3	2780	Alive	Yes
4	582	Alive	Unknown
7	64	Alive	Unknown
11	130	Alive	Unknown
14	132	Alive	Unknown
16	3734	Alive	Yes
17	1334	Alive	Unknown
20	3054	Alive	Yes
21	426	Dead	No
22	1478	Alive	Unknown
23	1786	Alive	Unknown
24	816	Alive	Unknown
25	2813	Alive	Yes
26	566	Dead	No
27	2900	Alive	Yes
28	514	Dead	No
29	61	Dead	No
30	299	Alive	Unknown
31	2947	Alive	Yes
32	1865	Alive	Yes
33	393	Dead	No
35	3906	Alive	Yes
39	64	Alive	Unknown
41	2728	Alive	Yes
42	3137	Alive	Yes
46	2528	Alive	Yes
47	1558	Dead	No
48	1004	Alive	Unknown
61	4136	Alive	Yes
64	232	Alive	Unknown

4.8. Supplementary Figure

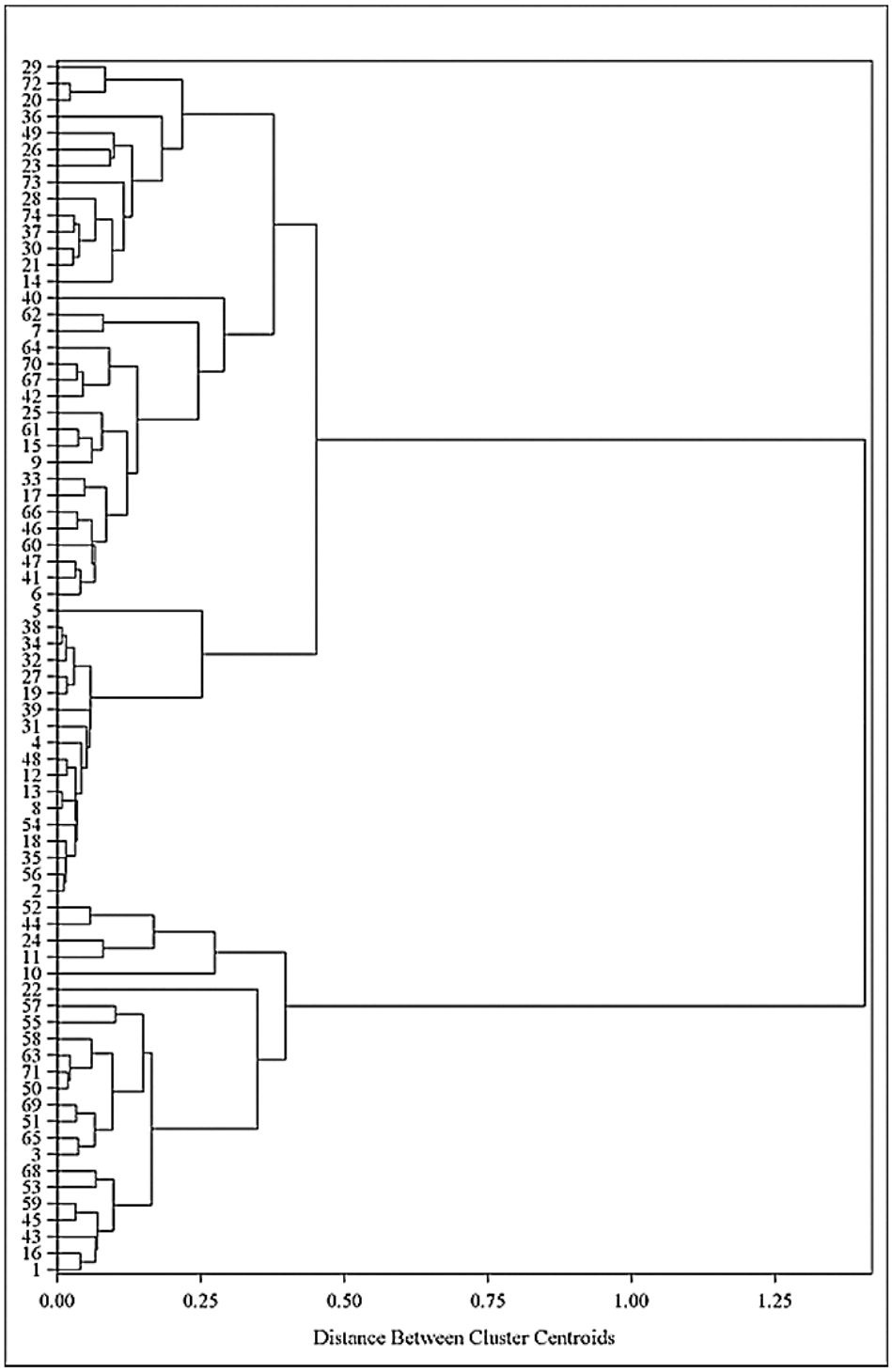

Supplementary Figure 4-1. Dendrogram Illustrating Hierarchical Cluster Analysis of Neuroblastoma Tissue Samples.

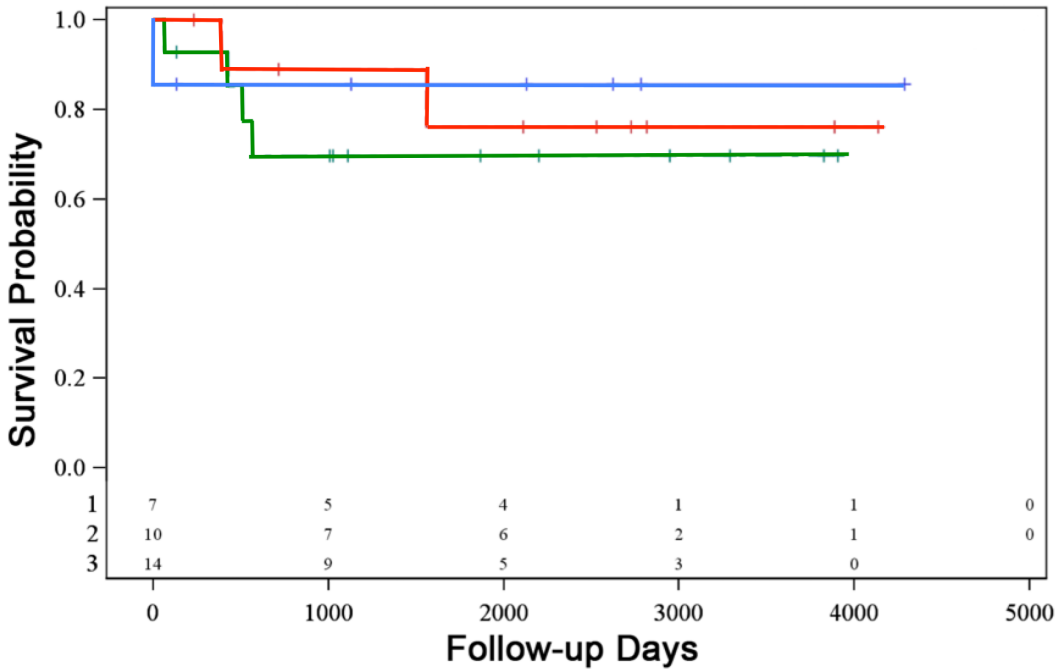

Supplementary Figure 4-2. Survival Analysis Neuroblastoma Tissue Samples. Survival analysis of the 31 patients in our cohort with clinical follow-up illustrated that tumors in Subgroup III (green) displayed the largest decrease in survival probability with time, compared to tumors in Subgroup I (red) and Subgroup II (blue). This trend was not statistically significant.

Chapter 5:

Discussion

5.1. 3D Telomere Organization as a Clinical Tool

A biomarker has been defined as "a characteristic that is objectively measured and evaluated as an indicator of normal biological processes, pathogenic processes, or pharmacologic responses to a therapeutic intervention" (569). A biomarker should also be accurately measurable and reproducible (570). Multiple studies from our lab have proposed 3D telomere organization to be used as a novel biomarker in cancer. In a study of 16 patients with esophageal squamous cell carcinoma, differences in telomere signatures were found between tumor and normal tissue from the same patient, leading to the suggestion of 3D telomere organization as a diagnostic biomarker (571). The identification of subgroups of circulating tumor cells within patients with melanoma, prostate, colon and breast cancer illustrated the potential of 3D telomere organization for diagnosis and staging of these cancers (261). In large patient cohort studies of AML and multiple myeloma, unique telomere profiles were identified for these cancers and their precursor stages, MDS and MGUS, respectively; therefore, 3D telomere organization was proposed as a tool to monitor disease progression (260, 262). 3D telomere organization

could also be used as a prognostic biomarker: a study of 26 patients with Hodgkin's lymphoma revealed the ability of telomere organization to identify patients at diagnosis that would be refractory to treatment or relapse (517); another study of 11 patients with glioblastoma identified unique telomere profiles associated with short, intermediate and long term survival (257). The potential of 3D telomere organization to be used as a biomarker to monitor treatment response is currently being investigated in patients with high risk prostate cancer, to determine whether patients responsive to hormone therapy or radiation therapy have a unique profile compared to those who have progressive disease (Landon Wark, in submission 2016); similar studies are being conducted in intermediate risk prostate cancers to determine if patients responsive and unresponsive to surgery have different telomere profiles (Julius Awe, unpublished results). The work presented in this thesis continues to support the use of telomere profiling as a clinical tool. The ability of 3D telomere organization to detect differences between normal mouse lymphocytes and PCT cells (Chapter 2) may be applicable to diagnosing human Burkitt lymphoma, as mouse PCT is cytogenetically identical to Burkitt lymphoma. Currently there is no single reliable prognostic biomarker in neuroblastoma. The correlation between neuroblastoma subgroups, generated from measured telomere parameters, and multiple histopathologic features of the disease (Chapter 4), suggest 3D telomere organization as a potential prognostic marker in neuroblastoma. One of our subgroups clearly identified a group of high-risk tumors. Although the other two subgroups were comprised of tumors with similar clinical characteristics, we propose that the subgroup with greater telomere dysfunction contains neuroblastomas of higher risk. Current prognostic markers in neuroblastoma may not be able to distinguish tumors in the way that telomere

organization can. Therefore, 3D telomere profiling may be a novel approach for classifying neuroblastomas that provides additional information than currently available prognostic markers.

A unique feature of 3D telomere organization is that unlike most biomarkers, it is not disease specific. Altered telomere organization has been proposed as a biomarker in multiple tumor types. It has also been proposed as a biomarker in diseases other than cancer, such Alzheimer's disease (572). The relevance of 3D telomere organization to multiple diseases is because it reflects the sample's genomic stability, not a disease-specific gene, protein or clinical feature. Greater levels of telomere dysfunction, indicated by high numbers of telomeres, telomeric aggregates and short telomeres, also reflect greater levels of genomic instability. Our findings suggested that a group of neuroblastomas, both *MYCN* amplified and non-amplified but with medium to high levels of MYCN expression, had the highest level of genomic instability (Chapter 4). Previous studies have determined that a subset of *MYCN* non-amplified harbor the most segmental chromosome aberrations (564, 573). To see if our results also supported this conclusion, we split our subset of neuroblastomas with the highest genomic instability into *MYCN* amplified and non-amplified groups, and then compared their 3D telomere organization. Indeed, we found that the *MYCN* non-amplified tumors displayed telomere characteristics that indicated higher genomic instability.

Our study of 3D telomere organization in neuroblastoma also examined intratumor heterogeneity of the measured telomere parameters. Intratumor variation of chromosome number has been previously observed in neuroblastoma (568). A study which determined average telomere length of multiple single cells per neuroblastoma tissue sample, found intratumor variation of average telomere length in 32 out of 105 samples (32/105); they stated this group of tumors had similar histopathologic characteristics as the group with homogenous tumor lengths (175). Although our methods of measuring telomere length and classifying telomeres as short, medium and long are different, our results suggest that there is intratumor heterogeneity in every sample. We also identified greater intratumor variation in tumors with unfavorable histopathological characteristics, and higher levels of telomere dysfunction and genomic instability. Our results are more consistent with previous findings that intratumor heterogeneity increases with genomic instability (574).

The study of telomeres in disease by 3D telomere organization is elaborate compared to other methods such as 2D Q-FISH, STELA, Q-PCR and TRF because it measures multiple telomere parameters on a single-cell basis (203), rather than solely individual or average telomere length. The conflicting results of previous studies of telomere length in neuroblastoma could be because they determined a single average telomere length for each patient sample by either TRF (452, 453, 513) or Q-FISH (451). When examining telomere length with 3D telomere Q-FISH, the length of each telomere is determined and the distribution of telomere lengths is compared between patients. In our study of telomere length in neuroblastoma (Chapter 4), we found two subgroups had

similar mean telomere intensities but unique percentages of short, medium and long telomeres. This finding demonstrates the ability of mean telomere length to overlook differences in telomere length between samples. Therefore our study uses novel methods and is more comprehensive than previous studies of neuroblastoma telomere length.

3D telomere organization is also an advantageous technique because it has been validated in multiple species and cell types. It has been studied in cell lines from multiple species (46, 250, 252, 253, 345) and in mouse cells of various origin (258, 259, 264, 567). It has also been validated in many human cell types: tissue sections from solid tumors (250, 260, 517, 571), bone marrow (260, 262, 263), circulating tumor cells (261), blood cells (262, 263) and buccal cells (572). This provides a promising future for diseases such as neuroblastoma, where 3D telomere organization has shown potential as a biomarker in tissue samples, findings that may be transferable to less invasive diagnostic methods such as CTCs or buccal swabs.

The drawback to studying 3D telomere organization is that the process is semi-automated and can be time consuming. This has led to the development of TeloScan (207), a high-throughput scanning/acquisition system that allows for the acquisition of 3D images and measurement of telomere parameters on a single-cell basis, at a speed of 10,000 to 15,000 cells per hour. This innovation has drastically reduced sample processing time and eliminates the sampling bias of non-automated imaging and analysis. It can also detect one aberrant cell in 1,000 normal cells (207). For certain cancers in which the available study material is tissue biopsies, it can be difficult to create TeloScan

parameters that identify correct and consistent cell populations for each sample. To ensure the automated method is accurately selecting cells, TeloScan reveals the analyzed cells after the scanning process and allows the use to manually delete and add cells to the analysis. However, the use of different equipment, such as objectives, lower magnification, 63x to 40 or 60x, and new automated software, can lead to differing results when directly comparing TeloView results with those from TeloScan. For example, 3D telomere profiles of Hodgkin lymphoma patients differ from TeloView to TeloScan (Cheryl Taylor, unpublished results) and a different number of neuroblastoma subgroups were identified using telomere parameter data from TeloView compared to TeloScan (Alexandra Kuzyk, unpublished results). Contrastingly, identical subgroups of glioblastoma that correlated with patient survival were determined with both the automated and semi-automated software (257). Although there may be differences when directly comparing samples between TeloView and TeloScan, the overall trends and conclusions may be indistinguishable; therefore, the role of automated software in future studies of 3D telomere organization will have to be determined on an individual basis.

5.2. MYCN Drives Tumorigenesis by Altering 3D Nuclear Organization

MYCC is a proto-oncogene whose deregulation is present in over 70% of tumors (270, 575). MYC is known to induce genomic instability though the formation of EEs (276, 343, 576), centromere and telomere fusion (343), chromosome and chromatid breaks (276, 343), ring chromosomes (343), translocations (338), deletions and inversions (338), aneuploidy (276, 340), Robertsonian chromosomes (259, 342), and

endoreduplication and polyploidy (316-318). The genomic instability induced by MYC also acts on the interphase nucleus remodeling its 3D organization (536, 560). A study by Louis *et al*. (2005) found conditional MYC deregulation resulted in changes in the 3D nuclear organization of telomeres and chromosomes (46). MYC overexpression led to cycles of telomeric aggregate formation that were proportional to the duration of MYC deregulation. The cycles continued when MYC overexpression was discontinued, leading to non-rcpTs, alteration in 3D telomere organization and genomic instability. It was concluded that MYC-induced nuclear remodeling preceded the onset of genomic instability. With MYC deregulation, chromosomes involved in structural rearrangements illustrated a change in their position in the interphase nucleus to be in closer proximity to each other; however chromosomes not involved in translocations did not exhibit a change in their nuclear location (46). Robertsonian fusions were also observed after MYC deregulation (342).

Although MYC is involved in remodeling of the interphase nucleus, the role of MYCN in this process has not been studied. The work in this thesis illustrates for the first time, the potential of MYCN deregulation to change the 3D nuclear organization of telomeres and chromosomes. MYCN deregulation in neuroblastoma cell lines led to altered telomere organization with an increase in the number of telomeres and telomeric aggregates, and more short and long telomeres (Chapter 4). With MYCN overexpression in neuroblastoma cell lines, chromosomal gains of the 17q region were observed (Chapter 3). Although gain of the 17q region is more commonly associated with *MYCN* amplified neuroblastomas (418), we provide evidence of a functional relationship between

increased MYCN expression and copy number gain of 17q. Altered nuclear location of the 17q region and increased expression of genes in this region was also observed with MYCN overexpression. Although the increased expression of genes on 17q may be because they are downstream targets of MYCN, previous studies have not identified them as such (485, 496, 577). This suggests the role of MYCN is to alter the nuclear location of the 17q region to one of higher transcriptional activity, rather than to act on a promoter.

The mechanism behind MYC and MYCN-dependent nuclear remodeling is not known. MYC and MYCN are associated with the amplification of genes involved in cell cycle progression and proliferation (334); therefore, affected cells will replicate at a quicker rate leading to critically short telomeres and genomic instability as a result of BFB cycles. As telomere repeat sequences can bind to the nuclear matrix (578, 579), short telomeres, which move more than long telomeres (580, 581), may have a looser attachment and readily alter their nuclear location. MYC overexpression results in telomere uncapping (46) and down-regulation of TRF2 (582). TRF2 is tightly associated with the nuclear matrix (583), therefore, telomere uncapping and the loss of TRF2 may also liberate chromosome ends to alter their nuclear position. In support of this hypothesis, disruption of the nuclear matrix through loss of A-type lamins, resulted in an increased speed of chromatin diffusion throughout the nucleus (78), altered nuclear distribution of telomeres, and increased genomic instability (79). Loss of TRF2, which protects and represses DDRs at telomeres, may also make telomeres more vulnerable to dysfunction creating telomere fusions; accordingly cancers with MYC (and MYCN)

overexpression illustrate an increase in telomeric aggregates (46, 567). Another possibility is that MYC and MYCN activate downstream target genes that are involved in nuclear motor activities, such as nuclear myosin 1 beta (NM1β) (584), and consequently cause chromosome movements.

5.3. The Potential of Studying CT Arrangement in Cancer

It has been widely accepted that CT arrangement in the interphase nucleus is non-random and cell-type specific (36-38, 518). The most thoroughly tested conclusion about CT arrangement is the more peripheral position of chromosome 19 compared to chromosome 18 (50). This arrangement was confirmed in multiple normal and tumor cell types (48) and was also found to be evolutionarily conserved in primates (51). All other aspects of CT are either unknown or debated. For example, a topic of heavy deliberation is which factors contribute to, and which one is most influential in, CT arrangement in a given cell type. Another controversial topic is whether transcriptional regulation is influenced by the gene's nuclear position and which nuclear environments are active versus repressive. Nonetheless, most would agree that although complex, nuclear organization contributes to cell function and is important to understand.

One of the reasons why it is difficult to draw conclusions about CT arrangement is because it is challenging to determine the exact location of an entity in the nucleus. Firstly, a CT's position in the nucleus always has to have a point of reference, such as the nuclear centre, the nuclear periphery, a gene locus or another CT. Consequently,

comparisons between samples can be problematic if the cell size or shape differs, or if the function of the reference entity is not conserved. This makes study conclusions very specific to the cell type analyzed and conditions used, rather than being able to generalize findings. Secondly, there is often great variation in a CT's position between cells in the same sample. Therefore, rather than being able to determine an exact position, the average or range of positions for an entity in the nucleus has to be reported (as shown for the position of 17q25 and 17p11 in neuroblastoma tissue samples and cell lines in Chapter 3). This variation could be due to differences in the transcriptional state or cell cycle status of the cells. Also, not only can there be variation in the nuclear position of the CT, there can also be variation in the orientation of the chromosome (585, 586). Another reason it is difficult to draw generalizations about CT arrangement is that model systems may not accurately reflect *in vivo* studies. Computer modeling and cell culture conditions may not be able to mimic the complex *in vivo* environment. For example, studies of milk protein genes in mammary epithelial tissue found a significant change in the gene's position *in vivo*, but not *in vitro* (81, 587). Because of these limitations, the potential and value of studying the arrangement of CTs in cancer is in understanding tumor pathogenesis rather than in identifying a tumor biomarker.

5.4. 3D Telomere Organization Reflects Telomere Maintenance Mechanism

Studies of telomere length regulation in neuroblastoma have identified a role for both telomerase and ALT. High telomerase expression is associated with *MYCN* amplification (453) and poor clinical outcomes (514, 515). As MYC directly activates

hTERT promotor sequences (588), MYCN may have a similar mechanism. However, studies have not found a clear relationship between telomerase and telomere length (175, 453). Neuroblastomas without *MYCN* amplification and increased telomere length also contained APBs, suggesting the presence of an ALT mechanism (451). These tumors were also associated with poor patient survival. One study identified the coexistence of high hTERT and ALT in a subset of tumors with significantly reduced overall survival (175).

We propose that the neuroblastoma subgroups identified by 3D telomere parameters (Chapter 4) represent a model of neuroblastoma pathogenesis regulated by MYCN expression and mechanisms of telomere length maintenance. Subgroup II compared to Subgroup I has a higher level of MYCN expression and fewer telomeres but more telomeric aggregates per cell. Therefore the progression from Subgroup I occurs as MYCN deregulation causes increased cellular proliferation and the formation of shorter telomeres to an extent that the telomeres are very short and may not be visible by telomere Q-FISH (Subgroup II). At this point of critically short telomere length, cells develop a telomere lengthening mechanism to continue to proliferate and progress into Subgroup III. Whether telomerase and/or ALT is acquired depends on the *MYCN* amplification status of the tumor. As discussed in Chapter 4, Subgroup III can be divided into two groups (IIIa and IIIb) that have different telomere profiles. Subgroup IIIa contains *MYCN* non-amplified tumors with fewer telomeric aggregates but a greater distribution of telomere lengths; therefore, these tumors have acquired the ALT mechanism. Subgroup IIIb contains *MYCN* amplified tumors with predominately one

length of telomere and many telomeric aggregates; therefore these tumors have acquired telomerase. Identifying if and which telomere healing mechanism is active in neuroblastomas at diagnosis is clinically useful because different treatment strategies may be needed to target the cellular mechanisms leading to the tumors' pathogenesis.

5.5. Conclusion

It is now known that cancer pathogenesis relies on much more than the underlying genomic sequence, and aberrations therein. Therefore, it is important to investigate new mechanisms that can contribute to tumorigenesis and assist in clinical management. The knowledge of the role of nuclear architecture in cancer is still in its infancy. The studies in this thesis demonstrate the contribution of 3D nuclear organization to two malignancies: mouse PCT and human neuroblastoma. 3D telomere organization has the capability of differentiating normal cells from tumor cells, and aggressive from less-aggressive tumors in mouse PCT. It can also stratify a neuroblastoma cohort by clinical prognostic risk factors. MYC and MYCN deregulation in these tumors is associated with unbalanced chromosome gain of a syntenic region: 11E2 in PCT and 17q25 in neuroblastoma. Their deregulation is also associated with changes in the nuclear position of these regions. Therefore, MYC and MYCN may be drivers of nuclear disorganization in cancer. In conclusion, this thesis demonstrates that multiples aspects of 3D nuclear organization contribute to the pathogenesis of PCT and neuroblastoma. The use of 3D telomere organization as a novel prognostic biomarker in neuroblastoma has been proposed, and should be validated with further clinical trials.

5.6. Future Directions

5.6.1. Relationship Between MYC Overexpression and CT Organization in Mouse PCT

An altered, more central nuclear location of chromosome T(X;11) containing cytoband 11E2 was seen in fast-onset PCTs compared to slow-onset PCTs and normal mouse lymphocytes (Alexandra Kuzyk, unpublished results). Conditional MYC deregulation was found to alter the position of CTs in a mouse lymphocyte cell line (46); however, the role of MYC in the nuclear positioning of chromosomes 11E2 in fast-onset PCTs has not been investigated. Whether repositioning of chromosome 11E2 or PCT formation occurs first, is also unknown.

To determine whether MYC drives the nuclear repositioning of chromosome 11E2 in fast-onset PCT and the mechanism by which it does so, a model system of fast-onset PCT can be used. MYC can be activated in PreB ABL/MYC cells by 4-hydroxy-tamoxifen (46). A cell line with an inducible MYC mutant, was previously shown to be unable to promote nuclear remodeling (345), could be used a control for MYC's effects. FISH can be used to monitor the nuclear position of chromosomes over time, to

determine relationship between MYC deregulation and 11E2 movement. Both telomere uncapping through the loss of TRF2 and activation of nuclear motor proteins have been hypothesized as the mechanism by which MYC alters nuclear organization (see Discussion Section 5.2). Silencing NM1β by RNA interference after MYC induction and performing FISH for chromosome 11 as indicated above, can determine if NM1β plays a role in the nuclear positioning of 11E2; no movement of 11E2 after silencing of NM1β would indicate a role of NM1β in chromosome movement. Telomere de-protection after MYC deregulation can be determined by 3D immuno-FISH for TRF2 and telomeres; telomeres without corresponding TRF2 signals would indicate loss of this protein at telomeres (252). Uncapped telomeres can be identified by immunofluorescence for DDR proteins, such as γH2AX, and TRF1; co-localization of signals would indicate uncapped telomeres. γH2AX could be used because it is not normally found at telomeres, its presence is an early event in DDR and it has been previously validated in multiple studies (254, 589).

To determine whether repositioning of chromosome 11E2 is a cause or consequence of fast-onset PCT development, the position of chromosome 11 can be followed in PreB cells before and after v-*abl/myc* infection and transformation into PCTs *in vivo*. Fast-onset PCTs can be induced in [T38HxBALB/c]N rcpT(X;11) mice by infection with v-*abl/myc* (402). B cells can be collected prior to infection and throughout the latency period by peritoneal washes in the same mouse. B cells and PCT cells can be identified by immunostaining with CD45 and anti-surface IgM, respectively (590). FISH can be conducted on the B cells at each harvest to determine the position of chromosome

11 over time. This experiment will establish whether repositioning of chromosome 11E2 precedes or is a consequence of tumor formation. Because all fast-onset PCTs have chromosome 11 aberrations (402) and overexpression of 11E2 genes, it is most likely that chromosome 11E2 repositioning precedes tumor formation.

5.6.2. 3D Nuclear Location of Transcription Factories

Mouse cytoband 11E2 and human cytoband 17q25 are syntenic regions. The 11E2 region in fast-onset PCTs, and the 17q region in high MYCN-expressing neuroblastomas, illustrate an altered, more central nuclear location compared to slow-onset PCTs and low MYCN-expressing neuroblastomas, respectively (566) (Alexandra Kuzyk, unpublished results). This repositioning may lead to increased transcription of these regions (67) through better access to transcription factories. This is supported by the findings of increased expression of genes located on 11E2 and 17q25 in the cases where these regions occupy a more central location (566) (Sabine Mai, unpublished results).

To determine whether the genes in these cytobands experience higher rates of transcription due to their central nuclear location, the co-localization of RNA transcripts and transcription factories can be determined. Slow-onset PCTs and neuroblastomas with low MYCN expression would be used as controls, as the cytobands are found in a more peripheral location in these conditions. RNA FISH could be used to determine the nuclear location of transcripts from the *ASPSCR1, FOXK2* and *TBCD* genes, which are

located on the 11E2 and 17q25 cytobands, and previously found to be overexpressed (566) (Sabine Mai, unpublished results); *GAPDH* transcripts could be used as a control. Concurrently, immunofluorescence with anti-polII-phospho-Ser5, which indicates transcription initiation (591), and anti-polII-phospho-Ser2, which indicates transcription elongation (592), would be conducted on the mouse cells and tissue samples. Co-localization of RNA transcript signals and transcription factories would indicate a nuclear location where the gene is being transcribed. It is expected that fast-onset PCTs and neuroblastomas with high MYCN expression would have more active transcription sites overall, as well as more localized to the nuclear centre, than their respective controls.

5.6.3. Telomerase versus ALT in Neuroblastoma

There is evidence for a role of both telomerase and ALT as a telomere maintenance mechanism in neuroblastoma (175, 451, 514). *MYCN* amplified tumors are associated with high telomerase expression (453). *MYCN* amplified neuroblastomas had a distinct 3D telomere organization (Kuzyk *et al.*, in submission) and could represent telomerase-positive neuroblastomas. *MYCN* non-amplified tumors with increased telomere length are associated with the ALT mechanism (451). 3D telomere organization also identified a subgroup of *MYCN* non-amplified neuroblastomas with heterogeneous telomere lengths (Kuzyk *et al.*, in submission), an indication of the ALT mechanism, and therefore this subgroup could represent ALT-positive neuroblastomas. However, the relationship between 3D telomere organization and telomere maintenance mechanisms has never been investigated.

Immunofluorescence can be used to determine the level of hTERT expression in neuroblastoma tissue samples. To determine the presence of ALT, immuno-FISH could be used with a PML antibody and telomere FISH probe; co-localization of PML staining and a large telomere signal, such as one of the five brightest signals, would indicate the presence of ALT (451). 3D telomere Q-FISH could be employed to determine 3D telomere organization of the samples. Tumor characteristics such as *MYCN* amplification, MYCN protein expression, age at diagnosis, histologic grade and tumor stage could be compared with the presence of telomerase and ALT. Patient outcome and survival data could also be correlated with the presence of telomerase and ALT. Determination of whether 3D telomere organization correlates with the type of telomere healing mechanism could be clinically useful for determining patient prognosis and treatment strategies.

Chapter 6:

References

1. Boveri T. Die Blastomerenkerne von *Ascaris megalocephala* und die Theorie der Chromosomenindividualitat. Arch Zellforsch. 1909;3:181-268.

2. Cremer T, Cremer C. Chromosome territories, nuclear architecture and gene regulation in mammalian cells. Nature reviews Genetics. 2001;2:292-301.

3. Shaw PJ, Abranches R, Paula Santos A, Beven AF, Stoger E, Wegel E, et al. The architecture of interphase chromosomes and nucleolar transcription sites in plants. Journal of structural biology. 2002;140:31-8.

4. Pecinka A, Schubert V, Meister A, Kreth G, Klatte M, Lysak MA, et al. Chromosome territory arrangement and homologous pairing in nuclei of Arabidopsis thaliana are predominantly random except for NOR-bearing chromosomes. Chromosoma. 2004;113:258-69.

5. Berr A, Pecinka A, Meister A, Kreth G, Fuchs J, Blattner FR, et al. Chromosome arrangement and nuclear architecture but not centromeric sequences are conserved between Arabidopsis thaliana and Arabidopsis lyrata. The Plant journal : for cell and molecular biology. 2006;48:771-83.

6. Bystricky K, Laroche T, van Houwe G, Blaszczyk M, Gasser SM. Chromosome looping in yeast: telomere pairing and coordinated movement reflect anchoring efficiency and territorial organization. The Journal of cell biology. 2005;168:375-87.

7. Molnar M, Kleckner N. Examination of interchromosomal interactions in vegetatively growing diploid Schizosaccharomyces pombe cells by Cre/loxP site-specific recombination. Genetics. 2008;178:99-112.

8. Jackson DA, Pombo A. Replicon clusters are stable units of chromosome structure: evidence that nuclear organization contributes to the efficient activation and propagation of S phase in human cells. The Journal of cell biology. 1998;140:1285-95.

9. Berezney R, Malyavantham KS, Pliss A, Bhattacharya S, Acharya R. Spatio-temporal dynamics of genomic organization and function in the mammalian cell nucleus. Advances in enzyme regulation. 2005;45:17-26.

10. Dixon JR, Selvaraj S, Yue F, Kim A, Li Y, Shen Y, et al. Topological domains in mammalian genomes identified by analysis of chromatin interactions. Nature. 2012;485:376-80.

11. Nora EP, Lajoie BR, Schulz EG, Giorgetti L, Okamoto I, Servant N, et al. Spatial partitioning of the regulatory landscape of the X-inactivation centre. Nature. 2012;485:381-5.

12. Albiez H, Cremer M, Tiberi C, Vecchio L, Schermelleh L, Dittrich S, et al. Chromatin domains and the interchromatin compartment form structurally defined and functionally interacting nuclear networks. Chromosome research : an international journal on the molecular, supramolecular and evolutionary aspects of chromosome biology. 2006;14:707-33.

13. Lyon MF. Sex chromatin and gene action in the mammalian X-chromosome. American journal of human genetics. 1962;14:135-48.

14. Teller K, Illner D, Thamm S, Casas-Delucchi CS, Versteeg R, Indemans M, et al. A top-down analysis of Xa- and Xi-territories reveals differences of higher order structure at >/= 20 Mb genomic length scales. Nucleus (Austin, Tex). 2011;2:465-77.

15. Marenduzzo D, Micheletti C, Cook PR. Entropy-driven genome organization. Biophysical journal. 2006;90:3712-21.

16. Visser AE, Jaunin F, Fakan S, Aten JA. High resolution analysis of interphase chromosome domains. Journal of cell science. 2000;113 (Pt 14):2585-93.

17. Fakan S, van Driel R. The perichromatin region: a functional compartment in the nucleus that determines large-scale chromatin folding. Seminars in cell & developmental biology. 2007;18:676-81.

18. Cmarko D, Verschure PJ, Martin TE, Dahmus ME, Krause S, Fu XD, et al. Ultrastructural analysis of transcription and splicing in the cell nucleus after bromo-UTP microinjection. Molecular biology of the cell. 1999;10:211-23.

19. Trentani A, Testillano PS, Risueno MC, Biggiogera M. Visualization of transcription sites at the electron microscope. European journal of histochemistry : EJH. 2003;47:195-200.

20. Fakan S, Bernhard W. Localisation of rapidly and slowly labelled nuclear RNA as visualized by high resolution autoradiography. Experimental cell research. 1971;67:129-41.

21. Jaunin F, Fakan S. DNA replication and nuclear architecture. Journal of cellular biochemistry. 2002;85:1-9.

22. Solimando L, Luijsterburg MS, Vecchio L, Vermeulen W, van Driel R, Fakan S. Spatial organization of nucleotide excision repair proteins after UV-induced DNA damage in the human cell nucleus. Journal of cell science. 2009;122:83-91.

23. Zirbel RM, Mathieu UR, Kurz A, Cremer T, Lichter P. Evidence for a nuclear compartment of transcription and splicing located at chromosome domain boundaries. Chromosome research : an international journal on the molecular, supramolecular and evolutionary aspects of chromosome biology. 1993;1:93-106.

24. Mahy NL, Perry PE, Gilchrist S, Baldock RA, Bickmore WA. Spatial organization of active and inactive genes and noncoding DNA within chromosome territories. The Journal of cell biology. 2002;157:579-89.

25. Verschure PJ, van Der Kraan I, Manders EM, van Driel R. Spatial relationship between transcription sites and chromosome territories. The Journal of cell biology. 1999;147:13-24.

26. Kupper K, Kolbl A, Biener D, Dittrich S, von Hase J, Thormeyer T, et al. Radial chromatin positioning is shaped by local gene density, not by gene expression. Chromosoma. 2007;116:285-306.

27. Branco MR, Pombo A. Intermingling of chromosome territories in interphase suggests role in translocations and transcription-dependent associations. PLoS biology. 2006;4:e138.

28. Chubb JR, Bickmore WA. Considering nuclear compartmentalization in the light of nuclear dynamics. Cell. 2003;112:403-6.

29. Fraser P, Bickmore W. Nuclear organization of the genome and the potential for gene regulation. Nature. 2007;447:413-7.

30. Kosak ST, Groudine M. Form follows function: The genomic organization of cellular differentiation. Genes & development. 2004;18:1371-84.

31. Rouquette J, Genoud C, Vazquez-Nin GH, Kraus B, Cremer T, Fakan S. Revealing the high-resolution three-dimensional network of chromatin and interchromatin space: a novel electron-microscopic approach to reconstructing nuclear architecture. Chromosome research : an international journal on the molecular, supramolecular and evolutionary aspects of chromosome biology. 2009;17:801-10.

32. Dekker J, Rippe K, Dekker M, Kleckner N. Capturing chromosome conformation. Science (New York, NY). 2002;295:1306-11.

33. Schermelleh L, Carlton PM, Haase S, Shao L, Winoto L, Kner P, et al. Subdiffraction multicolor imaging of the nuclear periphery with 3D structured illumination microscopy. Science (New York, NY). 2008;320:1332-6.

34. Gustafsson MG. Surpassing the lateral resolution limit by a factor of two using structured illumination microscopy. Journal of microscopy. 2000;198:82-7.

35. Lieberman-Aiden E, van Berkum NL, Williams L, Imakaev M, Ragoczy T, Telling A, et al. Comprehensive mapping of long-range interactions reveals folding principles of the human genome. Science (New York, NY). 2009;326:289-93.

36. Marella NV, Bhattacharya S, Mukherjee L, Xu J, Berezney R. Cell type specific chromosome territory organization in the interphase nucleus of normal and cancer cells. Journal of cellular physiology. 2009;221:130-8.

37. Meaburn KJ, Misteli T. Cell biology: chromosome territories. Nature. 2007;445:379-781.

38. Parada LA, McQueen PG, Munson PJ, Misteli T. Conservation of relative chromosome positioning in normal and cancer cells. Current biology : CB. 2002;12:1692-7.

39. Thomson I, Gilchrist S, Bickmore WA, Chubb JR. The radial positioning of chromatin is not inherited through mitosis but is established de novo in early G1. Current biology : CB. 2004;14:166-72.

40. Walter J, Schermelleh L, Cremer M, Tashiro S, Cremer T. Chromosome order in HeLa cells changes during mitosis and early G1, but is stably maintained during subsequent interphase stages. The Journal of cell biology. 2003;160:685-97.

41. Vourc'h C, Taruscio D, Boyle AL, Ward DC. Cell cycle-dependent distribution of telomeres, centromeres, and chromosome-specific subsatellite domains in the interphase nucleus of mouse lymphocytes. Experimental cell research. 1993;205:142-51.

42. Ferguson M, Ward DC. Cell cycle dependent chromosomal movement in pre-mitotic human T-lymphocyte nuclei. Chromosoma. 1992;101:557-65.

43. Marshall WF, Straight A, Marko JF, Swedlow J, Dernburg A, Belmont A, et al. Interphase chromosomes undergo constrained diffusional motion in living cells. Current biology : CB. 1997;7:930-9.

44. Martou G, De Boni U. Nuclear topology of murine, cerebellar Purkinje neurons: changes as a function of development. Experimental cell research. 2000;256:131-9.

45. Kuroda M, Tanabe H, Yoshida K, Oikawa K, Saito A, Kiyuna T, et al. Alteration of chromosome positioning during adipocyte differentiation. Journal of cell science. 2004;117:5897-903.

46. Louis SF, Vermolen BJ, Garini Y, Young IT, Guffei A, Lichtensztejn Z, et al. c-Myc induces chromosomal rearrangements through telomere and chromosome remodeling in the interphase nucleus. Proceedings of the National Academy of Sciences of the United States of America. 2005;102:9613-8.

47. Murata S, Nakazawa T, Ohno N, Terada N, Iwashina M, Mochizuki K, et al. Conservation and alteration of chromosome territory arrangements in thyroid carcinoma cell nuclei. Thyroid : official journal of the American Thyroid Association. 2007;17:489-96.

48. Cremer M, Kupper K, Wagler B, Wizelman L, von Hase J, Weiland Y, et al. Inheritance of gene density-related higher order chromatin arrangements in normal and tumor cell nuclei. The Journal of cell biology. 2003;162:809-20.

49. Guffei A, Sarkar R, Klewes L, Righolt C, Knecht H, Mai S. Dynamic chromosomal rearrangements in Hodgkin's lymphoma are due to ongoing three-dimensional nuclear remodeling and breakage-bridge-fusion cycles. Haematologica. 2010;95:2038-46.

50. Croft JA, Bridger JM, Boyle S, Perry P, Teague P, Bickmore WA. Differences in the localization and morphology of chromosomes in the human nucleus. The Journal of cell biology. 1999;145:1119-31.

51. Tanabe H, Muller S, Neusser M, von Hase J, Calcagno E, Cremer M, et al. Evolutionary conservation of chromosome territory arrangements in cell nuclei from higher primates. Proceedings of the National Academy of Sciences of the United States of America. 2002;99:4424-9.

52. Boyle S, Gilchrist S, Bridger JM, Mahy NL, Ellis JA, Bickmore WA. The spatial organization of human chromosomes within the nuclei of normal and emerin-mutant cells. Human molecular genetics. 2001;10:211-9.

53. Mayer R, Brero A, von Hase J, Schroeder T, Cremer T, Dietzel S. Common themes and cell type specific variations of higher order chromatin arrangements in the mouse. BMC cell biology. 2005;6:44.

54. Koehler D, Zakhartchenko V, Froenicke L, Stone G, Stanyon R, Wolf E, et al. Changes of higher order chromatin arrangements during major genome activation in bovine preimplantation embryos. Experimental cell research. 2009;315:2053-63.

55. Habermann FA, Cremer M, Walter J, Kreth G, von Hase J, Bauer K, et al. Arrangements of macro- and microchromosomes in chicken cells. Chromosome research : an international journal on the molecular, supramolecular and evolutionary aspects of chromosome biology. 2001;9:569-84.

56. Bolzer A, Kreth G, Solovei I, Koehler D, Saracoglu K, Fauth C, et al. Three-dimensional maps of all chromosomes in human male fibroblast nuclei and prometaphase rosettes. PLoS biology. 2005;3:e157.

57. Heride C, Ricoul M, Kieu K, von Hase J, Guillemot V, Cremer C, et al. Distance between homologous chromosomes results from chromosome positioning constraints. Journal of cell science. 2010;123:4063-75.

58. Botta M, Haider S, Leung IX, Lio P, Mozziconacci J. Intra- and inter-chromosomal interactions correlate with CTCF binding genome wide. Molecular systems biology. 2010;6:426.

59. Gaszner M, Felsenfeld G. Insulators: exploiting transcriptional and epigenetic mechanisms. Nature reviews Genetics. 2006;7:703-13.

60. Chung JH, Whiteley M, Felsenfeld G. A 5' element of the chicken beta-globin domain serves as an insulator in human erythroid cells and protects against position effect in Drosophila. Cell. 1993;74:505-14.

61. Cuddapah S, Jothi R, Schones DE, Roh TY, Cui K, Zhao K. Global analysis of the insulator binding protein CTCF in chromatin barrier regions reveals demarcation of active and repressive domains. Genome research. 2009;19:24-32.

62. Narendra V, Rocha PP, An D, Raviram R, Skok JA, Mazzoni EO, et al. Transcription. CTCF establishes discrete functional chromatin domains at the Hox clusters during differentiation. Science (New York, NY). 2015;347:1017-21.

63. Bell AC, West AG, Felsenfeld G. The protein CTCF is required for the enhancer blocking activity of vertebrate insulators. Cell. 1999;98:387-96.

64. Hou C, Zhao H, Tanimoto K, Dean A. CTCF-dependent enhancer-blocking by alternative chromatin loop formation. Proceedings of the National Academy of Sciences of the United States of America. 2008;105:20398-403.

65. Selvaraj S, J RD, Bansal V, Ren B. Whole-genome haplotype reconstruction using proximity-ligation and shotgun sequencing. Nature biotechnology. 2013;31:1111-8.

66. Solovei I, Kreysing M, Lanctot C, Kosem S, Peichl L, Cremer T, et al. Nuclear architecture of rod photoreceptor cells adapts to vision in mammalian evolution. Cell. 2009;137:356-68.

67. Lanctot C, Kaspar C, Cremer T. Positioning of the mouse Hox gene clusters in the nuclei of developing embryos and differentiating embryoid bodies. Experimental cell research. 2007;313:1449-59.

68. Morey C, Kress C, Bickmore WA. Lack of bystander activation shows that localization exterior to chromosome territories is not sufficient to up-regulate gene expression. Genome research. 2009;19:1184-94.

69. Volpi EV, Chevret E, Jones T, Vatcheva R, Williamson J, Beck S, et al. Large-scale chromatin organization of the major histocompatibility complex and other regions of human chromosome 6 and its response to interferon in interphase nuclei. Journal of cell science. 2000;113 (Pt 9):1565-76.

70. Osborne CS, Chakalova L, Mitchell JA, Horton A, Wood AL, Bolland DJ, et al. Myc dynamically and preferentially relocates to a transcription factory occupied by Igh. PLoS biology. 2007;5:e192.

71. Nolis IK, McKay DJ, Mantouvalou E, Lomvardas S, Merika M, Thanos D. Transcription factors mediate long-range enhancer-promoter interactions. Proceedings of the National Academy of Sciences of the United States of America. 2009;106:20222-7.

72. Deng W, Lee J, Wang H, Miller J, Reik A, Gregory PD, et al. Controlling long-range genomic interactions at a native locus by targeted tethering of a looping factor. Cell. 2012;149:1233-44.

73. Schneider R, Grosschedl R. Dynamics and interplay of nuclear architecture, genome organization, and gene expression. Genes & development. 2007;21:3027-43.

74. Andrulis ED, Neiman AM, Zappulla DC, Sternglanz R. Perinuclear localization of chromatin facilitates transcriptional silencing. Nature. 1998;394:592-5.

75. Pickersgill H, Kalverda B, de Wit E, Talhout W, Fornerod M, van Steensel B. Characterization of the Drosophila melanogaster genome at the nuclear lamina. Nature genetics. 2006;38:1005-14.

76. Mattout A, Pike BL, Towbin BD, Bank EM, Gonzalez-Sandoval A, Stadler MB, et al. An EDMD mutation in C. elegans lamin blocks muscle-specific gene relocation and compromises muscle integrity. Current biology : CB. 2011;21:1603-14.

77. Towbin BD, Gonzalez-Aguilera C, Sack R, Gaidatzis D, Kalck V, Meister P, et al. Step-wise methylation of histone H3K9 positions heterochromatin at the nuclear periphery. Cell. 2012;150:934-47.

78. Bronshtein I, Kepten E, Kanter I, Berezin S, Lindner M, Redwood AB, et al. Loss of lamin A function increases chromatin dynamics in the nuclear interior. 2015;6:8044.

79. Gonzalez-Suarez I, Redwood AB, Perkins SM, Vermolen B, Lichtensztejin D, Grotsky DA, et al. Novel roles for A-type lamins in telomere biology and the DNA damage response pathway. The EMBO journal. 2009;28:2414-27.

80. Kubben N, Adriaens M, Meuleman W, Voncken JW, van Steensel B, Misteli T. Mapping of lamin A- and progerin-interacting genome regions. Chromosoma. 2012;121:447-64.

81. Kress C, Kieu K, Droineau S, Galio L, Devinoy E. Specific positioning of the casein gene cluster in active nuclear domains in luminal mammary epithelial cells. Chromosome research : an international journal on the molecular, supramolecular and evolutionary aspects of chromosome biology. 2011;19:979-97.

82. Reddy KL, Zullo JM, Bertolino E, Singh H. Transcriptional repression mediated by repositioning of genes to the nuclear lamina. Nature. 2008;452:243-7.

83. Ragoczy T, Bender MA, Telling A, Byron R, Groudine M. The locus control region is required for association of the murine beta-globin locus with engaged transcription factories during erythroid maturation. Genes & development. 2006;20:1447-57.

84. Zink D, Amaral MD, Englmann A, Lang S, Clarke LA, Rudolph C, et al. Transcription-dependent spatial arrangements of CFTR and adjacent genes in human cell nuclei. The Journal of cell biology. 2004;166:815-25.

85. Williams RR, Azuara V, Perry P, Sauer S, Dvorkina M, Jorgensen H, et al. Neural induction promotes large-scale chromatin reorganisation of the Mash1 locus. Journal of cell science. 2006;119:132-40.

86. Finlan LE, Sproul D, Thomson I, Boyle S, Kerr E, Perry P, et al. Recruitment to the nuclear periphery can alter expression of genes in human cells. PLoS genetics. 2008;4:e1000039.

87. Kumaran RI, Spector DL. A genetic locus targeted to the nuclear periphery in living cells maintains its transcriptional competence. The Journal of cell biology. 2008;180:51-65.

88. Wansink DG, Schul W, van der Kraan I, van Steensel B, van Driel R, de Jong L. Fluorescent labeling of nascent RNA reveals transcription by RNA polymerase II in domains scattered throughout the nucleus. The Journal of cell biology. 1993;122:283-93.

89. Elcock LS, Bridger JM. Exploring the relationship between interphase gene positioning, transcriptional regulation and the nuclear matrix. Biochemical Society transactions. 2010;38:263-7.

90. Meyne J, Ratliff RL, Moyzis RK. Conservation of the human telomere sequence (TTAGGG)n among vertebrates. Proceedings of the National Academy of Sciences of the United States of America. 1989;86:7049-53.

91. Kipling D, Cooke HJ. Hypervariable ultra-long telomeres in mice. Nature. 1990;347:400-2.

92. Makarov VL, Hirose Y, Langmore JP. Long G tails at both ends of human chromosomes suggest a C strand degradation mechanism for telomere shortening. Cell. 1997;88:657-66.

93. McElligott R, Wellinger RJ. The terminal DNA structure of mammalian chromosomes. The EMBO journal. 1997;16:3705-14.

94. Griffith JD, Comeau L, Rosenfield S, Stansel RM, Bianchi A, Moss H, et al. Mammalian telomeres end in a large duplex loop. Cell. 1999;97:503-14.

95. Doksani Y, Wu JY, de Lange T, Zhuang X. Super-resolution fluorescence imaging of telomeres reveals TRF2-dependent T-loop formation. Cell. 2013;155:345-56.

96. Palm W, de Lange T. How shelterin protects mammalian telomeres. Annual review of genetics. 2008;42:301-34.

97. Lipps HJ, Rhodes D. G-quadruplex structures: in vivo evidence and function. Trends in cell biology. 2009;19:414-22.

98. Benetti R, Gonzalo S, Jaco I, Schotta G, Klatt P, Jenuwein T, et al. Suv4-20h deficiency results in telomere elongation and derepression of telomere recombination. The Journal of cell biology. 2007;178:925-36.

99. Garcia-Cao M, O'Sullivan R, Peters AH, Jenuwein T, Blasco MA. Epigenetic regulation of telomere length in mammalian cells by the Suv39h1 and Suv39h2 histone methyltransferases. Nature genetics. 2004;36:94-9.

100. Gonzalo S, Jaco I, Fraga MF, Chen T, Li E, Esteller M, et al. DNA methyltransferases control telomere length and telomere recombination in mammalian cells. Nature cell biology. 2006;8:416-24.

101. Schoeftner S, Blasco MA. A 'higher order' of telomere regulation: telomere heterochromatin and telomeric RNAs. The EMBO journal. 2009;28:2323-36.

102. Azzalin CM, Reichenbach P, Khoriauli L, Giulotto E, Lingner J. Telomeric repeat containing RNA and RNA surveillance factors at mammalian chromosome ends. Science (New York, NY). 2007;318:798-801.

103. Cusanelli E, Romero CA, Chartrand P. Telomeric noncoding RNA TERRA is induced by telomere shortening to nucleate telomerase molecules at short telomeres. Molecular cell. 2013;51:780-91.

104. Redon S, Zemp I, Lingner J. A three-state model for the regulation of telomerase by TERRA and hnRNPA1. Nucleic acids research. 2013;41:9117-28.

105. Flynn RL, Centore RC, O'Sullivan RJ, Rai R, Tse A, Songyang Z, et al. TERRA and hnRNPA1 orchestrate an RPA-to-POT1 switch on telomeric single-stranded DNA. Nature. 2011;471:532-6.

106. de Lange T. Shelterin: the protein complex that shapes and safeguards human telomeres. Genes & development. 2005;19:2100-10.

107. Lei M, Podell ER, Cech TR. Structure of human POT1 bound to telomeric single-stranded DNA provides a model for chromosome end-protection. Nature structural & molecular biology. 2004;11:1223-9.

108. Xin H, Liu D, Songyang Z. The telosome/shelterin complex and its functions. Genome biology. 2008;9:232.

109. van Steensel B, de Lange T. Control of telomere length by the human telomeric protein TRF1. Nature. 1997;385:740-3.

110. Smogorzewska A, van Steensel B, Bianchi A, Oelmann S, Schaefer MR, Schnapp G, et al. Control of human telomere length by TRF1 and TRF2. Molecular and cellular biology. 2000;20:1659-68.

111. Karlseder J, Kachatrian L, Takai H, Mercer K, Hingorani S, Jacks T, et al. Targeted deletion reveals an essential function for the telomere length regulator Trf1. Molecular and cellular biology. 2003;23:6533-41.

112. Celli GB, de Lange T. DNA processing is not required for ATM-mediated telomere damage response after TRF2 deletion. Nature cell biology. 2005;7:712-8.

113. Martinez P, Blasco MA. Telomeric and extra-telomeric roles for telomerase and the telomere-binding proteins. Nature reviews Cancer. 2011;11:161-76.

114. Hockemeyer D, Daniels JP, Takai H, de Lange T. Recent expansion of the telomeric complex in rodents: Two distinct POT1 proteins protect mouse telomeres. Cell. 2006;126:63-77.

115. Wu L, Multani AS, He H, Cosme-Blanco W, Deng Y, Deng JM, et al. Pot1 deficiency initiates DNA damage checkpoint activation and aberrant homologous recombination at telomeres. Cell. 2006;126:49-62.

116. Wang F, Podell ER, Zaug AJ, Yang Y, Baciu P, Cech TR, et al. The POT1-TPP1 telomere complex is a telomerase processivity factor. Nature. 2007;445:506-10.

117. Xin H, Liu D, Wan M, Safari A, Kim H, Sun W, et al. TPP1 is a homologue of ciliate TEBP-beta and interacts with POT1 to recruit telomerase. Nature. 2007;445:559-62.

118. Tejera AM, Stagno d'Alcontres M, Thanasoula M, Marion RM, Martinez P, Liao C, et al. TPP1 is required for TERT recruitment, telomere elongation during nuclear reprogramming, and normal skin development in mice. Developmental cell. 2010;18:775-89.

119. Takai KK, Kibe T, Donigian JR, Frescas D, de Lange T. Telomere protection by TPP1/POT1 requires tethering to TIN2. Molecular cell. 2011;44:647-59.

120. Carroll KA, Ly H. Telomere dysfunction in human diseases: the long and short of it! International journal of clinical and experimental pathology. 2009;2:528-43.

121. Yang D, He Q, Kim H, Ma W, Songyang Z. TIN2 protein dyskeratosis congenita missense mutants are defective in association with telomerase. The Journal of biological chemistry. 2011;286:23022-30.

122. Ramsay AJ, Quesada V, Foronda M, Conde L, Martinez-Trillos A, Villamor N, et al. POT1 mutations cause telomere dysfunction in chronic lymphocytic leukemia. Nature genetics. 2013;45:526-30.

123. Miyake Y, Nakamura M, Nabetani A, Shimamura S, Tamura M, Yonehara S, et al. RPA-like mammalian Ctc1-Stn1-Ten1 complex binds to single-stranded DNA and protects telomeres independently of the Pot1 pathway. Molecular cell. 2009;36:193-206.

124. Surovtseva YV, Churikov D, Boltz KA, Song X, Lamb JC, Warrington R, et al. Conserved telomere maintenance component 1 interacts with STN1 and maintains chromosome ends in higher eukaryotes. Molecular cell. 2009;36:207-18.

125. Wu P, Takai H, de Lange T. Telomeric 3' overhangs derive from resection by Exo1 and Apollo and fill-in by POT1b-associated CST. Cell. 2012;150:39-52.

126. Chen LY, Redon S, Lingner J. The human CST complex is a terminator of telomerase activity. Nature. 2012;488:540-4.

127. Olovnikov AM. A theory of marginotomy. The incomplete copying of template margin in enzymic synthesis of polynucleotides and biological significance of the phenomenon. Journal of theoretical biology. 1973;41:181-90.

128. Watson JD. Origin of concatemeric T7 DNA. Nature: New biology. 1972;239:197-201.

129. Hayflick L. THE LIMITED IN VITRO LIFETIME OF HUMAN DIPLOID CELL STRAINS. Experimental cell research. 1965;37:614-36.

130. Hara E, Tsurui H, Shinozaki A, Nakada S, Oda K. Cooperative effect of antisense-Rb and antisense-p53 oligomers on the extension of life span in human diploid fibroblasts, TIG-1. Biochemical and biophysical research communications. 1991;179:528-34.

131. Shay JW, Pereira-Smith OM, Wright WE. A role for both RB and p53 in the regulation of human cellular senescence. Experimental cell research. 1991;196:33-9.

132. Counter CM, Avilion AA, LeFeuvre CE, Stewart NG, Greider CW, Harley CB, et al. Telomere shortening associated with chromosome instability is arrested in immortal cells which express telomerase activity. The EMBO journal. 1992;11:1921-9.

133. Shay JW, Wright WE, Brasiskyte D, Van der Haegen BA. E6 of human papillomavirus type 16 can overcome the M1 stage of immortalization in human mammary epithelial cells but not in human fibroblasts. Oncogene. 1993;8:1407-13.

134. Bodnar AG, Ouellette M, Frolkis M, Holt SE, Chiu CP, Morin GB, et al. Extension of life-span by introduction of telomerase into normal human cells. Science (New York, NY). 1998;279:349-52.

135. Xu L, Blackburn EH. Human cancer cells harbor T-stumps, a distinct class of extremely short telomeres. Molecular cell. 2007;28:315-27.

136. Kim NW, Piatyszek MA, Prowse KR, Harley CB, West MD, Ho PL, et al. Specific association of human telomerase activity with immortal cells and cancer. Science (New York, NY). 1994;266:2011-5.

137. Harley CB, Futcher AB, Greider CW. Telomeres shorten during ageing of human fibroblasts. Nature. 1990;345:458-60.

138. Flores I, Canela A, Vera E, Tejera A, Cotsarelis G, Blasco MA. The longest telomeres: a general signature of adult stem cell compartments. Genes & development. 2008;22:654-67.

139. Nakamura TM, Morin GB, Chapman KB, Weinrich SL, Andrews WH, Lingner J, et al. Telomerase catalytic subunit homologs from fission yeast and human. Science (New York, NY). 1997;277:955-9.

140. Blasco MA. Telomeres and human disease: ageing, cancer and beyond. Nature reviews Genetics. 2005;6:611-22.

141. Shay JW, Bacchetti S. A survey of telomerase activity in human cancer. European journal of cancer (Oxford, England : 1990). 1997;33:787-91.

142. Shay JW, Wright WE. Telomerase activity in human cancer. Current opinion in oncology. 1996;8:66-71.

143. Blasco MA, Rizen M, Greider CW, Hanahan D. Differential regulation of telomerase activity and telomerase RNA during multi-stage tumorigenesis. Nature genetics. 1996;12:200-4.

144. Liu Y, Snow BE, Hande MP, Yeung D, Erdmann NJ, Wakeham A, et al. The telomerase reverse transcriptase is limiting and necessary for telomerase function in vivo. Current biology : CB. 2000;10:1459-62.

145. Cosme-Blanco W, Shen MF, Lazar AJ, Pathak S, Lozano G, Multani AS, et al. Telomere dysfunction suppresses spontaneous tumorigenesis in vivo by initiating p53-dependent cellular senescence. EMBO reports. 2007;8:497-503.

146. Feldser DM, Greider CW. Short telomeres limit tumor progression in vivo by inducing senescence. Cancer cell. 2007;11:461-9.

147. Gonzalez-Suarez E, Samper E, Flores JM, Blasco MA. Telomerase-deficient mice with short telomeres are resistant to skin tumorigenesis. Nature genetics. 2000;26:114-7.

148. Greenberg RA, Chin L, Femino A, Lee KH, Gottlieb GJ, Singer RH, et al. Short dysfunctional telomeres impair tumorigenesis in the INK4a(delta2/3) cancer-prone mouse. Cell. 1999;97:515-25.

149. Gonzalez-Suarez E, Samper E, Ramirez A, Flores JM, Martin-Caballero J, Jorcano JL, et al. Increased epidermal tumors and increased skin wound healing in transgenic mice overexpressing the catalytic subunit of telomerase, mTERT, in basal keratinocytes. The EMBO journal. 2001;20:2619-30.

150. Cayuela ML, Flores JM, Blasco MA. The telomerase RNA component Terc is required for the tumour-promoting effects of Tert overexpression. EMBO reports. 2005;6:268-74.

151. Tomas-Loba A, Flores I, Fernandez-Marcos PJ, Cayuela ML, Maraver A, Tejera A, et al. Telomerase reverse transcriptase delays aging in cancer-resistant mice. Cell. 2008;135:609-22.

152. Savage SA, Calado RT, Xin ZT, Ly H, Young NS, Chanock SJ. Genetic variation in telomeric repeat binding factors 1 and 2 in aplastic anemia. Experimental hematology. 2006;34:664-71.

153. Armanios MY, Chen JJ, Cogan JD, Alder JK, Ingersoll RG, Markin C, et al. Telomerase mutations in families with idiopathic pulmonary fibrosis. The New England journal of medicine. 2007;356:1317-26.

154. Teng SC, Zakian VA. Telomere-telomere recombination is an efficient bypass pathway for telomere maintenance in Saccharomyces cerevisiae. Molecular and cellular biology. 1999;19:8083-93.

155. Henson JD, Neumann AA, Yeager TR, Reddel RR. Alternative lengthening of telomeres in mammalian cells. Oncogene. 2002;21:598-610.

156. Cesare AJ, Reddel RR. Alternative lengthening of telomeres: models, mechanisms and implications. Nature reviews Genetics. 2010;11:319-30.

157. Reddel RR. Alternative lengthening of telomeres, telomerase, and cancer. Cancer letters. 2003;194:155-62.

158. Heaphy CM, Subhawong AP, Hong SM, Goggins MG, Montgomery EA, Gabrielson E, et al. Prevalence of the alternative lengthening of telomeres telomere

maintenance mechanism in human cancer subtypes. The American journal of pathology. 2011;179:1608-15.

159. Bryan TM, Englezou A, Dalla-Pozza L, Dunham MA, Reddel RR. Evidence for an alternative mechanism for maintaining telomere length in human tumors and tumor-derived cell lines. Nature medicine. 1997;3:1271-4.

160. Henson JD, Hannay JA, McCarthy SW, Royds JA, Yeager TR, Robinson RA, et al. A robust assay for alternative lengthening of telomeres in tumors shows the significance of alternative lengthening of telomeres in sarcomas and astrocytomas. Clinical cancer research : an official journal of the American Association for Cancer Research. 2005;11:217-25.

161. Celli GB, Denchi EL, de Lange T. Ku70 stimulates fusion of dysfunctional telomeres yet protects chromosome ends from homologous recombination. Nature cell biology. 2006;8:885-90.

162. Palm W, Hockemeyer D, Kibe T, de Lange T. Functional dissection of human and mouse POT1 proteins. Molecular and cellular biology. 2009;29:471-82.

163. Bryan TM, Englezou A, Gupta J, Bacchetti S, Reddel RR. Telomere elongation in immortal human cells without detectable telomerase activity. The EMBO journal. 1995;14:4240-8.

164. Tokutake Y, Matsumoto T, Watanabe T, Maeda S, Tahara H, Sakamoto S, et al. Extra-chromosomal telomere repeat DNA in telomerase-negative immortalized cell lines. Biochemical and biophysical research communications. 1998;247:765-72.

165. Muntoni A, Neumann AA, Hills M, Reddel RR. Telomere elongation involves intra-molecular DNA replication in cells utilizing alternative lengthening of telomeres. Human molecular genetics. 2009;18:1017-27.

166. Wang RC, Smogorzewska A, de Lange T. Homologous recombination generates T-loop-sized deletions at human telomeres. Cell. 2004;119:355-68.

167. Yeager TR, Neumann AA, Englezou A, Huschtscha LI, Noble JR, Reddel RR. Telomerase-negative immortalized human cells contain a novel type of promyelocytic leukemia (PML) body. Cancer research. 1999;59:4175-9.

168. Wu G, Lee WH, Chen PL. NBS1 and TRF1 colocalize at promyelocytic leukemia bodies during late S/G2 phases in immortalized telomerase-negative cells. Implication of NBS1 in alternative lengthening of telomeres. The Journal of biological chemistry. 2000;275:30618-22.

169. Cerone MA, Londono-Vallejo JA, Bacchetti S. Telomere maintenance by telomerase and by recombination can coexist in human cells. Human molecular genetics. 2001;10:1945-52.

170. Grobelny JV, Kulp-McEliece M, Broccoli D. Effects of reconstitution of telomerase activity on telomere maintenance by the alternative lengthening of telomeres (ALT) pathway. Human molecular genetics. 2001;10:1953-61.

171. Perrem K, Colgin LM, Neumann AA, Yeager TR, Reddel RR. Coexistence of alternative lengthening of telomeres and telomerase in hTERT-transfected GM847 cells. Molecular and cellular biology. 2001;21:3862-75.

172. Ford LP, Zou Y, Pongracz K, Gryaznov SM, Shay JW, Wright WE. Telomerase can inhibit the recombination-based pathway of telomere maintenance in human cells. The Journal of biological chemistry. 2001;276:32198-203.

173. Katoh M, Katoh M, Kameyama M, Kugoh H, Shimizu M, Oshimura M. A repressor function for telomerase activity in telomerase-negative immortal cells. Molecular carcinogenesis. 1998;21:17-25.

174. Costa A, Daidone MG, Daprai L, Villa R, Cantu S, Pilotti S, et al. Telomere maintenance mechanisms in liposarcomas: association with histologic subtypes and disease progression. Cancer research. 2006;66:8918-24.

175. Pezzolo A, Pistorio A, Gambini C, Haupt R, Ferraro M, Erminio G, et al. Intratumoral diversity of telomere length in individual neuroblastoma tumors. Oncotarget. 2015;6:7493-503.

176. Gocha AR, Nuovo G, Iwenofu OH, Groden J. Human sarcomas are mosaic for telomerase-dependent and telomerase-independent telomere maintenance mechanisms: implications for telomere-based therapies. The American journal of pathology. 2013;182:41-8.

177. Chin L, Artandi SE, Shen Q, Tam A, Lee SL, Gottlieb GJ, et al. p53 deficiency rescues the adverse effects of telomere loss and cooperates with telomere dysfunction to accelerate carcinogenesis. Cell. 1999;97:527-38.

178. Martinez P, Thanasoula M, Munoz P, Liao C, Tejera A, McNees C, et al. Increased telomere fragility and fusions resulting from TRF1 deficiency lead to degenerative pathologies and increased cancer in mice. Genes & development. 2009;23:2060-75.

179. Munoz P, Blanco R, Flores JM, Blasco MA. XPF nuclease-dependent telomere loss and increased DNA damage in mice overexpressing TRF2 result in premature aging and cancer. Nature genetics. 2005;37:1063-71.

180. Artandi SE, Chang S, Lee SL, Alson S, Gottlieb GJ, Chin L, et al. Telomere dysfunction promotes non-reciprocal translocations and epithelial cancers in mice. Nature. 2000;406:641-5.

181. O'Sullivan RJ, Karlseder J. Telomeres: protecting chromosomes against genome instability. Nature reviews Molecular cell biology. 2010;11:171-81.

182. de Lange T. How telomeres solve the end-protection problem. Science (New York, NY). 2009;326:948-52.

183. d'Adda di Fagagna F, Reaper PM, Clay-Farrace L, Fiegler H, Carr P, Von Zglinicki T, et al. A DNA damage checkpoint response in telomere-initiated senescence. Nature. 2003;426:194-8.

184. Murnane JP. Telomeres and chromosome instability. DNA repair. 2006;5:1082-92.

185. McClintock B. The Stability of Broken Ends of Chromosomes in Zea Mays. Genetics. 1941;26:234-82.

186. Mai S, Garini Y. Oncogenic remodeling of the three-dimensional organization of the interphase nucleus: c-Myc induces telomeric aggregates whose formation precedes chromosomal rearrangements. Cell cycle (Georgetown, Tex). 2005;4:1327-31.

187. Verdun RE, Karlseder J. The DNA damage machinery and homologous recombination pathway act consecutively to protect human telomeres. Cell. 2006;127:709-20.

188. Sfeir A, Kosiyatrakul ST, Hockemeyer D, MacRae SL, Karlseder J, Schildkraut CL, et al. Mammalian telomeres resemble fragile sites and require TRF1 for efficient replication. Cell. 2009;138:90-103.

189. Oikawa S, Tada-Oikawa S, Kawanishi S. Site-specific DNA damage at the GGG sequence by UVA involves acceleration of telomere shortening. Biochemistry. 2001;40:4763-8.

190. Ayouaz A, Raynaud C, Heride C, Revaud D, Sabatier L. Telomeres: hallmarks of radiosensitivity. Biochimie. 2008;90:60-72.

191. Rochette PJ, Brash DE. Human telomeres are hypersensitive to UV-induced DNA Damage and refractory to repair. PLoS genetics. 2010;6:e1000926.

192. de Lange T, Shiue L, Myers RM, Cox DR, Naylor SL, Killery AM, et al. Structure and variability of human chromosome ends. Molecular and cellular biology. 1990;10:518-27.

193. Cawthon RM. Telomere measurement by quantitative PCR. Nucleic acids research. 2002;30:e47.

194. Cawthon RM. Telomere length measurement by a novel monochrome multiplex quantitative PCR method. Nucleic acids research. 2009;37:e21.

195. Baird DM, Rowson J, Wynford-Thomas D, Kipling D. Extensive allelic variation and ultrashort telomeres in senescent human cells. Nature genetics. 2003;33:203-7.

196. Britt-Compton B, Rowson J, Locke M, Mackenzie I, Kipling D, Baird DM. Structural stability and chromosome-specific telomere length is governed by cis-acting determinants in humans. Human molecular genetics. 2006;15:725-33.

197. Lansdorp PM, Verwoerd NP, van de Rijke FM, Dragowska V, Little MT, Dirks RW, et al. Heterogeneity in telomere length of human chromosomes. Human molecular genetics. 1996;5:685-91.

198. Moyzis RK, Buckingham JM, Cram LS, Dani M, Deaven LL, Jones MD, et al. A highly conserved repetitive DNA sequence, (TTAGGG)n, present at the telomeres of human chromosomes. Proceedings of the National Academy of Sciences of the United States of America. 1988;85:6622-6.

199. Londono-Vallejo JA, DerSarkissian H, Cazes L, Thomas G. Differences in telomere length between homologous chromosomes in humans. Nucleic acids research. 2001;29:3164-71.

200. Martens UM, Zijlmans JM, Poon SS, Dragowska W, Yui J, Chavez EA, et al. Short telomeres on human chromosome 17p. Nature genetics. 1998;18:76-80.

201. Perner S, Bruderlein S, Hasel C, Waibel I, Holdenried A, Ciloglu N, et al. Quantifying telomere lengths of human individual chromosome arms by centromere-calibrated fluorescence in situ hybridization and digital imaging. The American journal of pathology. 2003;163:1751-6.

202. Poon SS, Martens UM, Ward RK, Lansdorp PM. Telomere length measurements using digital fluorescence microscopy. Cytometry. 1999;36:267-78.

203. Vermolen BJ, Garini Y, Mai S, Mougey V, Fest T, Chuang TC, et al. Characterizing the three-dimensional organization of telomeres. Cytometry Part A : the journal of the International Society for Analytical Cytology. 2005;67:144-50.

204. Solovei I, Cavallo A, Schermelleh L, Jaunin F, Scasselati C, Cmarko D, et al. Spatial preservation of nuclear chromatin architecture during three-dimensional

fluorescence in situ hybridization (3D-FISH). Experimental cell research. 2002;276:10-23.

205. Schaefer LH, Schuster D, Herz H. Generalized approach for accelerated maximum likelihood based image restoration applied to three-dimensional fluorescence microscopy. Journal of microscopy. 2001;204:99-107.

206. Klonisch T, Wark L, Hombach-Klonisch S, Mai S. Nuclear imaging in three dimensions: a unique tool in cancer research. Annals of anatomy = Anatomischer Anzeiger : official organ of the Anatomische Gesellschaft. 2010;192:292-301.

207. Klewes L, Hobsch C, Katzir N, Rourke D, Garini Y, Mai S. Novel automated three-dimensional genome scanning based on the nuclear architecture of telomeres. Cytometry Part A : the journal of the International Society for Analytical Cytology. 2011;79:159-66.

208. Vaziri H, Dragowska W, Allsopp RC, Thomas TE, Harley CB, Lansdorp PM. Evidence for a mitotic clock in human hematopoietic stem cells: loss of telomeric DNA with age. Proceedings of the National Academy of Sciences of the United States of America. 1994;91:9857-60.

209. Takubo K, Izumiyama-Shimomura N, Honma N, Sawabe M, Arai T, Kato M, et al. Telomere lengths are characteristic in each human individual. Experimental gerontology. 2002;37:523-31.

210. Hoffmann J, Erben Y, Zeiher AM, Dimmeler S, Spyridopoulos I. Telomere length-heterogeneity among myeloid cells is a predictor for chronological ageing. Experimental gerontology. 2009;44:363-6.

211. Moller P, Mayer S, Mattfeldt T, Muller K, Wiegand P, Bruderlein S. Sex-related differences in length and erosion dynamics of human telomeres favor females. Aging. 2009;1:733-9.

212. Okuda K, Bardeguez A, Gardner JP, Rodriguez P, Ganesh V, Kimura M, et al. Telomere length in the newborn. Pediatric research. 2002;52:377-81.

213. Slagboom PE, Droog S, Boomsma DI. Genetic determination of telomere size in humans: a twin study of three age groups. American journal of human genetics. 1994;55:876-82.

214. Graakjaer J, Bischoff C, Korsholm L, Holstebroe S, Vach W, Bohr VA, et al. The pattern of chromosome-specific variations in telomere length in humans is determined by inherited, telomere-near factors and is maintained throughout life. Mechanisms of ageing and development. 2003;124:629-40.

215. Valdes AM, Andrew T, Gardner JP, Kimura M, Oelsner E, Cherkas LF, et al. Obesity, cigarette smoking, and telomere length in women. Lancet (London, England). 2005;366:662-4.

216. Epel ES, Blackburn EH, Lin J, Dhabhar FS, Adler NE, Morrow JD, et al. Accelerated telomere shortening in response to life stress. Proceedings of the National Academy of Sciences of the United States of America. 2004;101:17312-5.

217. Simon NM, Smoller JW, McNamara KL, Maser RS, Zalta AK, Pollack MH, et al. Telomere shortening and mood disorders: preliminary support for a chronic stress model of accelerated aging. Biological psychiatry. 2006;60:432-5.

218. Ishii A, Nakamura K, Kishimoto H, Honma N, Aida J, Sawabe M, et al. Telomere shortening with aging in the human pancreas. Experimental gerontology. 2006;41:882-6.

219. Kimura M, Cherkas LF, Kato BS, Demissie S, Hjelmborg JB, Brimacombe M, et al. Offspring's leukocyte telomere length, paternal age, and telomere elongation in sperm. PLoS genetics. 2008;4:e37.

220. Haycock PC, Heydon EE, Kaptoge S, Butterworth AS, Thompson A, Willeit P. Leucocyte telomere length and risk of cardiovascular disease: systematic review and meta-analysis. BMJ (Clinical research ed). 2014;349:g4227.

221. Zhao J, Miao K, Wang H, Ding H, Wang DW. Association between telomere length and type 2 diabetes mellitus: a meta-analysis. PloS one. 2013;8:e79993.

222. Ma H, Zhou Z, Wei S, Liu Z, Pooley KA, Dunning AM, et al. Shortened telomere length is associated with increased risk of cancer: a meta-analysis. PloS one. 2011;6:e20466.

223. Wentzensen IM, Mirabello L, Pfeiffer RM, Savage SA. The association of telomere length and cancer: a meta-analysis. Cancer epidemiology, biomarkers & prevention : a publication of the American Association for Cancer Research, cosponsored by the American Society of Preventive Oncology. 2011;20:1238-50.

224. Shen J, Gammon MD, Terry MB, Wang Q, Bradshaw P, Teitelbaum SL, et al. Telomere length, oxidative damage, antioxidants and breast cancer risk. International journal of cancer Journal international du cancer. 2009;124:1637-43.

225. Shen J, Terry MB, Gurvich I, Liao Y, Senie RT, Santella RM. Short telomere length and breast cancer risk: a study in sister sets. Cancer research. 2007;67:5538-44.

226. Zheng YL, Loffredo CA, Shields PG, Selim SM. Chromosome 9 arm-specific telomere length and breast cancer risk. Carcinogenesis. 2009;30:1380-6.

227. Gramatges MM, Telli ML, Balise R, Ford JM. Longer relative telomere length in blood from women with sporadic and familial breast cancer compared with healthy controls. Cancer epidemiology, biomarkers & prevention : a publication of the American Association for Cancer Research, cosponsored by the American Society of Preventive Oncology. 2010;19:605-13.

228. Svenson U, Nordfjall K, Stegmayr B, Manjer J, Nilsson P, Tavelin B, et al. Breast cancer survival is associated with telomere length in peripheral blood cells. Cancer research. 2008;68:3618-23.

229. De Vivo I, Prescott J, Wong JY, Kraft P, Hankinson SE, Hunter DJ. A prospective study of relative telomere length and postmenopausal breast cancer risk. Cancer epidemiology, biomarkers & prevention : a publication of the American Association for Cancer Research, cosponsored by the American Society of Preventive Oncology. 2009;18:1152-6.

230. Zheng YL, Ambrosone C, Byrne C, Davis W, Nesline M, McCann SE. Telomere length in blood cells and breast cancer risk: investigations in two case-control studies. Breast cancer research and treatment. 2010;120:769-75.

231. Lee IM, Lin J, Castonguay AJ, Barton NS, Buring JE, Zee RY. Mean leukocyte telomere length and risk of incident colorectal carcinoma in women: a prospective, nested case-control study. Clinical chemistry and laboratory medicine : CCLM / FESCC. 2010;48:259-62.

232. Pooley KA, Sandhu MS, Tyrer J, Shah M, Driver KE, Luben RN, et al. Telomere length in prospective and retrospective cancer case-control studies. Cancer research. 2010;70:3170-6.

233. Zee RY, Castonguay AJ, Barton NS, Buring JE. Mean telomere length and risk of incident colorectal carcinoma: a prospective, nested case-control approach. Cancer epidemiology, biomarkers & prevention : a publication of the American Association for Cancer Research, cosponsored by the American Society of Preventive Oncology. 2009;18:2280-2.

234. Risques RA, Vaughan TL, Li X, Odze RD, Blount PL, Ayub K, et al. Leukocyte telomere length predicts cancer risk in Barrett's esophagus. Cancer epidemiology, biomarkers & prevention : a publication of the American Association for Cancer Research, cosponsored by the American Society of Preventive Oncology. 2007;16:2649-55.

235. Xing J, Ajani JA, Chen M, Izzo J, Lin J, Chen Z, et al. Constitutive short telomere length of chromosome 17p and 12q but not 11q and 2p is associated with an increased risk for esophageal cancer. Cancer prevention research (Philadelphia, Pa). 2009;2:459-65.

236. Hou L, Savage SA, Blaser MJ, Perez-Perez G, Hoxha M, Dioni L, et al. Telomere length in peripheral leukocyte DNA and gastric cancer risk. Cancer epidemiology, biomarkers & prevention : a publication of the American Association for Cancer Research, cosponsored by the American Society of Preventive Oncology. 2009;18:3103-9.

237. Liu X, Bao G, Huo T, Wang Z, He X, Dong G. Constitutive telomere length and gastric cancer risk: case-control analysis in Chinese Han population. Cancer science. 2009;100:1300-5.

238. Wu X, Amos CI, Zhu Y, Zhao H, Grossman BH, Shay JW, et al. Telomere dysfunction: a potential cancer predisposition factor. Journal of the National Cancer Institute. 2003;95:1211-8.

239. Jang JS, Choi YY, Lee WK, Choi JE, Cha SI, Kim YJ, et al. Telomere length and the risk of lung cancer. Cancer science. 2008;99:1385-9.

240. Hosgood HD, 3rd, Cawthon R, He X, Chanock S, Lan Q. Genetic variation in telomere maintenance genes, telomere length, and lung cancer susceptibility. Lung cancer (Amsterdam, Netherlands). 2009;66:157-61.

241. Mirabello L, Garcia-Closas M, Cawthon R, Lissowska J, Brinton LA, Peplonska B, et al. Leukocyte telomere length in a population-based case-control study of ovarian cancer: a pilot study. Cancer causes & control : CCC. 2010;21:77-82.

242. Shao L, Wood CG, Zhang D, Tannir NM, Matin S, Dinney CP, et al. Telomere dysfunction in peripheral lymphocytes as a potential predisposition factor for renal cancer. The Journal of urology. 2007;178:1492-6.

243. Broberg K, Bjork J, Paulsson K, Hoglund M, Albin M. Constitutional short telomeres are strong genetic susceptibility markers for bladder cancer. Carcinogenesis. 2005;26:1263-71.

244. McGrath M, Wong JY, Michaud D, Hunter DJ, De Vivo I. Telomere length, cigarette smoking, and bladder cancer risk in men and women. Cancer epidemiology, biomarkers & prevention : a publication of the American Association for Cancer Research, cosponsored by the American Society of Preventive Oncology. 2007;16:815-9.

245. Willeit P, Willeit J, Mayr A, Weger S, Oberhollenzer F, Brandstatter A, et al. Telomere length and risk of incident cancer and cancer mortality. Jama. 2010;304:69-75.

246. Mayer S, Bruderlein S, Perner S, Waibel I, Holdenried A, Ciloglu N, et al. Sex-specific telomere length profiles and age-dependent erosion dynamics of individual chromosome arms in humans. Cytogenetic and genome research. 2006;112:194-201.

247. Samassekou O, Ntwari A, Hebert J, Yan J. Individual telomere lengths in chronic myeloid leukemia. Neoplasia (New York, NY). 2009;11:1146-54.

248. Surralles J, Hande MP, Marcos R, Lansdorp PM. Accelerated telomere shortening in the human inactive X chromosome. American journal of human genetics. 1999;65:1617-22.

249. Samassekou O, Li H, Hebert J, Ntwari A, Wang H, Cliche CG, et al. Chromosome arm-specific long telomeres: a new clonal event in primary chronic myelogenous leukemia cells. Neoplasia (New York, NY). 2011;13:550-60.

250. Chuang TC, Moshir S, Garini Y, Chuang AY, Young IT, Vermolen B, et al. The three-dimensional organization of telomeres in the nucleus of mammalian cells. BMC biology. 2004;2:12.

251. De Vos WH, Hoebe RA, Joss GH, Haffmans W, Baatout S, Van Oostveldt P, et al. Controlled light exposure microscopy reveals dynamic telomere microterritories throughout the cell cycle. Cytometry Part A : the journal of the International Society for Analytical Cytology. 2009;75:428-39.

252. Lacoste S, Wiechec E, Dos Santos Silva AG, Guffei A, Williams G, Lowbeer M, et al. Chromosomal rearrangements after ex vivo Epstein-Barr virus (EBV) infection of human B cells. Oncogene. 2010;29:503-15.

253. Knecht H, Bruderlein S, Wegener S, Lichtensztejn D, Lichtensztejn Z, Lemieux B, et al. 3D nuclear organization of telomeres in the Hodgkin cell lines U-HO1 and U-

HO1-PTPN1: PTPN1 expression prevents the formation of very short telomeres including "t-stumps". BMC cell biology. 2010;11:99.

254. Knecht H, Sawan B, Lichtensztejn D, Lemieux B, Wellinger RJ, Mai S. The 3D nuclear organization of telomeres marks the transition from Hodgkin to Reed-Sternberg cells. Leukemia. 2009;23:565-73.

255. Knecht H, Sawan B, Lichtensztejn Z, Lichtensztejn D, Mai S. 3D Telomere FISH defines LMP1-expressing Reed-Sternberg cells as end-stage cells with telomere-poor 'ghost' nuclei and very short telomeres. Laboratory investigation; a journal of technical methods and pathology. 2010;90:611-9.

256. Knecht H, Bruderlein S, Mai S, Moller P, Sawan B. 3D structural and functional characterization of the transition from Hodgkin to Reed-Sternberg cells. Annals of anatomy = Anatomischer Anzeiger : official organ of the Anatomische Gesellschaft. 2010;192:302-8.

257. Gadji M, Fortin D, Tsanaclis AM, Garini Y, Katzir N, Wienburg Y, et al. Three-dimensional nuclear telomere architecture is associated with differential time to progression and overall survival in glioblastoma patients. Neoplasia (New York, NY). 2010;12:183-91.

258. Danescu A, Herrero Gonzalez S, Di Cristofano A, Mai S, Hombach-Klonisch S. Three-dimensional nuclear telomere architecture changes during endometrial carcinoma development. Genes, chromosomes & cancer. 2013;52:716-32.

259. Silva AG, Graves HA, Guffei A, Ricca TI, Mortara RA, Jasiulionis MG, et al. Telomere-centromere-driven genomic instability contributes to karyotype evolution in a mouse model of melanoma. Neoplasia (New York, NY). 2010;12:11-9.

260. Gadji M, Adebayo Awe J, Rodrigues P, Kumar R, Houston DS, Klewes L, et al. Profiling three-dimensional nuclear telomeric architecture of myelodysplastic syndromes and acute myeloid leukemia defines patient subgroups. Clinical cancer research : an official journal of the American Association for Cancer Research. 2012;18:3293-304.

261. Adebayo Awe J, Xu MC, Wechsler J, Benali-Furet N, Cayre YE, Saranchuk J, et al. Three-Dimensional Telomeric Analysis of Isolated Circulating Tumor Cells (CTCs) Defines CTC Subpopulations. Translational oncology. 2013;6:51-65.

262. Klewes L, Vallente R, Dupas E, Brand C, Grun D, Guffei A, et al. Three-dimensional Nuclear Telomere Organization in Multiple Myeloma. Translational oncology. 2013;6:749-56.

263. Samassekou O, Hebert J, Mai S, Yan J. Nuclear remodeling of telomeres in chronic myeloid leukemia. Genes, chromosomes & cancer. 2013;52:495-502.

264. Wark L, Danescu A, Natarajan S, Zhu X, Cheng SY, Hombach-Klonisch S, et al. Three-dimensional telomere dynamics in follicular thyroid cancer. Thyroid : official journal of the American Thyroid Association. 2014;24:296-304.

265. Levens D. Cellular MYCro economics: Balancing MYC function with MYC expression. Cold Spring Harbor perspectives in medicine. 2013;3.

266. Boxer LM, Dang CV. Translocations involving c-myc and c-myc function. Oncogene. 2001;20:5595-610.

267. Eilers M, Eisenman RN. Myc's broad reach. Genes & development. 2008;22:2755-66.

268. Dang CV. MYC on the path to cancer. Cell. 2012;149:22-35.

269. Sauter G, Carroll P, Moch H, Kallioniemi A, Kerschmann R, Narayan P, et al. c-myc copy number gains in bladder cancer detected by fluorescence in situ hybridization. The American journal of pathology. 1995;146:1131-9.

270. Nesbit CE, Tersak JM, Prochownik EV. MYC oncogenes and human neoplastic disease. Oncogene. 1999;18:3004-16.

271. Shachaf CM, Felsher DW. Tumor dormancy and MYC inactivation: pushing cancer to the brink of normalcy. Cancer research. 2005;65:4471-4.

272. Bachireddy P, Rakhra K, Felsher DW. Immunology in the clinic review series; focus on cancer: multiple roles for the immune system in oncogene addiction. Clinical and experimental immunology. 2012;167:188-94.

273. Gabay M, Li Y, Felsher DW. MYC activation is a hallmark of cancer initiation and maintenance. Cold Spring Harbor perspectives in medicine. 2014;4.

274. Evan GI, Wyllie AH, Gilbert CS, Littlewood TD, Land H, Brooks M, et al. Induction of apoptosis in fibroblasts by c-myc protein. Cell. 1992;69:119-28.

275. Gibson AW, Cheng T, Johnston RN. Apoptosis induced by c-myc overexpression is dependent on growth conditions. Experimental cell research. 1995;218:351-8.

276. Felsher DW, Bishop JM. Transient excess of MYC activity can elicit genomic instability and tumorigenesis. Proceedings of the National Academy of Sciences of the United States of America. 1999;96:3940-4.

277. Felsher DW, Zetterberg A, Zhu J, Tlsty T, Bishop JM. Overexpression of MYC causes p53-dependent G2 arrest of normal fibroblasts. Proceedings of the National Academy of Sciences of the United States of America. 2000;97:10544-8.

278. Mai S, Hanley-Hyde J, Fluri M. c-Myc overexpression associated DHFR gene amplification in hamster, rat, mouse and human cell lines. Oncogene. 1996;12:277-88.

279. Karlsson A, Deb-Basu D, Cherry A, Turner S, Ford J, Felsher DW. Defective double-strand DNA break repair and chromosomal translocations by MYC overexpression. Proceedings of the National Academy of Sciences of the United States of America. 2003;100:9974-9.

280. Schmitt CA, Lowe SW. Bcl-2 mediates chemoresistance in matched pairs of primary E(mu)-myc lymphomas in vivo. Blood cells, molecules & diseases. 2001;27:206-16.

281. Zindy F, Eischen CM, Randle DH, Kamijo T, Cleveland JL, Sherr CJ, et al. Myc signaling via the ARF tumor suppressor regulates p53-dependent apoptosis and immortalization. Genes & development. 1998;12:2424-33.

282. D'Cruz CM, Gunther EJ, Boxer RB, Hartman JL, Sintasath L, Moody SE, et al. c-MYC induces mammary tumorigenesis by means of a preferred pathway involving spontaneous Kras2 mutations. Nature medicine. 2001;7:235-9.

283. Felsher DW, Bishop JM. Reversible tumorigenesis by MYC in hematopoietic lineages. Molecular cell. 1999;4:199-207.

284. Jain M, Arvanitis C, Chu K, Dewey W, Leonhardt E, Trinh M, et al. Sustained loss of a neoplastic phenotype by brief inactivation of MYC. Science (New York, NY). 2002;297:102-4.

285. Lawlor ER, Soucek L, Brown-Swigart L, Shchors K, Bialucha CU, Evan GI. Reversible kinetic analysis of Myc targets in vivo provides novel insights into Myc-mediated tumorigenesis. Cancer research. 2006;66:4591-601.

286. Marinkovic D, Marinkovic T, Mahr B, Hess J, Wirth T. Reversible lymphomagenesis in conditionally c-MYC expressing mice. International journal of cancer Journal international du cancer. 2004;110:336-42.

287. Shachaf CM, Kopelman AM, Arvanitis C, Karlsson A, Beer S, Mandl S, et al. MYC inactivation uncovers pluripotent differentiation and tumour dormancy in hepatocellular cancer. Nature. 2004;431:1112-7.

288. Choi PS, van Riggelen J, Gentles AJ, Bachireddy P, Rakhra K, Adam SJ, et al. Lymphomas that recur after MYC suppression continue to exhibit oncogene addiction. Proceedings of the National Academy of Sciences of the United States of America. 2011;108:17432-7.

289. Chou YT, Lin HH, Lien YC, Wang YH, Hong CF, Kao YR, et al. EGFR promotes lung tumorigenesis by activating miR-7 through a Ras/ERK/Myc pathway that targets the Ets2 transcriptional repressor ERF. Cancer research. 2010;70:8822-31.

290. Palomero T, Lim WK, Odom DT, Sulis ML, Real PJ, Margolin A, et al. NOTCH1 directly regulates c-MYC and activates a feed-forward-loop transcriptional network promoting leukemic cell growth. Proceedings of the National Academy of Sciences of the United States of America. 2006;103:18261-6.

291. Rahl PB, Lin CY, Seila AC, Flynn RA, McCuine S, Burge CB, et al. c-Myc regulates transcriptional pause release. Cell. 2010;141:432-45.

292. Lin CY, Loven J, Rahl PB, Paranal RM, Burge CB, Bradner JE, et al. Transcriptional amplification in tumor cells with elevated c-Myc. Cell. 2012;151:56-67.

293. Nie Z, Hu G, Wei G, Cui K, Yamane A, Resch W, et al. c-Myc is a universal amplifier of expressed genes in lymphocytes and embryonic stem cells. Cell. 2012;151:68-79.

294. Wolf E, Lin CY, Eilers M, Levens DL. Taming of the beast: shaping Myc-dependent amplification. Trends in cell biology. 2015;25:241-8.

295. Dang CV. MYC, metabolism, cell growth, and tumorigenesis. Cold Spring Harbor perspectives in medicine. 2013;3.

296. Sabo A, Kress TR, Pelizzola M, de Pretis S, Gorski MM, Tesi A, et al. Selective transcriptional regulation by Myc in cellular growth control and lymphomagenesis. Nature. 2014;511:488-92.

297. Walz S, Lorenzin F, Morton J, Wiese KE, von Eyss B, Herold S, et al. Activation and repression by oncogenic MYC shape tumour-specific gene expression profiles. Nature. 2014;511:483-7.

298. Osthus RC, Shim H, Kim S, Li Q, Reddy R, Mukherjee M, et al. Deregulation of glucose transporter 1 and glycolytic gene expression by c-Myc. The Journal of biological chemistry. 2000;275:21797-800.

299. Wise DR, DeBerardinis RJ, Mancuso A, Sayed N, Zhang XY, Pfeiffer HK, et al. Myc regulates a transcriptional program that stimulates mitochondrial glutaminolysis and leads to glutamine addiction. Proceedings of the National Academy of Sciences of the United States of America. 2008;105:18782-7.

300. Li F, Wang Y, Zeller KI, Potter JJ, Wonsey DR, O'Donnell KA, et al. Myc stimulates nuclearly encoded mitochondrial genes and mitochondrial biogenesis. Molecular and cellular biology. 2005;25:6225-34.

301. van Riggelen J, Yetil A, Felsher DW. MYC as a regulator of ribosome biogenesis and protein synthesis. Nature reviews Cancer. 2010;10:301-9.

302. Liu YC, Li F, Handler J, Huang CR, Xiang Y, Neretti N, et al. Global regulation of nucleotide biosynthetic genes by c-Myc. PloS one. 2008;3:e2722.

303. Mannava S, Grachtchouk V, Wheeler LJ, Im M, Zhuang D, Slavina EG, et al. Direct role of nucleotide metabolism in C-MYC-dependent proliferation of melanoma cells. Cell cycle (Georgetown, Tex). 2008;7:2392-400.

304. Zeller KI, Jegga AG, Aronow BJ, O'Donnell KA, Dang CV. An integrated database of genes responsive to the Myc oncogenic transcription factor: identification of direct genomic targets. Genome biology. 2003;4:R69.

305. Bouchard C, Dittrich O, Kiermaier A, Dohmann K, Menkel A, Eilers M, et al. Regulation of cyclin D2 gene expression by the Myc/Max/Mad network: Myc-dependent TRRAP recruitment and histone acetylation at the cyclin D2 promoter. Genes & development. 2001;15:2042-7.

306. Hermeking H, Rago C, Schuhmacher M, Li Q, Barrett JF, Obaya AJ, et al. Identification of CDK4 as a target of c-MYC. Proceedings of the National Academy of Sciences of the United States of America. 2000;97:2229-34.

307. Rempel RE, Mori S, Gasparetto M, Glozak MA, Andrechek ER, Adler SB, et al. A role for E2F activities in determining the fate of Myc-induced lymphomagenesis. PLoS genetics. 2009;5:e1000640.

308. Khanna KK, Jackson SP. DNA double-strand breaks: signaling, repair and the cancer connection. Nature genetics. 2001;27:247-54.

309. Vafa O, Wade M, Kern S, Beeche M, Pandita TK, Hampton GM, et al. c-Myc can induce DNA damage, increase reactive oxygen species, and mitigate p53 function: a mechanism for oncogene-induced genetic instability. Molecular cell. 2002;9:1031-44.

310. Tanaka H, Matsumura I, Ezoe S, Satoh Y, Sakamaki T, Albanese C, et al. E2F1 and c-Myc potentiate apoptosis through inhibition of NF-kappaB activity that facilitates MnSOD-mediated ROS elimination. Molecular cell. 2002;9:1017-29.

311. Dang CV, Li F, Lee LA. Could MYC induction of mitochondrial biogenesis be linked to ROS production and genomic instability? Cell cycle (Georgetown, Tex). 2005;4:1465-6.

312. Prochownik EV. c-Myc: linking transformation and genomic instability. Current molecular medicine. 2008;8:446-58.

313. Wonsey DR, Zeller KI, Dang CV. The c-Myc target gene PRDX3 is required for mitochondrial homeostasis and neoplastic transformation. Proceedings of the National Academy of Sciences of the United States of America. 2002;99:6649-54.

314. Ray S, Atkuri KR, Deb-Basu D, Adler AS, Chang HY, Herzenberg LA, et al. MYC can induce DNA breaks in vivo and in vitro independent of reactive oxygen species. Cancer research. 2006;66:6598-605.

315. Campaner S, Amati B. Two sides of the Myc-induced DNA damage response: from tumor suppression to tumor maintenance. Cell division. 2012;7:6.

316. Li Q, Dang CV. c-Myc overexpression uncouples DNA replication from mitosis. Molecular and cellular biology. 1999;19:5339-51.

317. Gandarillas A, Davies D, Blanchard JM. Normal and c-Myc-promoted human keratinocyte differentiation both occur via a novel cell cycle involving cellular growth and endoreplication. Oncogene. 2000;19:3278-89.

318. Pierce SB, Yost C, Britton JS, Loo LW, Flynn EM, Edgar BA, et al. dMyc is required for larval growth and endoreplication in Drosophila. Development (Cambridge, England). 2004;131:2317-27.

319. Barlow JH, Faryabi RB, Callen E, Wong N, Malhowski A, Chen HT, et al. Identification of early replicating fragile sites that contribute to genome instability. Cell. 2013;152:620-32.

320. Li Z, Owonikoko TK, Sun SY, Ramalingam SS, Doetsch PW, Xiao ZQ, et al. c-Myc suppression of DNA double-strand break repair. Neoplasia (New York, NY). 2012;14:1190-202.

321. Luoto KR, Meng AX, Wasylishen AR, Zhao H, Coackley CL, Penn LZ, et al. Tumor cell kill by c-MYC depletion: role of MYC-regulated genes that control DNA double-strand break repair. Cancer research. 2010;70:8748-59.

322. Kuzyk A, Mai S. c-MYC-induced genomic instability. Cold Spring Harbor perspectives in medicine. 2014;4:a014373.

323. Denis N, Kitzis A, Kruh J, Dautry F, Corcos D. Stimulation of methotrexate resistance and dihydrofolate reductase gene amplification by c-myc. Oncogene. 1991;6:1453-7.

324. Guijon FB, Greulich-Bode K, Paraskevas M, Baker P, Mai S. Premalignant cervical lesions are characterized by dihydrofolate reductase gene amplification and c-

Myc overexpression: possible biomarkers. Journal of lower genital tract disease. 2007;11:265-72.

325. Mai S. Overexpression of c-myc precedes amplification of the gene encoding dihydrofolate reductase. Gene. 1994;148:253-60.

326. Taylor C, Mai S. c-Myc-associated genomic instability of the dihydrofolate reductase locus in vivo. Cancer detection and prevention. 1998;22:350-6.

327. Benner SE, Wahl GM, Von Hoff DD. Double minute chromosomes and homogeneously staining regions in tumors taken directly from patients versus in human tumor cell lines. Anti-cancer drugs. 1991;2:11-25.

328. Windle B, Draper BW, Yin YX, O'Gorman S, Wahl GM. A central role for chromosome breakage in gene amplification, deletion formation, and amplicon integration. Genes & development. 1991;5:160-74.

329. Chernova OB, Chernov MV, Ishizaka Y, Agarwal ML, Stark GR. MYC abrogates p53-mediated cell cycle arrest in N-(phosphonacetyl)-L-aspartate-treated cells, permitting CAD gene amplification. Molecular and cellular biology. 1998;18:536-45.

330. Eberhardy SR, Farnham PJ. c-Myc mediates activation of the cad promoter via a post-RNA polymerase II recruitment mechanism. The Journal of biological chemistry. 2001;276:48562-71.

331. Fukasawa K, Wiener F, Vande Woude GF, Mai S. Genomic instability and apoptosis are frequent in p53 deficient young mice. Oncogene. 1997;15:1295-302.

332. George RE, Kenyon RM, McGuckin AG, Malcolm AJ, Pearson AD, Lunec J. Investigation of co-amplification of the candidate genes ornithine decarboxylase, ribonucleotide reductase, syndecan-1 and a DEAD box gene, DDX1, with N-myc in

neuroblastoma. United Kingdom Children's Cancer Study Group. Oncogene. 1996;12:1583-7.

333. Kuschak TI, Taylor C, McMillan-Ward E, Israels S, Henderson DW, Mushinski JF, et al. The ribonucleotide reductase R2 gene is a non-transcribed target of c-Myc-induced genomic instability. Gene. 1999;238:351-65.

334. Mai S, Hanley-Hyde J, Rainey GJ, Kuschak TI, Paul JT, Littlewood TD, et al. Chromosomal and extrachromosomal instability of the cyclin D2 gene is induced by Myc overexpression. Neoplasia (New York, NY). 1999;1:241-52.

335. Miltenberger RJ, Sukow KA, Farnham PJ. An E-box-mediated increase in cad transcription at the G1/S-phase boundary is suppressed by inhibitory c-Myc mutants. Molecular and cellular biology. 1995;15:2527-35.

336. Rounbehler RJ, Li W, Hall MA, Yang C, Fallahi M, Cleveland JL. Targeting ornithine decarboxylase impairs development of MYCN-amplified neuroblastoma. Cancer research. 2009;69:547-53.

337. Kuschak TI, Kuschak BC, Taylor CL, Wright JA, Wiener F, Mai S. c-Myc initiates illegitimate replication of the ribonucleotide reductase R2 gene. Oncogene. 2002;21:909-20.

338. Rockwood LD, Torrey TA, Kim JS, Coleman AE, Kovalchuk AL, Xiang S, et al. Genomic instability in mouse Burkitt lymphoma is dominated by illegitimate genetic recombinations, not point mutations. Oncogene. 2002;21:7235-40.

339. Smith G, Taylor-Kashton C, Dushnicky L, Symons S, Wright J, Mai S. c-Myc-induced extrachromosomal elements carry active chromatin. Neoplasia (New York, NY). 2003;5:110-20.

340. Chen Q, Shi X, Rudolph C, Yu Y, Zhang D, Zhao X, et al. Recurrent trisomy and Robertsonian translocation of chromosome 14 in murine iPS cell lines. Chromosome research : an international journal on the molecular, supramolecular and evolutionary aspects of chromosome biology. 2011;19:857-68.

341. Goncalves Dos Santos Silva A, Sarkar R, Harizanova J, Guffei A, Mowat M, Garini Y, et al. Centromeres in cell division, evolution, nuclear organization and disease. Journal of cellular biochemistry. 2008;104:2040-58.

342. Guffei A, Lichtensztejn Z, Goncalves Dos Santos Silva A, Louis SF, Caporali A, Mai S. c-Myc-dependent formation of Robertsonian translocation chromosomes in mouse cells. Neoplasia (New York, NY). 2007;9:578-88.

343. Mai S, Fluri M, Siwarski D, Huppi K. Genomic instability in MycER-activated Rat1A-MycER cells. Chromosome research : an international journal on the molecular, supramolecular and evolutionary aspects of chromosome biology. 1996;4:365-71.

344. Prochownik EV, Li Y. The ever expanding role for c-Myc in promoting genomic instability. Cell cycle (Georgetown, Tex). 2007;6:1024-9.

345. Caporali A, Wark L, Vermolen BJ, Garini Y, Mai S. Telomeric aggregates and end-to-end chromosomal fusions require myc box II. Oncogene. 2007;26:1398-406.

346. Fest T, Guffei A, Williams G, Silva S, Mai S. Uncoupling of genomic instability and tumorigenesis in a mouse model of Burkitt's lymphoma expressing a conditional box II-deleted Myc protein. Oncogene. 2005;24:2944-53.

347. Fest T, Mougey V, Dalstein V, Hagerty M, Milette D, Silva S, et al. c-MYC overexpression in Ba/F3 cells simultaneously elicits genomic instability and apoptosis. Oncogene. 2002;21:2981-90.

348. Neiman PE, Thomas SJ, Loring G. Induction of apoptosis during normal and neoplastic B-cell development in the bursa of Fabricius. Proceedings of the National Academy of Sciences of the United States of America. 1991;88:5857-61.

349. Askew DS, Ashmun RA, Simmons BC, Cleveland JL. Constitutive c-myc expression in an IL-3-dependent myeloid cell line suppresses cell cycle arrest and accelerates apoptosis. Oncogene. 1991;6:1915-22.

350. Martin-Subero JI, Odero MD, Hernandez R, Cigudosa JC, Agirre X, Saez B, et al. Amplification of IGH/MYC fusion in clinically aggressive IGH/BCL2-positive germinal center B-cell lymphomas. Genes, chromosomes & cancer. 2005;43:414-23.

351. Ozdek A, Sarac S, Akyol MU, Sungur A, Yilmaz T. c-myc and bcl-2 Expression in supraglottic squamous cell carcinoma of the larynx. Otolaryngology--head and neck surgery : official journal of American Academy of Otolaryngology-Head and Neck Surgery. 2004;131:77-83.

352. Letai A, Sorcinelli MD, Beard C, Korsmeyer SJ. Antiapoptotic BCL-2 is required for maintenance of a model leukemia. Cancer cell. 2004;6:241-9.

353. Zhang XY, Pfeiffer HK, Mellert HS, Stanek TJ, Sussman RT, Kumari A, et al. Inhibition of the single downstream target BAG1 activates the latent apoptotic potential of MYC. Molecular and cellular biology. 2011;31:5037-45.

354. McMahon SB. MYC and the control of apoptosis. Cold Spring Harbor perspectives in medicine. 2014;4:a014407.

355. Eischen CM, Weber JD, Roussel MF, Sherr CJ, Cleveland JL. Disruption of the ARF-Mdm2-p53 tumor suppressor pathway in Myc-induced lymphomagenesis. Genes & development. 1999;13:2658-69.

356. Amanullah A, Liebermann DA, Hoffman B. p53-independent apoptosis associated with c-Myc-mediated block in myeloid cell differentiation. Oncogene. 2000;19:2967-77.

357. Boone DN, Qi Y, Li Z, Hann SR. Egr1 mediates p53-independent c-Myc-induced apoptosis via a noncanonical ARF-dependent transcriptional mechanism. Proceedings of the National Academy of Sciences of the United States of America. 2011;108:632-7.

358. Hagiyama H, Adachi T, Yoshida T, Nomura T, Miyasaka N, Honjo T, et al. Signaling through the antigen receptor of B lymphocytes activates a p53-independent pathway of c-Myc-induced apoptosis. Oncogene. 1999;18:4091-8.

359. Sakamuro D, Eviner V, Elliott KJ, Showe L, White E, Prendergast GC. c-Myc induces apoptosis in epithelial cells by both p53-dependent and p53-independent mechanisms. Oncogene. 1995;11:2411-8.

360. Trudel M, Lanoix J, Barisoni L, Blouin MJ, Desforges M, L'Italien C, et al. C-myc-induced apoptosis in polycystic kidney disease is Bcl-2 and p53 independent. The Journal of experimental medicine. 1997;186:1873-84.

361. Gamberi G, Benassi MS, Bohling T, Ragazzini P, Molendini L, Sollazzo MR, et al. C-myc and c-fos in human osteosarcoma: prognostic value of mRNA and protein expression. Oncology. 1998;55:556-63.

362. Bettess MD, Dubois N, Murphy MJ, Dubey C, Roger C, Robine S, et al. c-Myc is required for the formation of intestinal crypts but dispensable for homeostasis of the adult intestinal epithelium. Molecular and cellular biology. 2005;25:7868-78.

363. Hurlin PJ. Control of vertebrate development by MYC. Cold Spring Harbor perspectives in medicine. 2013;3:a014332.

364. Fletcher S, Hamilton AD. Protein-protein interaction inhibitors: small molecules from screening techniques. Current topics in medicinal chemistry. 2007;7:922-7.

365. Farrell AS, Sears RC. MYC degradation. Cold Spring Harbor perspectives in medicine. 2014;4.

366. Gsponer J, Babu MM. The rules of disorder or why disorder rules. Progress in biophysics and molecular biology. 2009;99:94-103.

367. McKeown MR, Bradner JE. Therapeutic strategies to inhibit MYC. Cold Spring Harbor perspectives in medicine. 2014;4.

368. Wells JA, McClendon CL. Reaching for high-hanging fruit in drug discovery at protein-protein interfaces. Nature. 2007;450:1001-9.

369. Clausen DM, Guo J, Parise RA, Beumer JH, Egorin MJ, Lazo JS, et al. In vitro cytotoxicity and in vivo efficacy, pharmacokinetics, and metabolism of 10074-G5, a novel small-molecule inhibitor of c-Myc/Max dimerization. The Journal of pharmacology and experimental therapeutics. 2010;335:715-27.

370. Guo J, Parise RA, Joseph E, Egorin MJ, Lazo JS, Prochownik EV, et al. Efficacy, pharmacokinetics, tisssue distribution, and metabolism of the Myc-Max disruptor, 10058-F4 [Z,E]-5-[4-ethylbenzylidine]-2-thioxothiazolidin-4-one, in mice. Cancer chemotherapy and pharmacology. 2009;63:615-25.

371. Savino M, Annibali D, Carucci N, Favuzzi E, Cole MD, Evan GI, et al. The action mechanism of the Myc inhibitor termed Omomyc may give clues on how to target Myc for cancer therapy. PloS one. 2011;6:e22284.

372. Soucek L, Whitfield J, Martins CP, Finch AJ, Murphy DJ, Sodir NM, et al. Modelling Myc inhibition as a cancer therapy. Nature. 2008;455:679-83.

373. Delmore JE, Issa GC, Lemieux ME, Rahl PB, Shi J, Jacobs HM, et al. BET bromodomain inhibition as a therapeutic strategy to target c-Myc. Cell. 2011;146:904-17.

374. Zuber J, Shi J, Wang E, Rappaport AR, Herrmann H, Sison EA, et al. RNAi screen identifies Brd4 as a therapeutic target in acute myeloid leukaemia. Nature. 2011;478:524-8.

375. Potter M. Immunoglobulin-producing tumors and myeloma proteins of mice. Physiological reviews. 1972;52:631-719.

376. Dunn TB. Plasma-cell neoplasms beginning in the ileocecal area in strain C3H mice. Journal of the National Cancer Institute. 1957;19:371-91.

377. Potter M, Wax JS, Blankenhorn E. BALB/c subline differences in susceptibility to plasmacytoma induction. Current topics in microbiology and immunology. 1985;122:234-41.

378. Warner N. Autoimmunity and the pathogenesis of plasma cell tumor induction in NZB and hybrid mice. Immunogenetics. 1975;2:1-20.

379. Merwin RM, Algire GH. Induction of plasma-cell neoplasms and fibrosarcomas in BALB/c mice carrying diffusion chambers. Proceedings of the Society for Experimental Biology and Medicine Society for Experimental Biology and Medicine (New York, NY). 1959;101:437-9.

380. Merwin RM, Redmon LW. INDUCTION OF PLASMA CELL TUMORS AND SARCOMAS IN MICE BY DIFFUSION CHAMBERS PLACED IN THE PERITONEAL CAVITY. Journal of the National Cancer Institute. 1963;31:997-1017.

381. Potter M, Wax JS. Peritoneal plasmacytomagenesis in mice: comparison of different pristane dose regimens. Journal of the National Cancer Institute. 1983;71:391-5.

382. Potter M, Wiener F. Plasmacytomagenesis in mice: model of neoplastic development dependent upon chromosomal translocations. Carcinogenesis. 1992;13:1681-97.

383. Anderson AO, Wax JS, Potter M. Differences in the peritoneal response to pristane in BALB/cAnPt and BALB/cJ mice. Current topics in microbiology and immunology. 1985;122:242-53.

384. Leak LV, Potter M, Mayfield WJ. Response of the peritoneal mesothelium to the mineral oil, pristane. Current topics in microbiology and immunology. 1985;122:221-33.

385. Potter M, Maccardle RC. HISTOLOGY OF DEVELOPING PLASMA CELL NEOPLASIA INDUCED BY MINERAL OIL IN BALB/C MICE. Journal of the National Cancer Institute. 1964;33:497-515.

386. Potter M. Neoplastic development in plasma cells. Immunological reviews. 2003;194:177-95.

387. Hilbert DM, Kopf M, Mock BA, Kohler G, Rudikoff S. Interleukin 6 is essential for in vivo development of B lineage neoplasms. The Journal of experimental medicine. 1995;182:243-8.

388. Potter M, Pumphrey JG, Walters JL. Growth of primary plasmacytomas in the mineral oil-conditioned peritoneal environment. Journal of the National Cancer Institute. 1972;49:305-8.

389. Vink A, Coulie P, Warnier G, Renauld JC, Stevens M, Donckers D, et al. Mouse plasmacytoma growth in vivo: enhancement by interleukin 6 (IL-6) and inhibition by antibodies directed against IL-6 or its receptor. The Journal of experimental medicine. 1990;172:997-1000.

390. Lattanzio G, Libert C, Aquilina M, Cappelletti M, Ciliberto G, Musiani P, et al. Defective development of pristane-oil-induced plasmacytomas in interleukin-6-deficient BALB/c mice. The American journal of pathology. 1997;151:689-96.

391. Adams JM, Gerondakis S, Webb E, Corcoran LM, Cory S. Cellular myc oncogene is altered by chromosome translocation to an immunoglobulin locus in murine plasmacytomas and is rearranged similarly in human Burkitt lymphomas. Proceedings of the National Academy of Sciences of the United States of America. 1983;80:1982-6.

392. Klein G. Specific chromosomal translocations and the genesis of B-cell-derived tumors in mice and men. Cell. 1983;32:311-5.

393. Evan GI, Littlewood TD. The role of c-myc in cell growth. Current opinion in genetics & development. 1993;3:44-9.

394. Pelengaris S, Khan M, Evan GI. Suppression of Myc-induced apoptosis in beta cells exposes multiple oncogenic properties of Myc and triggers carcinogenic progression. Cell. 2002;109:321-34.

395. Nordan RP, Potter M. A macrophage-derived factor required by plasmacytomas for survival and proliferation in vitro. Science (New York, NY). 1986;233:566-9.

396. Takakura K, Yamada H, Hollander VP. Studies on the pathogenesis of plasma cell tumors. II. The role of mast cells and pituitary glycoprotein hormones in the inhibition of plasma cell tumorigenesis. Cancer research. 1966;26:2564-9.

397. Clynes R, Wax J, Stanton LW, Smith-Gill S, Potter M, Marcu KB. Rapid induction of IgM-secreting murine plasmacytomas by pristane and an immunoglobulin heavy-chain promoter/enhancer-driven c-myc/v-Ha-ras retrovirus. Proceedings of the National Academy of Sciences of the United States of America. 1988;85:6067-71.

398. Ohno S, Migita S, Wiener F, Babonits M, Klein G, Mushinski JF, et al. Chromosomal translocations activating myc sequences and transduction of v-abl are critical events in the rapid induction of plasmacytomas by pristane and abelson virus. The Journal of experimental medicine. 1984;159:1762-77.

399. Wiener F, Coleman A, Mock BA, Potter M. Nonrandom chromosomal change (trisomy 11) in murine plasmacytomas induced by an ABL-MYC retrovirus. Cancer research. 1995;55:1181-8.

400. Ohno S, Babonits M, Wiener F, Spira J, Klein G, Potter M. Nonrandom chromosome changes involving the Ig gene-carrying chromosomes 12 and 6 in pristane-induced mouse plasmacytomas. Cell. 1979;18:1001-7.

401. Potter M, Mushinski JF, Mushinski EB, Brust S, Wax JS, Wiener F, et al. Avian v-myc replaces chromosomal translocation in murine plasmacytomagenesis. Science (New York, NY). 1987;235:787-9.

402. Wiener F, Schmalter AK, Mowat MR, Mai S. Duplication of Subcytoband 11E2 of Chromosome 11 Is Regularly Associated with Accelerated Tumor Development in v-abl/myc-Induced Mouse Plasmacytomas. Genes & cancer. 2010;1:847-58.

403. Benedek K, Chudoba I, Klein G, Wiener F, Mai S. Rearrangements of the telomeric region of mouse chromosome 11 in Pre-B ABL/MYC cells revealed by mBANDing, spectral karyotyping, and fluorescence in-situ hybridization with a subtelomeric probe. Chromosome research : an international journal on the molecular, supramolecular and evolutionary aspects of chromosome biology. 2004;12:777-85.

404. Robertson DL, Yau P, Dobbertin DC, Sweeney TK, Thach SS, Brendler T, et al. Relationships between intracisternal type A and extracellular oncornavirus-like particles produced in murine MOPC-460 myeloma cells. Journal of virology. 1976;18:344-55.

405. Sarkar R, Guffei A, Vermolen BJ, Garini Y, Mai S. Alterations of centromere positions in nuclei of immortalized and malignant mouse lymphocytes. Cytometry Part A : the journal of the International Society for Analytical Cytology. 2007;71:386-92.

406. Righolt CH, Wiener F, Taylor-Kashton C, Harizanova J, Vermolen BJ, Garini Y, et al. Translocation frequencies and chromosomal proximities for selected mouse chromosomes in primary B lymphocytes. Cytometry Part A : the journal of the International Society for Analytical Cytology. 2011;79:276-83.

407. Helou K, Walentinsson A, Beckmann B, Johansson A, Hedrich HJ, Szpirer C, et al. Analysis of genetic changes in rat endometrial carcinomas by means of comparative genomic hybridization. Cancer genetics and cytogenetics. 2001;127:118-27.

408. Bermudo R, Abia D, Ferrer B, Nayach I, Benguria A, Zaballos A, et al. Co-regulation analysis of closely linked genes identifies a highly recurrent gain on chromosome 17q25.3 in prostate cancer. BMC cancer. 2008;8:315.

409. Zou H, Kang X, Pang LJ, Hu W, Zhao J, Qi Y, et al. Xp11 translocation renal cell carcinoma in adults: a clinicopathological and comparative genomic hybridization study. International journal of clinical and experimental pathology. 2014;7:236-45.

410. Rice KL, Lin X, Wolniak K, Ebert BL, Berkofsky-Fessler W, Buzzai M, et al. Analysis of genomic aberrations and gene expression profiling identifies novel lesions and pathways in myeloproliferative neoplasms. Blood cancer journal. 2011;1:e40.

411. Toffoli S, Bar I, Abdel-Sater F, Delree P, Hilbert P, Cavallin F, et al. Identification by array comparative genomic hybridization of a new amplicon on chromosome 17q highly recurrent in BRCA1 mutated triple negative breast cancer. Breast cancer research : BCR. 2014;16:466.

412. Kawasaki H, Altieri DC, Lu CD, Toyoda M, Tenjo T, Tanigawa N. Inhibition of apoptosis by survivin predicts shorter survival rates in colorectal cancer. Cancer research. 1998;58:5071-4.

413. Sarela AI, Macadam RC, Farmery SM, Markham AF, Guillou PJ. Expression of the antiapoptosis gene, survivin, predicts death from recurrent colorectal carcinoma. Gut. 2000;46:645-50.

414. Shinohara ET, Gonzalez A, Massion PP, Chen H, Li M, Freyer AS, et al. Nuclear survivin predicts recurrence and poor survival in patients with resected nonsmall cell lung carcinoma. Cancer. 2005;103:1685-92.

415. Brinkschmidt C, Christiansen H, Terpe HJ, Simon R, Boecker W, Lampert F, et al. Comparative genomic hybridization (CGH) analysis of neuroblastomas--an important methodological approach in paediatric tumour pathology. The Journal of pathology. 1997;181:394-400.

416. Lastowska M, Nacheva E, McGuckin A, Curtis A, Grace C, Pearson A, et al. Comparative genomic hybridization study of primary neuroblastoma tumors. United Kingdom Children's Cancer Study Group. Genes, chromosomes & cancer. 1997;18:162-9.

417. Plantaz D, Mohapatra G, Matthay KK, Pellarin M, Seeger RC, Feuerstein BG. Gain of chromosome 17 is the most frequent abnormality detected in neuroblastoma by comparative genomic hybridization. The American journal of pathology. 1997;150:81-9.

418. Bown N, Cotterill S, Lastowska M, O'Neill S, Pearson AD, Plantaz D, et al. Gain of chromosome arm 17q and adverse outcome in patients with neuroblastoma. The New England journal of medicine. 1999;340:1954-61.

419. Lastowska M, Cotterill S, Pearson AD, Roberts P, McGuckin A, Lewis I, et al. Gain of chromosome arm 17q predicts unfavourable outcome in neuroblastoma patients. U.K. Children's Cancer Study Group and the U.K. Cancer Cytogenetics Group. European journal of cancer (Oxford, England : 1990). 1997;33:1627-33.

420. Trakhtenbrot L, Cohen N, Betts DR, Niggli FK, Amariglio N, Brok-Simoni F, et al. Interphase fluorescence in situ hybridization detection of chromosome 17 and 17q region gains in neuroblastoma: are they secondary events? Cancer genetics and cytogenetics. 2002;137:95-101.

421. Caron H. Allelic loss of chromosome 1 and additional chromosome 17 material are both unfavourable prognostic markers in neuroblastoma. Medical and pediatric oncology. 1995;24:215-21.

422. Vandesompele J, Baudis M, De Preter K, Van Roy N, Ambros P, Bown N, et al. Unequivocal delineation of clinicogenetic subgroups and development of a new model for improved outcome prediction in neuroblastoma. Journal of clinical oncology : official journal of the American Society of Clinical Oncology. 2005;23:2280-99.

423. Theissen J, Oberthuer A, Hombach A, Volland R, Hertwig F, Fischer M, et al. Chromosome 17/17q gain and unaltered profiles in high resolution array-CGH are

prognostically informative in neuroblastoma. Genes, chromosomes & cancer. 2014;53:639-49.

424. Lastowska M, Viprey V, Santibanez-Koref M, Wappler I, Peters H, Cullinane C, et al. Identification of candidate genes involved in neuroblastoma progression by combining genomic and expression microarrays with survival data. Oncogene. 2007;26:7432-44.

425. Lastowska M, Chung YJ, Cheng Ching N, Haber M, Norris MD, Kees UR, et al. Regions syntenic to human 17q are gained in mouse and rat neuroblastoma. Genes, chromosomes & cancer. 2004;40:158-63.

426. Combaret V, Brejon S, Iacono I, Schleiermacher G, Pierron G, Ribeiro A, et al. Determination of 17q gain in patients with neuroblastoma by analysis of circulating DNA. Pediatric blood & cancer. 2011;56:757-61.

427. Gurney JG, Ross JA, Wall DA, Bleyer WA, Severson RK, Robison LL. Infant cancer in the U.S.: histology-specific incidence and trends, 1973 to 1992. Journal of pediatric hematology/oncology. 1997;19:428-32.

428. Howlander NN, AM; Krapcho M; et al. SEER Cancer Statistics Review, 1975-2009. In: Institute NC, editor. Bethesda, Md.; 2012.

429. London WB, Castleberry RP, Matthay KK, Look AT, Seeger RC, Shimada H, et al. Evidence for an age cutoff greater than 365 days for neuroblastoma risk group stratification in the Children's Oncology Group. Journal of clinical oncology : official journal of the American Society of Clinical Oncology. 2005;23:6459-65.

430. Henderson TO, Bhatia S, Pinto N, London WB, McGrady P, Crotty C, et al. Racial and ethnic disparities in risk and survival in children with neuroblastoma: a

Children's Oncology Group study. Journal of clinical oncology : official journal of the American Society of Clinical Oncology. 2011;29:76-82.

431. Schilling FH, Spix C, Berthold F, Erttmann R, Fehse N, Hero B, et al. Neuroblastoma screening at one year of age. The New England journal of medicine. 2002;346:1047-53.

432. Takeuchi LA, Hachitanda Y, Woods WG, Tuchman M, Lemieux B, Brisson L, et al. Screening for neuroblastoma in North America. Preliminary results of a pathology review from the Quebec Project. Cancer. 1995;76:2363-71.

433. Woods WG, Gao RN, Shuster JJ, Robison LL, Bernstein M, Weitzman S, et al. Screening of infants and mortality due to neuroblastoma. The New England journal of medicine. 2002;346:1041-6.

434. Horner MR, LA; Krapcho, M; et al. SEER Cancer Statistics Review, 1975-2006. In: Institute NC, editor. Bethesda, Md.; 2009.

435. Mosse YP, Deyell RJ, Berthold F, Nagakawara A, Ambros PF, Monclair T, et al. Neuroblastoma in older children, adolescents and young adults: a report from the International Neuroblastoma Risk Group project. Pediatric blood & cancer. 2014;61:627-35.

436. Cotterill SJ, Pearson AD, Pritchard J, Foot AB, Roald B, Kohler JA, et al. Clinical prognostic factors in 1277 patients with neuroblastoma: results of The European Neuroblastoma Study Group 'Survey' 1982-1992. European journal of cancer (Oxford, England : 1990). 2000;36:901-8.

437. Evans AE, Albo V, D'Angio GJ, Finklestein JZ, Leiken S, Santulli T, et al. Factors influencing survival of children with nonmetastatic neuroblastoma. Cancer. 1976;38:661-6.

438. Schmidt ML, Lukens JN, Seeger RC, Brodeur GM, Shimada H, Gerbing RB, et al. Biologic factors determine prognosis in infants with stage IV neuroblastoma: A prospective Children's Cancer Group study. Journal of clinical oncology : official journal of the American Society of Clinical Oncology. 2000;18:1260-8.

439. Vo KT, Matthay KK, Neuhaus J, London WB, Hero B, Ambros PF, et al. Clinical, biologic, and prognostic differences on the basis of primary tumor site in neuroblastoma: a report from the international neuroblastoma risk group project. Journal of clinical oncology : official journal of the American Society of Clinical Oncology. 2014;32:3169-76.

440. Shimada H, Ambros IM, Dehner LP, Hata J, Joshi VV, Roald B, et al. The International Neuroblastoma Pathology Classification (the Shimada system). Cancer. 1999;86:364-72.

441. Shimada H, Umehara S, Monobe Y, Hachitanda Y, Nakagawa A, Goto S, et al. International neuroblastoma pathology classification for prognostic evaluation of patients with peripheral neuroblastic tumors: a report from the Children's Cancer Group. Cancer. 2001;92:2451-61.

442. Schwab M. Amplification of N-myc as a prognostic marker for patients with neuroblastoma. Seminars in cancer biology. 1993;4:13-8.

443. Seeger RC, Brodeur GM, Sather H, Dalton A, Siegel SE, Wong KY, et al. Association of multiple copies of the N-myc oncogene with rapid progression of neuroblastomas. The New England journal of medicine. 1985;313:1111-6.

444. Attiyeh EF, London WB, Mosse YP, Wang Q, Winter C, Khazi D, et al. Chromosome 1p and 11q deletions and outcome in neuroblastoma. The New England journal of medicine. 2005;353:2243-53.

445. Defferrari R, Mazzocco K, Ambros IM, Ambros PF, Bedwell C, Beiske K, et al. Influence of segmental chromosome abnormalities on survival in children over the age of 12 months with unresectable localised peripheral neuroblastic tumours without MYCN amplification. British journal of cancer. 2015;112:290-5.

446. Janoueix-Lerosey I, Schleiermacher G, Michels E, Mosseri V, Ribeiro A, Lequin D, et al. Overall genomic pattern is a predictor of outcome in neuroblastoma. Journal of clinical oncology : official journal of the American Society of Clinical Oncology. 2009;27:1026-33.

447. Maris JM. The biologic basis for neuroblastoma heterogeneity and risk stratification. Current opinion in pediatrics. 2005;17:7-13.

448. Schleiermacher G, Janoueix-Lerosey I, Ribeiro A, Klijanienko J, Couturier J, Pierron G, et al. Accumulation of segmental alterations determines progression in neuroblastoma. Journal of clinical oncology : official journal of the American Society of Clinical Oncology. 2010;28:3122-30.

449. Bresler SC, Weiser DA, Huwe PJ, Park JH, Krytska K, Ryles H, et al. ALK mutations confer differential oncogenic activation and sensitivity to ALK inhibition therapy in neuroblastoma. Cancer cell. 2014;26:682-94.

450. Mosse YP, Laudenslager M, Longo L, Cole KA, Wood A, Attiyeh EF, et al. Identification of ALK as a major familial neuroblastoma predisposition gene. Nature. 2008;455:930-5.

451. Lundberg G, Sehic D, Lansberg JK, Ora I, Frigyesi A, Castel V, et al. Alternative lengthening of telomeres--an enhanced chromosomal instability in aggressive non-MYCN amplified and telomere elongated neuroblastomas. Genes, chromosomes & cancer. 2011;50:250-62.

452. Ohali A, Avigad S, Ash S, Goshen Y, Luria D, Feinmesser M, et al. Telomere length is a prognostic factor in neuroblastoma. Cancer. 2006;107:1391-9.

453. Onitake Y, Hiyama E, Kamei N, Yamaoka H, Sueda T, Hiyama K. Telomere biology in neuroblastoma: telomere binding proteins and alternative strengthening of telomeres. Journal of pediatric surgery. 2009;44:2258-66.

454. Cozzi DA, Mele E, Ceccanti S, Natale F, Clerico A, Schiavetti A, et al. Long-term follow-up of the "wait and see" approach to localized perinatal adrenal neuroblastoma. World journal of surgery. 2013;37:459-65.

455. Kushner BH, Cheung NK, LaQuaglia MP, Ambros PF, Ambros IM, Bonilla MA, et al. Survival from locally invasive or widespread neuroblastoma without cytotoxic therapy. Journal of clinical oncology : official journal of the American Society of Clinical Oncology. 1996;14:373-81.

456. Nickerson HJ, Matthay KK, Seeger RC, Brodeur GM, Shimada H, Perez C, et al. Favorable biology and outcome of stage IV-S neuroblastoma with supportive care or minimal therapy: a Children's Cancer Group study. Journal of clinical oncology : official journal of the American Society of Clinical Oncology. 2000;18:477-86.

457. Goto S, Umehara S, Gerbing RB, Stram DO, Brodeur GM, Seeger RC, et al. Histopathology (International Neuroblastoma Pathology Classification) and MYCN status in patients with peripheral neuroblastic tumors: a report from the Children's Cancer Group. Cancer. 2001;92:2699-708.

458. Brodeur GM, Pritchard J, Berthold F, Carlsen NL, Castel V, Castelberry RP, et al. Revisions of the international criteria for neuroblastoma diagnosis, staging, and response to treatment. Journal of clinical oncology : official journal of the American Society of Clinical Oncology. 1993;11:1466-77.

459. Maris JM, Hogarty MD, Bagatell R, Cohn SL. Neuroblastoma. Lancet (London, England). 2007;369:2106-20.

460. Strother DR, London WB, Schmidt ML, Brodeur GM, Shimada H, Thorner P, et al. Outcome after surgery alone or with restricted use of chemotherapy for patients with low-risk neuroblastoma: results of Children's Oncology Group study P9641. Journal of clinical oncology : official journal of the American Society of Clinical Oncology. 2012;30:1842-8.

461. Nuchtern JG, London WB, Barnewolt CE, Naranjo A, McGrady PW, Geiger JD, et al. A prospective study of expectant observation as primary therapy for neuroblastoma in young infants: a Children's Oncology Group study. Annals of surgery. 2012;256:573-80.

462. Baker DL, Schmidt ML, Cohn SL, Maris JM, London WB, Buxton A, et al. Outcome after reduced chemotherapy for intermediate-risk neuroblastoma. The New England journal of medicine. 2010;363:1313-23.

463. De Bernardi B, Gerrard M, Boni L, Rubie H, Canete A, Di Cataldo A, et al. Excellent outcome with reduced treatment for infants with disseminated neuroblastoma without MYCN gene amplification. Journal of clinical oncology : official journal of the American Society of Clinical Oncology. 2009;27:1034-40.

464. Rubie H, De Bernardi B, Gerrard M, Canete A, Ladenstein R, Couturier J, et al. Excellent outcome with reduced treatment in infants with nonmetastatic and unresectable neuroblastoma without MYCN amplification: results of the prospective INES 99.1. Journal of clinical oncology : official journal of the American Society of Clinical Oncology. 2011;29:449-55.

465. Adkins ES, Sawin R, Gerbing RB, London WB, Matthay KK, Haase GM. Efficacy of complete resection for high-risk neuroblastoma: a Children's Cancer Group study. Journal of pediatric surgery. 2004;39:931-6.

466. DeCou JM, Bowman LC, Rao BN, Santana VM, Furman WL, Luo X, et al. Infants with metastatic neuroblastoma have improved survival with resection of the primary tumor. Journal of pediatric surgery. 1995;30:937-40; discussion 40-1.

467. Haas-Kogan DA, Swift PS, Selch M, Haase GM, Seeger RC, Gerbing RB, et al. Impact of radiotherapy for high-risk neuroblastoma: a Children's Cancer Group study. International journal of radiation oncology, biology, physics. 2003;56:28-39.

468. Matthay KK, Reynolds CP, Seeger RC, Shimada H, Adkins ES, Haas-Kogan D, et al. Long-term results for children with high-risk neuroblastoma treated on a randomized trial of myeloablative therapy followed by 13-cis-retinoic acid: a children's oncology group study. Journal of clinical oncology : official journal of the American Society of Clinical Oncology. 2009;27:1007-13.

469. Pearson AD, Pinkerton CR, Lewis IJ, Imeson J, Ellershaw C, Machin D. High-dose rapid and standard induction chemotherapy for patients aged over 1 year with stage 4 neuroblastoma: a randomised trial. The Lancet Oncology. 2008;9:247-56.

470. Castel V, Segura V, Berlanga P. Emerging drugs for neuroblastoma. Expert opinion on emerging drugs. 2013;18:155-71.

471. Park JR, Scott JR, Stewart CF, London WB, Naranjo A, Santana VM, et al. Pilot induction regimen incorporating pharmacokinetically guided topotecan for treatment of newly diagnosed high-risk neuroblastoma: a Children's Oncology Group study. Journal of clinical oncology : official journal of the American Society of Clinical Oncology. 2011;29:4351-7.

472. Zimmerman KA, Yancopoulos GD, Collum RG, Smith RK, Kohl NE, Denis KA, et al. Differential expression of myc family genes during murine development. Nature. 1986;319:780-3.

473. Knoepfler PS, Cheng PF, Eisenman RN. N-myc is essential during neurogenesis for the rapid expansion of progenitor cell populations and the inhibition of neuronal differentiation. Genes & development. 2002;16:2699-712.

474. Charron J, Malynn BA, Fisher P, Stewart V, Jeannotte L, Goff SP, et al. Embryonic lethality in mice homozygous for a targeted disruption of the N-myc gene. Genes & development. 1992;6:2248-57.

475. Stanton BR, Perkins AS, Tessarollo L, Sassoon DA, Parada LF. Loss of N-myc function results in embryonic lethality and failure of the epithelial component of the embryo to develop. Genes & development. 1992;6:2235-47.

476. Yancopoulos GD, Nisen PD, Tesfaye A, Kohl NE, Goldfarb MP, Alt FW. N-myc can cooperate with ras to transform normal cells in culture. Proceedings of the National Academy of Sciences of the United States of America. 1985;82:5455-9.

477. Weiss WA, Aldape K, Mohapatra G, Feuerstein BG, Bishop JM. Targeted expression of MYCN causes neuroblastoma in transgenic mice. The EMBO journal. 1997;16:2985-95.

478. Brodeur GM, Seeger RC, Schwab M, Varmus HE, Bishop JM. Amplification of N-myc in untreated human neuroblastomas correlates with advanced disease stage. Science (New York, NY). 1984;224:1121-4.

479. Look AT, Hayes FA, Shuster JJ, Douglass EC, Castleberry RP, Bowman LC, et al. Clinical relevance of tumor cell ploidy and N-myc gene amplification in childhood neuroblastoma: a Pediatric Oncology Group study. Journal of clinical oncology : official journal of the American Society of Clinical Oncology. 1991;9:581-91.

480. Schwab M. MYCN in neuronal tumours. Cancer letters. 2004;204:179-87.

481. Bordow SB, Norris MD, Haber PS, Marshall GM, Haber M. Prognostic significance of MYCN oncogene expression in childhood neuroblastoma. Journal of clinical oncology : official journal of the American Society of Clinical Oncology. 1998;16:3286-94.

482. Chan HS, Gallie BL, DeBoer G, Haddad G, Ikegaki N, Dimitroulakos J, et al. MYCN protein expression as a predictor of neuroblastoma prognosis. Clinical cancer research : an official journal of the American Association for Cancer Research. 1997;3:1699-706.

483. Hiyama E, Hiyama K, Yokoyama T, Ishii T. Immunohistochemical analysis of N-myc protein expression in neuroblastoma: correlation with prognosis of patients. Journal of pediatric surgery. 1991;26:838-43.

484. Nakada K, Fujioka T, Kitagawa H, Takakuwa T, Yamate N. Expressions of N-myc and ras oncogene products in neuroblastoma and their correlations with prognosis. Japanese journal of clinical oncology. 1993;23:149-55.

485. Valentijn LJ, Koster J, Haneveld F, Aissa RA, van Sluis P, Broekmans ME, et al. Functional MYCN signature predicts outcome of neuroblastoma irrespective of MYCN amplification. Proceedings of the National Academy of Sciences of the United States of America. 2012;109:19190-5.

486. Chesler L, Schlieve C, Goldenberg DD, Kenney A, Kim G, McMillan A, et al. Inhibition of phosphatidylinositol 3-kinase destabilizes Mycn protein and blocks malignant progression in neuroblastoma. Cancer research. 2006;66:8139-46.

487. Kenney AM, Widlund HR, Rowitch DH. Hedgehog and PI-3 kinase signaling converge on Nmyc1 to promote cell cycle progression in cerebellar neuronal precursors. Development (Cambridge, England). 2004;131:217-28.

488. Carter DR, Murray J, Cheung BB, Gamble L, Koach J, Tsang J, et al. Therapeutic targeting of the MYC signal by inhibition of histone chaperone FACT in neuroblastoma. Science translational medicine. 2015;7:312ra176.

489. Beltran H. The N-myc Oncogene: Maximizing its Targets, Regulation, and Therapeutic Potential. Molecular cancer research : MCR. 2014.

490. Huang M, Weiss WA. Neuroblastoma and MYCN. Cold Spring Harbor perspectives in medicine. 2013;3:a014415.

491. Lutz W, Stohr M, Schurmann J, Wenzel A, Lohr A, Schwab M. Conditional expression of N-myc in human neuroblastoma cells increases expression of alpha-prothymosin and ornithine decarboxylase and accelerates progression into S-phase early after mitogenic stimulation of quiescent cells. Oncogene. 1996;13:803-12.

492. Goodman LA, Liu BC, Thiele CJ, Schmidt ML, Cohn SL, Yamashiro JM, et al. Modulation of N-myc expression alters the invasiveness of neuroblastoma. Clinical & experimental metastasis. 1997;15:130-9.

493. Jiang R, Xue S, Jin Z. Stable knockdown of MYCN by lentivirus-based RNAi inhibits human neuroblastoma cells growth in vitro and in vivo. Biochemical and biophysical research communications. 2011;410:364-70.

494. Cotterman R, Knoepfler PS. N-Myc regulates expression of pluripotency genes in neuroblastoma including lif, klf2, klf4, and lin28b. PloS one. 2009;4:e5799.

495. Hatzi E, Murphy C, Zoephel A, Ahorn H, Tontsch U, Bamberger AM, et al. N-myc oncogene overexpression down-regulates leukemia inhibitory factor in neuroblastoma. European journal of biochemistry / FEBS. 2002;269:3732-41.

496. Alaminos M, Mora J, Cheung NK, Smith A, Qin J, Chen L, et al. Genome-wide analysis of gene expression associated with MYCN in human neuroblastoma. Cancer research. 2003;63:4538-46.

497. Biedler JL, Meyers MB, Spengler BA. Homogeneously Staining Regions and Double Minute Chromosomes, Prevalent Cytogenetic Abnormalities of Human Neuroblastoma Cells. In: Sergey F, Leif H, editors. Advances in Cellular Neurobiology: Elsevier; 1983. p. 267-307.

498. Brodeur GM, Green AA, Hayes FA, Williams KJ, Williams DL, Tsiatis AA. Cytogenetic features of human neuroblastomas and cell lines. Cancer research. 1981;41:4678-86.

499. Brodeur GM, Sekhon G, Goldstein MN. Chromosomal aberrations in human neuroblastomas. Cancer. 1977;40:2256-63.

500. Caron H, van Sluis P, de Kraker J, Bokkerink J, Egeler M, Laureys G, et al. Allelic loss of chromosome 1p as a predictor of unfavorable outcome in patients with neuroblastoma. The New England journal of medicine. 1996;334:225-30.

501. Lastowska M, Cullinane C, Variend S, Cotterill S, Bown N, O'Neill S, et al. Comprehensive genetic and histopathologic study reveals three types of neuroblastoma tumors. Journal of clinical oncology : official journal of the American Society of Clinical Oncology. 2001;19:3080-90.

502. Michels E, Vandesompele J, De Preter K, Hoebeeck J, Vermeulen J, Schramm A, et al. ArrayCGH-based classification of neuroblastoma into genomic subgroups. Genes, chromosomes & cancer. 2007;46:1098-108.

503. Mosse YP, Diskin SJ, Wasserman N, Rinaldi K, Attiyeh EF, Cole K, et al. Neuroblastomas have distinct genomic DNA profiles that predict clinical phenotype and regional gene expression. Genes, chromosomes & cancer. 2007;46:936-49.

504. Plantaz D, Vandesompele J, Van Roy N, Lastowska M, Bown N, Combaret V, et al. Comparative genomic hybridization (CGH) analysis of stage 4 neuroblastoma reveals high frequency of 11q deletion in tumors lacking MYCN amplification. International journal of cancer Journal international du cancer. 2001;91:680-6.

505. Schleiermacher G, Michon J, Huon I, d'Enghien CD, Klijanienko J, Brisse H, et al. Chromosomal CGH identifies patients with a higher risk of relapse in neuroblastoma without MYCN amplification. British journal of cancer. 2007;97:238-46.

506. Tomioka N, Oba S, Ohira M, Misra A, Fridlyand J, Ishii S, et al. Novel risk stratification of patients with neuroblastoma by genomic signature, which is independent of molecular signature. Oncogene. 2008;27:441-9.

507. Vandesompele J, Speleman F, Van Roy N, Laureys G, Brinskchmidt C, Christiansen H, et al. Multicentre analysis of patterns of DNA gains and losses in 204 neuroblastoma tumors: how many genetic subgroups are there? Medical and pediatric oncology. 2001;36:5-10.

508. Hiyama E, Hiyama K, Yamaoka H, Sueda T, Reynolds CP, Yokoyama T. Expression profiling of favorable and unfavorable neuroblastomas. Pediatric surgery international. 2004;20:33-8.

509. Oberthuer A, Hero B, Berthold F, Juraeva D, Faldum A, Kahlert Y, et al. Prognostic impact of gene expression-based classification for neuroblastoma. Journal of clinical oncology : official journal of the American Society of Clinical Oncology. 2010;28:3506-15.

510. Ohira M, Oba S, Nakamura Y, Isogai E, Kaneko S, Nakagawa A, et al. Expression profiling using a tumor-specific cDNA microarray predicts the prognosis of intermediate risk neuroblastomas. Cancer cell. 2005;7:337-50.

511. Vermeulen J, De Preter K, Naranjo A, Vercruysse L, Van Roy N, Hellemans J, et al. Predicting outcomes for children with neuroblastoma using a multigene-expression

signature: a retrospective SIOPEN/COG/GPOH study. The Lancet Oncology. 2009;10:663-71.

512. Wei JS, Greer BT, Westermann F, Steinberg SM, Son CG, Chen QR, et al. Prediction of clinical outcome using gene expression profiling and artificial neural networks for patients with neuroblastoma. Cancer research. 2004;64:6883-91.

513. Hiyama E, Hiyama K, Yokoyama T, Ichikawa T, Matsuura Y. Length of telomeric repeats in neuroblastoma: correlation with prognosis and other biological characteristics. Japanese journal of cancer research : Gann. 1992;83:159-64.

514. Hiyama E, Hiyama K, Yokoyama T, Matsuura Y, Piatyszek MA, Shay JW. Correlating telomerase activity levels with human neuroblastoma outcomes. Nature medicine. 1995;1:249-55.

515. Poremba C, Willenbring H, Hero B, Christiansen H, Schafer KL, Brinkschmidt C, et al. Telomerase activity distinguishes between neuroblastomas with good and poor prognosis. Annals of oncology : official journal of the European Society for Medical Oncology / ESMO. 1999;10:715-21.

516. Farooqi AS, Dagg RA, Choi LM, Shay JW, Reynolds CP, Lau LM. Alternative lengthening of telomeres in neuroblastoma cell lines is associated with a lack of MYCN genomic amplification and with p53 pathway aberrations. Journal of neuro-oncology. 2014;119:17-26.

517. Knecht H, Kongruttanachok N, Sawan B, Brossard J, Prevost S, Turcotte E, et al. Three-dimensional Telomere Signatures of Hodgkin- and Reed-Sternberg Cells at Diagnosis Identify Patients with Poor Response to Conventional Chemotherapy. Translational oncology. 2012;5:269-77.

518. Parada LA, McQueen PG, Misteli T. Tissue-specific spatial organization of genomes. Genome biology. 2004;5:R44.

519. Olovnikov AM. [The immune response and the process of marginotomy in lymphoid cells]. Vestnik Akademii meditsinskikh nauk SSSR. 1972;27:85-7.

520. Deng Y, Chan SS, Chang S. Telomere dysfunction and tumour suppression: the senescence connection. Nature reviews Cancer. 2008;8:450-8.

521. Hayflick L, Moorhead PS. The serial cultivation of human diploid cell strains. Experimental cell research. 1961;25:585-621.

522. Collins K, Mitchell JR. Telomerase in the human organism. Oncogene. 2002;21:564-79.

523. Lansdorp PM. Telomeres and disease. The EMBO journal. 2009;28:2532-40.

524. Misri S, Pandita S, Kumar R, Pandita TK. Telomeres, histone code, and DNA damage response. Cytogenetic and genome research. 2008;122:297-307.

525. Zvereva MI, Shcherbakova DM, Dontsova OA. Telomerase: structure, functions, and activity regulation. Biochemistry Biokhimiia. 2010;75:1563-83.

526. Blackburn EH. Switching and signaling at the telomere. Cell. 2001;106:661-73.

527. Greider CW, Blackburn EH. Identification of a specific telomere terminal transferase activity in Tetrahymena extracts. Cell. 1985;43:405-13.

528. Dunham MA, Neumann AA, Fasching CL, Reddel RR. Telomere maintenance by recombination in human cells. Nature genetics. 2000;26:447-50.

529. Muntoni A, Reddel RR. The first molecular details of ALT in human tumor cells. Human molecular genetics. 2005;14 Spec No. 2:R191-6.

530. Meeker AK, Hicks JL, Iacobuzio-Donahue CA, Montgomery EA, Westra WH, Chan TY, et al. Telomere length abnormalities occur early in the initiation of epithelial carcinogenesis. Clinical cancer research : an official journal of the American Association for Cancer Research. 2004;10:3317-26.

531. Odagiri E, Kanada N, Jibiki K, Demura R, Aikawa E, Demura H. Reduction of telomeric length and c-erbB-2 gene amplification in human breast cancer, fibroadenoma, and gynecomastia. Relationship to histologic grade and clinical parameters. Cancer. 1994;73:2978-84.

532. Rampazzo E, Bertorelle R, Serra L, Terrin L, Candiotto C, Pucciarelli S, et al. Relationship between telomere shortening, genetic instability, and site of tumour origin in colorectal cancers. British journal of cancer. 2010;102:1300-5.

533. Gisselsson D, Jonson T, Petersen A, Strombeck B, Dal Cin P, Hoglund M, et al. Telomere dysfunction triggers extensive DNA fragmentation and evolution of complex chromosome abnormalities in human malignant tumors. Proceedings of the National Academy of Sciences of the United States of America. 2001;98:12683-8.

534. Hanahan D, Weinberg RA. The hallmarks of cancer. Cell. 2000;100:57-70.

535. Murnane JP, Sabatier L. Chromosome rearrangements resulting from telomere dysfunction and their role in cancer. BioEssays : news and reviews in molecular, cellular and developmental biology. 2004;26:1164-74.

536. Mai S. Initiation of telomere-mediated chromosomal rearrangements in cancer. Journal of cellular biochemistry. 2010;109:1095-102.

537. Blasco MA, Lee HW, Hande MP, Samper E, Lansdorp PM, DePinho RA, et al. Telomere shortening and tumor formation by mouse cells lacking telomerase RNA. Cell. 1997;91:25-34.

538. Rudolph KL, Chang S, Lee HW, Blasco M, Gottlieb GJ, Greider C, et al. Longevity, stress response, and cancer in aging telomerase-deficient mice. Cell. 1999;96:701-12.

539. Willeit P, Willeit J, Brandstatter A, Ehrlenbach S, Mayr A, Gasperi A, et al. Cellular aging reflected by leukocyte telomere length predicts advanced atherosclerosis and cardiovascular disease risk. Arteriosclerosis, thrombosis, and vascular biology. 2010;30:1649-56.

540. Hande P, Slijepcevic P, Silver A, Bouffler S, van Buul P, Bryant P, et al. Elongated telomeres in scid mice. Genomics. 1999;56:221-3.

541. Hemann MT, Greider CW. Wild-derived inbred mouse strains have short telomeres. Nucleic acids research. 2000;28:4474-8.

542. Mai S, Wiener F. The impact of p53 loss on murine plasmacytoma development. Chromosome research : an international journal on the molecular, supramolecular and evolutionary aspects of chromosome biology. 2002;10:239-51.

543. Mai S, Garini Y. The significance of telomeric aggregates in the interphase nuclei of tumor cells. Journal of cellular biochemistry. 2006;97:904-15.

544. Koelsch BU, Rajewsky MF, Kindler-Rohrborn A. A 6-Mb contig-based comparative gene and linkage map of the rat schwannoma tumor suppressor region at 10q32.3. Genomics. 2005;85:322-9.

545. Montagna C, Lyu MS, Hunter K, Lukes L, Lowther W, Reppert T, et al. The Septin 9 (MSF) gene is amplified and overexpressed in mouse mammary gland adenocarcinomas and human breast cancer cell lines. Cancer research. 2003;63:2179-87.

546. Langan JE, Cole CG, Huckle EJ, Byrne S, McRonald FE, Rowbottom L, et al. Novel microsatellite markers and single nucleotide polymorphisms refine the tylosis with oesophageal cancer (TOC) minimal region on 17q25 to 42.5 kb: sequencing does not identify the causative gene. Human genetics. 2004;114:534-40.

547. Russell SE, McIlhatton MA, Burrows JF, Donaghy PG, Chanduloy S, Petty EM, et al. Isolation and mapping of a human septin gene to a region on chromosome 17q, commonly deleted in sporadic epithelial ovarian tumors. Cancer research. 2000;60:4729-34.

548. Turhan N, Yurur-Kutlay N, Topcuoglu P, Sayki M, Yuksel M, Gurman G, et al. Translocation (13;17)(q14;q25) as a novel chromosomal abnormality in acute myeloid leukemia-M4. Leukemia research. 2006;30:903-5.

549. Evans AE, Silber JH, Shpilsky A, D'Angio GJ. Successful management of low-stage neuroblastoma without adjuvant therapies: a comparison of two decades, 1972 through 1981 and 1982 through 1992, in a single institution. Journal of clinical oncology : official journal of the American Society of Clinical Oncology. 1996;14:2504-10.

550. Cohn SL, London WB, Huang D, Katzenstein HM, Salwen HR, Reinhart T, et al. MYCN expression is not prognostic of adverse outcome in advanced-stage neuroblastoma with nonamplified MYCN. Journal of clinical oncology : official journal of the American Society of Clinical Oncology. 2000;18:3604-13.

551. Spitz R, Hero B, Ernestus K, Berthold F. Gain of distal chromosome arm 17q is not associated with poor prognosis in neuroblastoma. Clinical cancer research : an official journal of the American Association for Cancer Research. 2003;9:4835-40.

552. Godfried MB, Veenstra M, v Sluis P, Boon K, v Asperen R, Hermus MC, et al. The N-myc and c-myc downstream pathways include the chromosome 17q genes nm23-H1 and nm23-H2. Oncogene. 2002;21:2097-101.

553. Mai S, Wiener F. Murine FISH. In: Beatty BG, Mai S, Squire JA, editors. FISH. Oxford: Oxford University Press; 2002. p. 55-76.

554. Wenzel A, Cziepluch C, Hamann U, Schurmann J, Schwab M. The N-Myc oncoprotein is associated in vivo with the phosphoprotein Max(p20/22) in human neuroblastoma cells. The EMBO journal. 1991;10:3703-12.

555. Robertson D, Isacke CM. Multiple immunofluorescence labeling of formalin-fixed paraffin-embedded tissue. Methods in molecular biology (Clifton, NJ). 2011;724:69-77.

556. Chin SF, Daigo Y, Huang HE, Iyer NG, Callagy G, Kranjac T, et al. A simple and reliable pretreatment protocol facilitates fluorescent in situ hybridisation on tissue microarrays of paraffin wax embedded tumour samples. Molecular pathology : MP. 2003;56:275-9.

557. Ridler TW, Calvard S. Picture thresholding using an iterative selection method. IEEE Transactions on Systems, Man and Cybernetics. 1978;8:631-2.

558. Chuang CH, Carpenter AE, Fuchsova B, Johnson T, de Lanerolle P, Belmont AS. Long-range directional movement of an interphase chromosome site. Current biology : CB. 2006;16:825-31.

559. Schleiermacher G, Janoueix-Lerosey I, Combaret V, Derre J, Couturier J, Aurias A, et al. Combined 24-color karyotyping and comparative genomic hybridization analysis indicates predominant rearrangements of early replicating chromosome regions in neuroblastoma. Cancer genetics and cytogenetics. 2003;141:32-42.

560. Gadji M, Vallente R, Klewes L, Righolt C, Wark L, Kongruttanachok N, et al. Nuclear remodeling as a mechanism for genomic instability in cancer. Advances in cancer research. 2011;112:77-126.

561. Breslow N, McCann B. Statistical estimation of prognosis for children with neuroblastoma. Cancer research. 1971;31:2098-103.

562. George RE, London WB, Cohn SL, Maris JM, Kretschmar C, Diller L, et al. Hyperdiploidy plus nonamplified MYCN confers a favorable prognosis in children 12 to 18 months old with disseminated neuroblastoma: a Pediatric Oncology Group study. Journal of clinical oncology : official journal of the American Society of Clinical Oncology. 2005;23:6466-73.

563. Brodeur GM. Neuroblastoma: biological insights into a clinical enigma. Nature reviews Cancer. 2003;3:203-16.

564. Coco S, Theissen J, Scaruffi P, Stigliani S, Moretti S, Oberthuer A, et al. Age-dependent accumulation of genomic aberrations and deregulation of cell cycle and telomerase genes in metastatic neuroblastoma. International journal of cancer Journal international du cancer. 2012;131:1591-600.

565. Pienta KJ, Partin AW, Coffey DS. Cancer as a disease of DNA organization and dynamic cell structure. Cancer research. 1989;49:2525-32.

566. Kuzyk A, Booth S, Righolt C, Mathur S, Gartner J, Mai S. MYCN overexpression is associated with unbalanced copy number gain, altered nuclear location, and overexpression of chromosome arm 17q genes in neuroblastoma tumors and cell lines. Genes, chromosomes & cancer. 2015;54:616-28.

567. Kuzyk A, Mai S. Selected telomere length changes and aberrant three-dimensional nuclear telomere organization during fast-onset mouse plasmacytomas. Neoplasia (New York, NY). 2012;14:344-51.

568. Lundberg G, Jin Y, Sehic D, Ora I, Versteeg R, Gisselsson D. Intratumour diversity of chromosome copy numbers in neuroblastoma mediated by on-going chromosome loss from a polyploid state. PloS one. 2013;8:e59268.

569. Group BDW. Biomarkers and surrogate endpoints: preferred definitions and conceptual framework. Clinical pharmacology and therapeutics. 2001;69:89-95.

570. Strimbu K, Tavel JA. What are biomarkers? Current opinion in HIV and AIDS. 2010;5:463-6.

571. Sunpaweravong S, Sunpaweravong P, Sathitruangsak C, Mai S. Three-dimensional telomere architecture of esophageal squamous cell carcinoma: comparison of tumor and normal epithelial cells. Diseases of the esophagus : official journal of the International Society for Diseases of the Esophagus / ISDE. 2015.

572. Mathur S, Glogowska A, McAvoy E, Righolt C, Rutherford J, Willing C, et al. Three-dimensional quantitative imaging of telomeres in buccal cells identifies mild, moderate, and severe Alzheimer's disease patients. Journal of Alzheimer's disease : JAD. 2014;39:35-48.

573. Caren H, Kryh H, Nethander M, Sjoberg RM, Trager C, Nilsson S, et al. High-risk neuroblastoma tumors with 11q-deletion display a poor prognostic, chromosome instability phenotype with later onset. Proceedings of the National Academy of Sciences of the United States of America. 2010;107:4323-8.

574. Sun XX, Yu Q. Intra-tumor heterogeneity of cancer cells and its implications for cancer treatment. Acta pharmacologica Sinica. 2015;36:1219-27.

575. Beckman RA, Loeb LA. Genetic instability in cancer: theory and experiment. Seminars in cancer biology. 2005;15:423-35.

576. Kuttler F, Mai S. Formation of non-random extrachromosomal elements during development, differentiation and oncogenesis. Seminars in cancer biology. 2007;17:56-64.

577. Wang Q, Diskin S, Rappaport E, Attiyeh E, Mosse Y, Shue D, et al. Integrative genomics identifies distinct molecular classes of neuroblastoma and shows that multiple genes are targeted by regional alterations in DNA copy number. Cancer research. 2006;66:6050-62.

578. de Lange T. Human telomeres are attached to the nuclear matrix. The EMBO journal. 1992;11:717-24.

579. Luderus ME, van Steensel B, Chong L, Sibon OC, Cremers FF, de Lange T. Structure, subnuclear distribution, and nuclear matrix association of the mammalian telomeric complex. The Journal of cell biology. 1996;135:867-81.

580. Bronstein I, Israel Y, Kepten E, Mai S, Shav-Tal Y, Barkai E, et al. Transient anomalous diffusion of telomeres in the nucleus of mammalian cells. Physical review letters. 2009;103:018102.

581. Wang X, Kam Z, Carlton PM, Xu L, Sedat JW, Blackburn EH. Rapid telomere motions in live human cells analyzed by highly time-resolved microscopy. Epigenetics & chromatin. 2008;1:4.

582. Ermler S, Krunic D, Knoch TA, Moshir S, Mai S, Greulich-Bode KM, et al. Cell cycle-dependent 3D distribution of telomeres and telomere repeat-binding factor 2 (TRF2) in HaCaT and HaCaT-myc cells. European journal of cell biology. 2004;83:681-90.

583. Mitchell TR, Zhu XD. Methylated TRF2 associates with the nuclear matrix and serves as a potential biomarker for cellular senescence. Aging. 2014;6:248-63.

584. Mehta IS, Amira M, Harvey AJ, Bridger JM. Rapid chromosome territory relocation by nuclear motor activity in response to serum removal in primary human fibroblasts. Genome biology. 2010;11:R5.

585. Schmalter AK, Kuzyk A, Righolt CH, Neusser M, Steinlein OK, Muller S, et al. Distinct nuclear orientation patterns for mouse chromosome 11 in normal B lymphocytes. BMC cell biology. 2014;15:22.

586. Schmalter AK, Righolt CH, Kuzyk A, Mai S. Changes in Nuclear Orientation Patterns of Chromosome 11 during Mouse Plasmacytoma Development. Translational oncology. 2015;8:417-23.

587. Ballester M, Kress C, Hue-Beauvais C, Kieu K, Lehmann G, Adenot P, et al. The nuclear localization of WAP and CSN genes is modified by lactogenic hormones in HC11 cells. Journal of cellular biochemistry. 2008;105:262-70.

588. Wu KJ, Grandori C, Amacker M, Simon-Vermot N, Polack A, Lingner J, et al. Direct activation of TERT transcription by c-MYC. Nature genetics. 1999;21:220-4.

589. Takai H, Smogorzewska A, de Lange T. DNA damage foci at dysfunctional telomeres. Current biology : CB. 2003;13:1549-56.

590. Bhoopalam N, Chen Y, Yakulis V, Heller P. Surface immunoglobulins of lymphocytes in plasmacytoma. V. The effect of RNA-rich extract from mouse plasmacytoma MOPC 104E on the immune response. Clinical and experimental immunology. 1976;24:357-67.

591. Sutherland H, Bickmore WA. Transcription factories: gene expression in unions? Nature reviews Genetics. 2009;10:457-66.

592. Phatnani HP, Greenleaf AL. Phosphorylation and functions of the RNA polymerase II CTD. Genes & development. 2006;20:2922-36.